Biomaterials Translational

Quarterly Established in December 2020. Volume 4, Issue 1 March 28, 2023

Contents

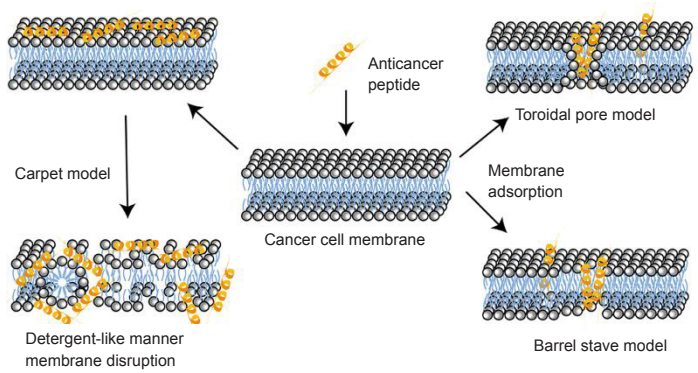

Anticancer peptides (ACPs), derived from naturally occurring and modified peptides, have received great attention in these years and emerge as novel therapeutic and diagnostic candidates for cancer therapies, because of numerous advantages over the current treatment modalities.

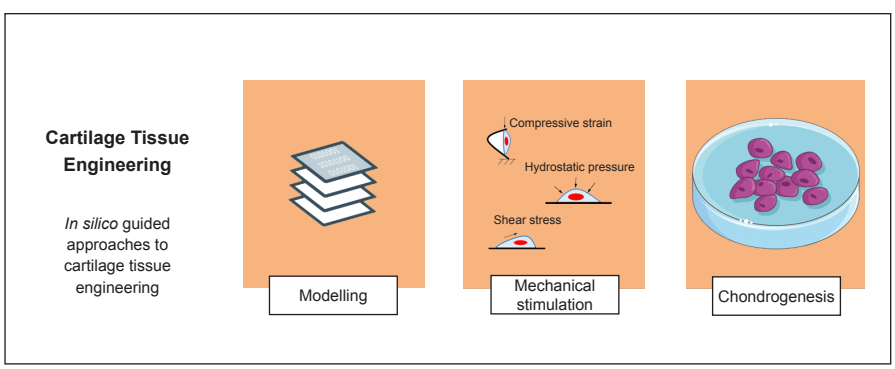

Different types of mechanical stimulation are applied on stem cells and/or chondrocytes for *in vitro* cartilage tissue engineering. Determining/optimising the mechanical stimulation for *in vitro* experiments can be assisted by *in silico* modelling and simulation (partly created by Servier Medical Art).

RESEARCH ARTICLES

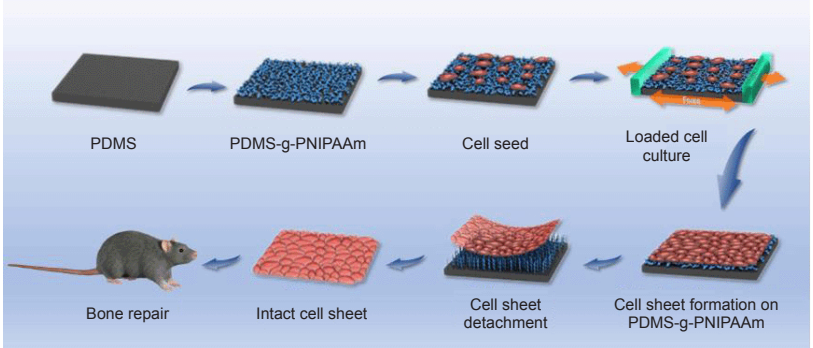

High-quality cell sheets through combining mechanical stimulation and thermosensitive poly(N-isopropyl acrylamide) (PNIPAAm) were prepared. Both *in vitro* and *in vivo* studies have proven that cell sheets function to facilitate osteogenesis and bone repair, and therefore present an effective strategy for bone tissue engineering.

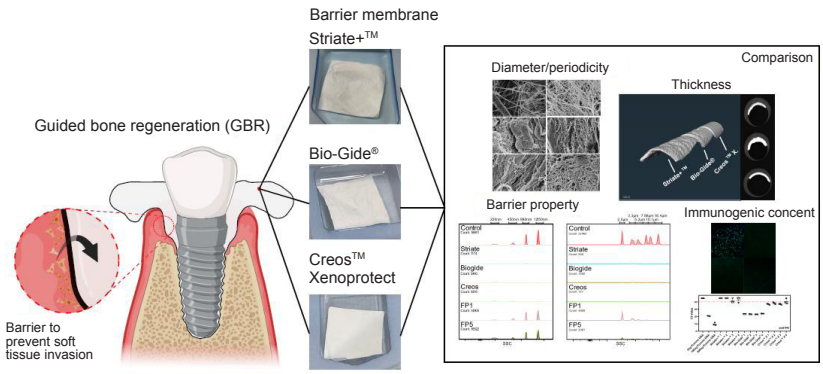

Guided bone regeneration is a dental surgical procedure that uses a barrier membrane to prevent soft tissue invasion into bone cavity and implants. Three porcine-derived collagen barrier membranes were systemically evaluated. All showed excellent barrier property, but significant difference in D-periodicity of collagen fibres, thickness of membrane and immunogenic content.

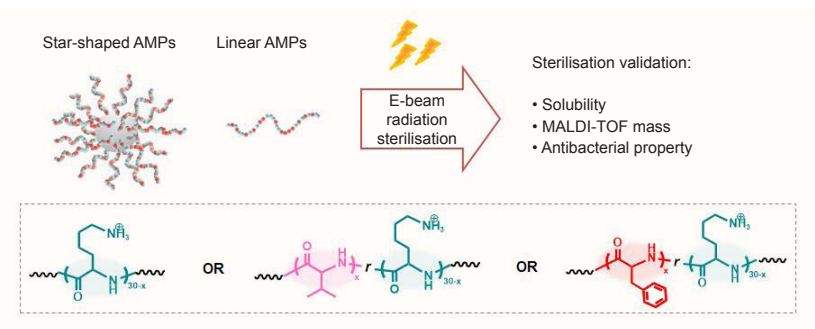

Antimicrobial peptides (AMPs) with different structures were successfully constructed from three types of amino acid monomers. The AMPs were then successfully sterilised using commercial electron beam radiation. The effects of radiation on the structure and properties of the AMPs were subsequently studied by solubility assay, matrix-assisted laser desorption/ionisation time of flight mass spectrometry, and antibacterial assay.

The emergence of AI tools in scientific writing and research

Zhidao Xia[1,*], *Qian Wang*[2,*]

Biomaterials Translational is now in its third year since its establishment. On March 19, the first virtual forums in 2023 on 'Advanced Technology for Biomaterial Research' hosted by *Biomaterials Translational* received a great response. The forum covered topics including angiogenesis of biomaterials presented by Professor Jake Barralet, McGill University, Canada, and a new lasermicrotome technology from Dr. Heiko Rechter, LLS ROWIAK LaserLabSolutions, Germany. Lasermicrotome and its related platform are expected to have wide applications for histology, pathology, and tissue/biomaterial interfaces, as shown in the cover art. The online forum was jointly supported by the Welsh Government to celebrate the successful collaboration between McGill University (Canada) and Swansea University (UK), and over 3100 people attended the online forum through virtual broadcast platforms.

In this issue, we present a collection of papers from different fields of translational biomaterials research. There are two review articles: the first, by Xingming Li and co-authors,[1] discusses bioactive peptides for anticancer therapies; the second, by Feihu Zhao's team,[2] explores how the combination of *in vitro* and *in silico* approaches can greatly facilitate the optimization of the micro-mechanical environment for cartilage tissue engineering. Additionally, this issue presents three original research articles, including a report on the development of mechanically conditioned cell sheets cultured on thermo-responsive surfaces for bone tissue engineering applications,[3] a comprehensive investigation on the application of porcine-derived collagen membranes for guided bone regeneration,[4] and a systematic study on how irradiation sterilization impacts the structure and antibacterial performance of antimicrobial peptides.[5]

The first quarter of 2023 has marked a significant milestone in the world of artificial intelligence (AI) with the announcement of ChatGPT4 and GoogleBard. Despite being in its infancy, ChatGPT4 has already made a considerable impact on the future of scientific publications. Many users have utilized ChatGPT to write essays, articles, emails, and other documents for publication. However, there are polarized views on the use of AI in scientific writing.

ChatGPT asserts that while it can generate text for scientific writing, its impact on scientific journals will depend on how researchers, editors, and publishers use it. One potential use of ChatGPT is to generate initial drafts of scientific papers, which could potentially save time and effort in the writing process. However, it is crucial to note that ChatGPT is not a substitute for human expertise and judgment, which are essential for scientific writing.

For Biomaterials Translational, where authors can use AI and AI-assisted technologies in the writing process, we request that authors:

- Only apply AI tools to improve the readability and language of their manuscript
- Always use AI tools with careful oversight
- Avoid using AI technologies to perform data interpretation
- Be mindful that AI technologies very often generate authoritative conclusions that can be biased or even incorrect
- Remember that AI technologies cannot be listed as a co-author

More importantly, as editors, we assure you that our journal is not and will not be controlled or edited by AI!

We thank ChatGPT from OpenAI for manuscript editing.

1 Institute of Life Science, Swansea University Medical School, Swansea, UK;
2 Department of Chemistry and Biochemistry, University of South Carolina, Columbia, SC, USA

***Corresponding author:**
Zhidao Xia, z.xia@swansea.ac.uk;
Qian Wang, Wang263@mailbox.sc.edu.

http://doi.org/10.12336/biomatertransl.2023.01.001

How to cite this article: Xia, Z.; Wang, Q. The emergence of AI tools in scientific writing and research. *Biomater Transl.* **2023**, *4*(1), 1-2.

1. Zhang, Y.; Wang, C.; Zhang, W.; Li X. Bioactive peptides for anticancer therapies. *Biomater Transl.* **2023**, *4*, 5-17.
2. Jess, R.; Ling, T.; Xiong, Y.; Wright, C. J.; Zhao, F. Mechanical environment for in vitro cartilage tissue engineering assisted by in silico models. *Biomater Transl.* **2023**, *4*, 18-26.
3. Wang, G.; Yuan, Z.; Yu, L.; Yu, Y.; Zhou, P.; Chu, G.; Wang, H.; Guo, Q.; Zhu, C.; Han, F.; Chen, S.; Li, B. Mechanically conditioned cell sheets cultured on thermo-responsive surfaces promote bone regeneration. *Biomater Transl.* **2023**, *4*, 27-40.
4. Tai, A.; Landao-Bassonga, E.; Chen, Z.; Tran, M.; Allan, B.; Ruan, R.; Calder, D.; Goonewardene, M.; Ngo, H.; Zheng, M. H. Systematic evaluation of three porcine-derived collagen membranes for guided bone regeneration. *Biomater Transl.* **2023**, *4*, 41-50.
5. Wang, X.; Li, Q.; Yang, H. Effect of radiation sterilisation on the structure and antibacterial properties of antimicrobial peptides. *Biomater Transl.* **2023**, *4*, 51-61.

Implantable immune stents: a new opportunity for cancer treatment

Fengxia Chen[1], *Feifei Pu*[2,*]

1 Department of Radiation and Medical Oncology, Zhongnan Hospital of Wuhan University, Wuhan, Hubei Province, China;
2 Department of Orthopedics, Wuhan Hospital of Traditional Chinese and Western Medicine (Wuhan No.1 Hospital), Tongji Medical College, Huazhong University of Science and Technology, Wuhan, Hubei Province, China

***Corresponding author:**
Feifei Pu,
pufeifei@hust.edu.cn.

http://doi.org/10.12336/biomatertransl.2023.01.002

How to cite this article:
Chen, F.; Pu, F. Implantable immune stents: a new opportunity for cancer treatment. *Biomater Transl.* **2023**, *4*(1), 3-4.

The poor efficacy of immunotherapy in clinical trials of solid tumours is mainly due to their highly immunosuppressive tumour microenvironment (TME).[1] Regulatory T cells (Tregs), a subset of T cells that control the autoimmune response and are one of the main components of immunosuppressive TME, can regulate the immune response intensity and inhibit the function and activity of effector T cells, thus inducing immune tolerance and maintaining immune response homeostasis. In solid TME, Tregs mediate the immune escape of tumour cells by inhibiting the body's immune response, affecting the efficacy of prognosis.[2]

Based on the characteristics of Tregs in TME, reducing their infiltration and immunosuppressive effect helps explore new treatment strategies for solid tumours. The design, manufacture, and therapeutic properties of biologically degradable immunomodulatory macroporous scaffolds have been reported recently in Nature Biomedical Engineering.[3] In this study, immunomodulatory macroporous scaffold implantation around the tumour released small-molecule inhibitors of transforming growth factor β, which selectively target Treg cells, while chemokines attracted effector T cells and antibodies to activate tumour cells. In animal models with malignant tumours, immunomodulatory macroporous scaffolds are beneficial to recruit and activate effector T cells into the tumours, released small-molecule inhibitors of transforming growth factor β, and suppressed Treg cells, which resulted in an "immunoectopic effect" against distant metastases and established long-term memory to prevent tumour recurrence. This study also revealed that immunomodulatory macroporous scaffolds can be regarded as a vehicle to deliver antigen-specific T cells into the tumours. Overall, implanting immunomodulatory macroporous scaffolds around tumours can enhance cellular immunity and avoid systemic toxicity (**Figure 1**).

Mesoporous silica nanomaterials have the advantages of high porosity, high biocompatibility, and easy surface modification and are ideal materials for improving tumour immunotherapy efficacy.[4] The two most common types of mesoporous-silica-based immunotherapies are internalization of mesoporous silica nanoparticles into antigen-presenting cells, and recruitment of antigen-presenting cells by micrometer-sized mesoporous silica rods that can form a three-dimensional (3D) space.[4] mesoporous silica nanoparticle-based cancer vaccines can be taken up by peripheral or lymphoid cells to stimulate the immune system to fight cancer cells, and mesoporous silica rod cancer vaccines can aggregate immune cells into their scaffold to induce tumour-specific immunity. Therefore, mesoporous silica can successfully stimulate adaptive immune response and can treat cancer and other infectious diseases.[5]

There are many types of immunotherapy carriers of biological scaffolds, which are divided into different types according to their composition, preparation method, route of administration, or immune regulation principle.[6] In addition to mesoporous silica, collagen, alginate, and hyaluronic acid are typically composed of natural ingredients or synthetic polymers.[7] The preparation methods include simple crosslinking *in vitro*, rapid sol-gel phase transformation *in vivo*, *in situ* chemical polymerization assembly, or 3D printing and self-assembly technology. These scaffolds are also becoming more diverse with tumour antigens and adjuvants, immunostimulatory or immunosuppressive molecules, and biologically active immune cells.[6] Moreover, because of the importance of 3D *in vitro* models in scientific research, 3D macroscale scaffolds have shown great potential for the development of biomimetic organoids.[8]

This work highlighted the unique advantage of using mesoporous materials for the modulation of cancer immunotherapy. However, such scaffold materials face challenges like limited penetration depth into solid tumours, the demand to deal with the high individual heterogeneity

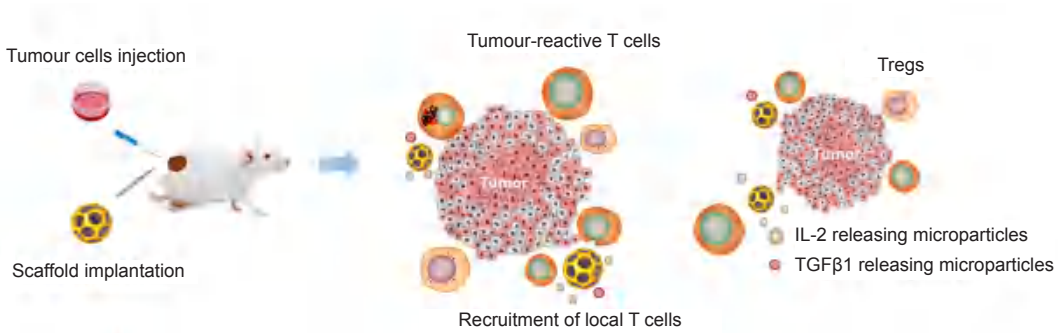

Figure 1. The schematic representation showed that the anti-tumour immunity was enhanced by immunomodulatory macroporous scaffolds. Sustained release of scaffolds can recruit endogenous T cells, whereas the presentation of surface-conjugated activation cues and the sustained release of IL-2 can activate recruited T cells. Sustained release of TGF-β depletes Tregs in tumours. IL-2: interleukin-2; TGF-β: transforming growth factor β; TGFβ1: transforming growth factor β 1; Treg: regulatory T cell.

of tumours, the challenge to achieve precise regulation, and the hurdle in large-scale production and potential market transformation, etc. Further research efforts are necessary to further explore the molecular mechanism of tumour immune microenvironment regulation and the influence of biological scaffold materials on cell fate. Eventually, the development of more personalised biological scaffold materials in combination with advanced biomaterials manufacturing technology will provide more efficient immunotherapies for solid tumours and other cancers.

Author contributions
Conceptualization, investigation, and writing-original draft: FXC; software, supervision, and writing-review & editing: FFP. Both authors read and approved the final version of the manuscript.

Financial support
None.
Acknowledgement
None.

Conflicts of interest statement
None.

1. Ho, W. J.; Jaffee, E. M.; Zheng, L. The tumour microenvironment in pancreatic cancer - clinical challenges and opportunities. *Nat Rev Clin Oncol.* **2020**, *17*, 527-540.
2. Dees, S.; Ganesan, R.; Singh, S.; Grewal, I. S. Regulatory T cell targeting in cancer: Emerging strategies in immunotherapy. *Eur J Immunol.* **2021**, *51*, 280-291.
3. Majedi, F. S.; Hasani-Sadrabadi, M. M.; Thauland, T. J.; Keswani, S. G.; Li, S.; Bouchard, L. S.; Butte, M. J. Systemic enhancement of antitumour immunity by peritumourally implanted immunomodulatory macroporous scaffolds. *Nat Biomed Eng.* **2023**, *7*, 56-71.
4. Yu, A.; Dai, X.; Wang, Z.; Chen, H.; Guo, B.; Huang, L. Recent advances of mesoporous silica as a platform for cancer immunotherapy. *Biosensors (Basel).* **2022**, *12*, 109.
5. Nguyen, T. L.; Choi, Y.; Kim, J. Mesoporous silica as a versatile platform for cancer immunotherapy. *Adv Mater.* **2019**, *31*, e1803953.
6. Huang, P.; Wang, X.; Liang, X.; Yang, J.; Zhang, C.; Kong, D.; Wang, W. Nano-, micro-, and macroscale drug delivery systems for cancer immunotherapy. *Acta Biomater.* **2019**, *85*, 1-26.
7. Jung, K.; Corrigan, N.; Wong, E. H. H.; Boyer, C. Bioactive synthetic polymers. *Adv Mater.* **2022**, *34*, e2105063.
8. Marchini, A.; Gelain, F. Synthetic scaffolds for 3D cell cultures and organoids: applications in regenerative medicine. *Crit Rev Biotechnol.* **2022**, *42*, 468-486.

Received: February 23, 2023
Revised: February 28, 2023
Accepted: March 1, 2023
Available online: March 28, 2023

Biomaterials Translational

Bioactive peptides for anticancer therapies

*Yehao Zhang, Cong Wang, Wenhui Zhang, Xinming Li**

Key Words:
anticancer peptide; antimicrobial peptide; apoptosis; natural resources

From the Contents

ABSTRACT

Cancer is a serious concern in public health worldwide. Numerous modalities including surgery, radiotherapy, and chemotherapy, have been used for cancer therapies in clinic. Despite progress in anticancer therapies, the usage of these methods for cancer treatment is often related to deleterious side effects and multidrug resistance of conventional anticancer drugs, which have prompted the development of novel therapeutic methods. Anticancer peptides (ACPs), derived from naturally occurring and modified peptides, have received great attention in these years and emerge as novel therapeutic and diagnostic candidates for cancer therapies, because of several advantages over the current treatment modalities. In this review, the classification and properties of ACPs, the mode of action and mechanism of membrane disruption, as well as the natural sources of bioactive peptides with anticancer activities were summarised. Because of their high efficacy for inducing cancer cell death, certain ACPs have been developed to work as drugs and vaccines, evaluated in varied phases of clinical trials. We expect that this summary could facilitate the understanding and design of ACPs with increased specificity and toxicity towards malignant cells and with reduced side effects to normal cells.

College of Chemistry, Chemical Engineering and Materials Science, Soochow University, Suzhou, Jiangsu Province, China

***Corresponding author:**
Xinming Li,
xinmingli@suda.edu.cn.

http://doi.org/10.12336/biomatertransl.2023.01.003

How to cite this article:
Zhang, Y.; Wang, C.; Zhang, W.; Li X. Bioactive peptides for anticancer therapies. *Biomater Transl.* **2023**, *4*(1), 5-17.

Introduction

As a leading cause of death, cancer threatens human health and life worldwide.[1, 2] Based on the report of the World Health Organization, cancer accounts for about 20 million deaths in 2020, including the occurrence of lung, prostate, colorectal, and stomach cancer in men, and breast, colorectal, lung, cervical and thyroid cancer in women.[3] Cancer results from the transformation of normal cells into tumour cells that grow uncontrollably and go beyond their boundaries to invade the surrounding tissues and organs via the process of metastasis, which is the principal reason of death from cancer.[4]

The current strategies for cancer therapies mainly include surgery, radiotherapy, and chemotherapy, which serve as the most frequently used modalities for cancer treatment in clinic. Despite progress in anticancer therapies, the usage of these methods for cancer therapy is often related to deleterious side effects. For example, surgery generally can quickly remove obvious cancer cells from the body, but the process of operation often results in serious trauma, bleeding, infection, and other risks. Radiotherapy as a modality of cancer therapy, relies on the application of high-energy rays or radioactive substances to damage cancer cells or prevent cancer growth.[5] However, radiotherapy often causes a wide range of side effects, such as tiredness and sore skin in the tumour area, due to the exposure of healthy cells and tissues around the tumour site to high doses of radiation.[6] Chemotherapy as a systemic therapy, depends on the administration of chemical drugs into the body to kill cancer cells.[7] But, most classical anticancer drugs lack the property to distinguish cancer cells from normal ones, thus resulting in systemic toxicity and adverse side effects (e.g., anaemia, gastrointestinal mucositis, alopecia, or cardiotoxicity).[8, 9] And, long-term usage of anticancer drugs increases the risk of drug resistance through the development of

mechanisms to deactivate or transport drugs out of the cells.[10] Thus, the development or discovery of a new class of anticancer agents with low toxicities, high selectivity and overcoming the influence of drug resistance is urgently required.[11, 12]

With the advance of biology and biomedicine, a great many bioactive peptides have been discovered and isolated from natural animal and plant sources, which exhibit antioxidant, antiinflammatory, antimicrobial and anticancer activities (**Figure 1A**).[13] In this review, the recent studies on naturally occurring cationic antimicrobial peptides with anticancer activities for cancer treatment were reviewed.[14] Most cationic anticancer peptides (ACPs) are usually short in length, with 5–50 amino acids, and mainly consist of positively charged amino acids, such as Lys and Arg and hydrophobic residues.[15] Because of the presence of positively charged amino acids and high proportions of hydrophobic residues, ACPs can electrostatically interact with cancer cell membranes with net negative charges, and elicit a cytotoxic effect on cancer cells via disruption of cell membranes.[16] Molecular sequences and chemical compositions of peptides can seriously affect the abilities to interact with cancers and the cytotoxicity (**Figure 1B** and **Table 1**).[17] Because of their unique mechanisms of action, ACPs have many advantages, including low toxicity and chance of developing multi-drug resistance problems, compared with conventional chemotherapeutic drugs, and thus offer the opportunity of developing a novel class of anticancer agents with improved cell selectivity for cancer cells and decreased side effects on normal tissues.[18, 19] Due to the limitation of space, the information about pharmaceutical characteristics of therapeutic peptides, such as peptide design, synthesis, modification, and evaluation of peptide drugs is not included in this review. For further details on these aspects, the readers are referred to several recent reviews.[2, 20-23]

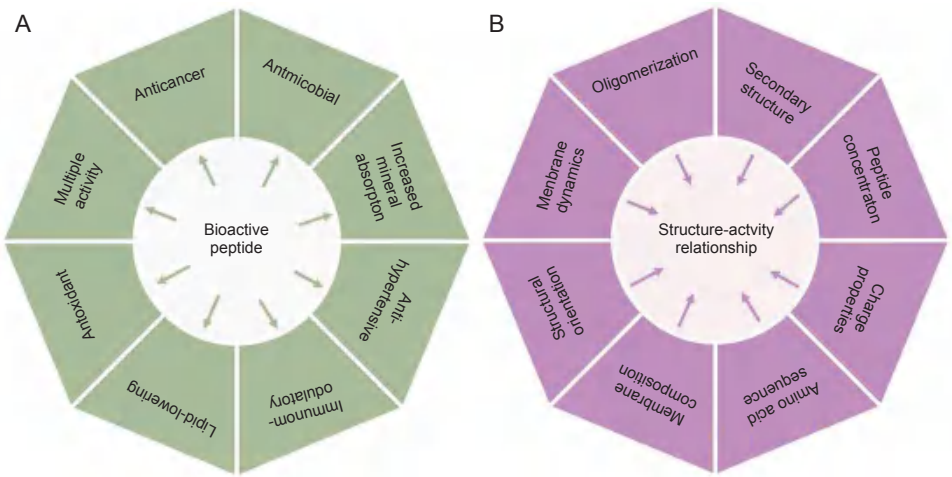

Figure 1. (A) Multipurpose bioactivities exhibited by peptides from natural resources, (B) Physicochemical and physiological factors of bioactive peptides that determine their anticancer activities.

Table 1. Effects of amino acid residues in ACPs on cancer cells

Amino acid residue	Amino acid properties	Action on cancer cells	References
Effect on cell membrane interactions			
Lysine Arginine	Positively charged, polar and hydrophilic	Disrupt cell membrane integrity and penetrate cell membrane, leading to cancer cell cytotoxicity	24
Histidine		Induce cancer cytotoxicity via membrane permeability under acidic condition	25, 26
Glutamic acid Aspartic acid	Negatively charged, polar and hydrophilic	Antiproliferative activities on tumour cells	27
Effect on cancer cell structure			
Cysteine	Polar, non-charged	Interact with numerous cell surface receptors for stabilizing and maintaining extracellular motif/domain structure	28
Proline	Non-polar, aliphatic	Membrane interaction and conformational flexibility of peptide chains	29
Glycine		Membrane interaction and conformational flexibility	29
Phenylalanine	Aromatic	Enhance the affinity with cancer cell membrane	30
Effect on cancer cell metabolism			
Methionine	Polar, non-charged	Reduced methionine will arrest cancer cell proliferation	31
Tyrosine	Aromatic	increase cytotoxic activity	32
Tryptophan	Aromatic	binding at the major groove of nuclear DNA	33

Note: Reprinted from Chiangjong et al.[17]

Characteristics of Cancer Cells for Selective Treatment by Anticancer Peptide

Although the selectivity and mechanism of membrane disruption by ACPs to kill cancer cells are not yet fully understood, the structural and compositional differences between cell membranes of cancer cells and normal cells may be responsible for the selectivity of ACPs towards cancer cells over healthy cells.[34] Compared with normal cells, malignant cells show several different characteristics with regard to the membrane components.[35] For example, the membrane of malignant normally carries a net negative charge because of the presence of a higher number of anionic components such as the phospholipid phosphatidylserine, O-glycosylated mucins, sialylated gangliosides and heparin sulphate than normal cells, which contributes to the selective cytotoxic property of ACPs.[36] Another distinctive trait of malignant cells is associated with the content of cholesterol within cell membranes.[37] Cholesterol is an integral component in cell membranes of eukaryotic cells to regulate membrane fluidity. Normal cells have large amounts of cholesterol which works as a protective layer to modulate the cell fluidity and block the entrance or passage of cationic ACPs. In contrast, most malignant cells have increased membrane fluidity, due to the low content of cholesterol in cell membranes, which may make them susceptible to ACPs. In addition, cancer cells also contain an increased number of microvilli, in contrast to healthy cells. The presence of microvilli with irregular size and shape on cancer cells can increase the surface area of cells for ACP binding and interactions,[38] influences cell adhesion, and the communications between cancer cells and their environments, and facilities the specific interaction of ACPs with cancer cells. Therefore, the high selectivity and cell-killing efficacy of ACPs towards cancer cells over normal cells could attribute to different compositions in cell membranes, as well as higher fluidity and surface areas of cancer cells than normal cells. Relying on electrostatic interactions, ACPs with positive charges and amphiphilicity target and bind the membrane of cancer cells with highly negative charges, destabilise and destroy cell membranes through hydrophobic interactions, leading to cell necrosis.[2]

With in-depth studies, scientists discovered that certain membrane-active peptides can disrupt the membrane of mitochondria, causing the release of cytochrome c, after they were internalised inside eukaryotic cells.[39] The released cytochrome c from damaged mitochondria to cytosol can induce oligomerization of Apaf-1, activation of caspase-9 and the transformation of pro-caspase-3 to caspase-3, initiating apoptosis in many cancer cells.[40] For example, the cationic membrane-active peptide (KLAKLAKKLAKLAK) has been shown to target mitochondria and trigger apoptosis after fusing to a CNGRC homing domain (**Figure 2**).[41]

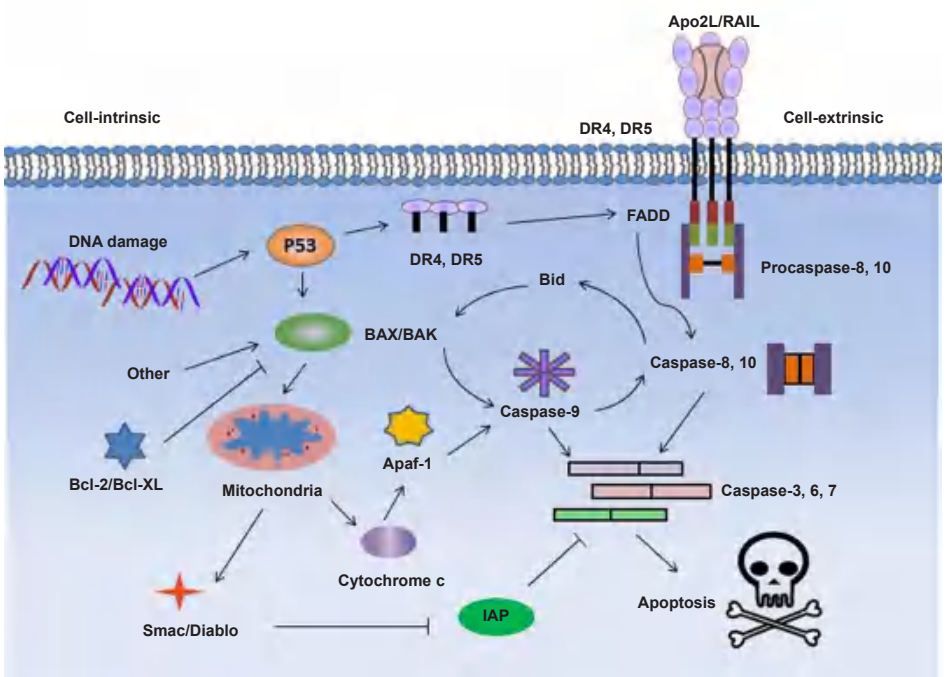

Figure 2. Proposed signaling pathways for induced apoptosis of cancer cells by pro-apoptotic peptides. Apaf-1: apoptotic protease activating factor 1; Apo2L: Apo2 ligand; Diablo: direct IAP binding protein with low pI; DR: death receptor; FADD: Fas associated via death domain; IAP: inhibitor of apoptosis protein; TRAIL: tumour necrosis factor-related apoptosis-inducing ligand.

Besides direct disruption of plasma or mitochondrial membranes, some ACPs can also kill cancer cells via other indirect pathways, such as gene targeting and immunomodulation.[42, 43] For example, melittin, is an ACP

consisting of 26 amino acid residues, and can preferentially activate phospholipase A2 in cells that overexpress the Ras oncogene, and result in selective destruction of cells. In another study, scientists discovered that a histidine-rich alloferons derivative could stimulate properly the activity of the natural killer cell of lymphocytes in a mouse model for tumour killing.[44] Currently, more and more evidence suggests that drugs with immunomodulatory effects could provide beneficial effects for cancer therapies.[45]

Properties and Classification of Anticancer Peptide

Based on their secondary molecular structures, most ACPs can be classified into four typical classes (**Figure 3**): (1) α-helices (e.g., bovine myeloid antimicrobial peptide (BMAP), melittin, cecropins, and magainins); (2) β-sheets (α- and β-defensins, lactoferrin and tachyplesin I); (3) ACPs with extended structures and enriched with glycine, proline, tryptophan, arginine, and/or histidine residues; and (4) cyclic loops (diffusa cytides 1–3).[46]

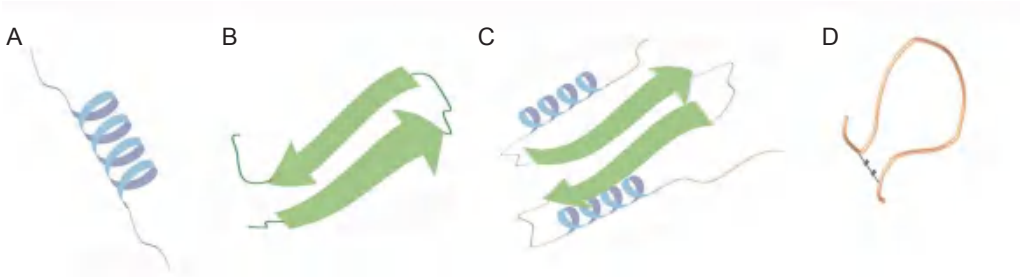

Figure 3. Schematic illustration of ACP structures containing α-helices (A), β-sheets (B), extended structures (C) or cyclic loops (D). ACP: anticancer peptide.

α-Helical anticancer peptides

The ACPs with α-helical structures are a major group of ACPs with short sequences and simple structures and compositions, which generally are composed of basic amino acids, such as lysine and arginine. Lysine (K) and arginine (R) are two kinds of hydrophilic amino acids with an amine group and a guanidinium group in their side chains, which contributes to the formation of peptides with net positive charges in neutral pH.[47] Compared with lysine, arginine containing the guanidinium group has a higher potential to perform electrostatic attraction and hydrogen bonding with the anionic membrane in a high affinity.[48] In contrast, lysine with ε-amino group in the side chain exhibits more hydrophobicity than arginine, and the long nonpolar alkyl side chain can insert into the hydrophobic area of the cell membrane, increasing the cytotoxicity of α-helical ACPs against cancer cells.[49] Based on statistical studies, lysine is an essential component of α-helical ACPs.

Besides positive net charge, the hydrophobicity of ACPs can also influence their biological activities.[50] Normally, the percentage of hydrophobic residues within ACPs can reach 30%, which makes these molecules possess a helical conformation with both polar and nonpolar faces in hydrophobic environments.[51] Peptides with increased hydrophobicity on the nonpolar face would increase their helicities and self-assembling abilities, which could insert deeper into the hydrophobic area of the cell membrane, increasing the potential to form pore or channel structures in the cancer cell membrane.[52] Therefore, ACPs with increased hydrophobicity would accordingly exhibit enhanced anticancer and hemolytic activities towards cancer cells.

β-Sheet anticancer peptides

The second class of ACPs shows a β-sheet structure that contains at least a pair of two β-strands, as well as 2–8 cysteine amino acids which form 1–4 pairs of intramolecular S–S bonds.[53] Formation of disulfide bonds within the molecular structures of β-sheet ACPs is often essential for the stabilization of the structure and biological activities of these peptides.[54] The β-sheet peptides also show amphipathic characteristics with spatially distributed polar and non-polar regions. Because of the high stability of β-sheet structures of ACPs, they will not conduct conformational transitions after binding with phospholipid membranes. Defensins are one of the well-researched and cationic ACPs which consist of 29 to 45 amino acid residues. Defensins generally are composed of three to six disulfide linkages, which create cyclic, triple-stranded β-sheet structures with spatially separated hydrophobic and hydrophilic domains.[53] In addition, the pattern and position of intramolecular disulfide bonds within peptide structures can define the class of the defensin. For example, α-defensins contain disulfide linkages in the positions Cys1–Cys6, Cys2–Cys4 and Cys3–Cys5, while Cys1–Cys5, Cys2–Cys4 and Cys3–Cys6 are for β-defensins. The formation of cyclic cysteine ladder conformation plays an essential role in determining the anticancer activity of defensins by sustaining the structure and molecular stability of the cyclic backbone. The stable, cyclic structures have high surface areas and reduced conformational flexibilities, which improve the capability and selectivity to bind with cancer cells.

Anticancer peptides with extended structures

ACPs with extended structures are generally rich in arginine, proline, tryptophan, glycine and histidine, but lack typical secondary structures. The extended structures are only stabilised by hydrogen bonds and other non-covalent interactions.[55] Typically, PR-39 is a linear ACP formed from proline (49%)

and arginine (24%), which is isolated from porcine neutrophils. PR-39 consists of 39 amino acid residues and lacks a regular structure.[56] PR-39 exerts anticancer activities on human hepatocellular carcinoma cell lines by inducing the expression of syndecan-1. Similar anticancer effects were also observed on hepatic leukaemia factor hepatocellular carcinoma cells when they were transfected with the PR-39 gene. Alloferon is another group of ACP derived from insects with glycine-rich domains, which can activate natural killer cells and the synthesis of interferon for antitumour treatment in mice.[57]

Cyclic anticancer peptides

Cyclic ACPs consist of a head-to-tail cyclization peptide backbone or disulfide linkages, which show much higher stability than that of linear molecules.[58] Diffusa cytides 1–3, as three new cyclic peptides, were extracted from the leaves and roots of the white snake plant, and have an obvious preventive effect on the growth and the migration of prostate cancer cells *in vitro*.[59] H-10 is another cyclic pentapeptide, which exhibits a concentration-dependent cytotoxic effect on mouse malignant melanoma B16 cells, without obvious cytotoxicity to human peripheral lymphocytes and rat aortic smooth muscle cells.[60] Because of its intense inhibitory activity against cancer cells, cyclic ACPs account for the majority of ACPs in clinical studies.

Natural Sources of Peptides with Anticancer Activity

Recently, a number of natural ACPs with cationic, anionic or neutral properties have been discovered in various organisms, including marine, plant, yeast, fungi, bacteria and bovine.[61] In addition, some nutrient proteins from milk and soybean can release biofunctional peptides via enzymatic degradation, and show antiproliferative effects on the growth of human cancer cells (**Figure 4**).[62]

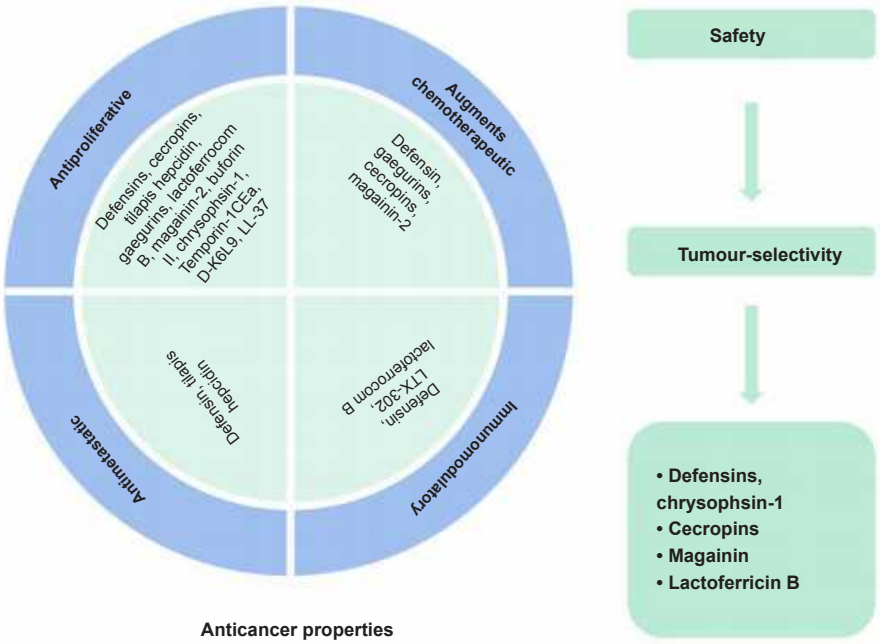

Figure 4. Lists of bioactive peptides with potentials for anticancer therapies via varied mechanisms.

Bioactive peptide compounds from both human and terrestrial animals have been reported to have anticancer properties. For example, LL-37 is a typical antimicrobial peptide derived from human cathelicidin and shows antimicrobial activities towards both Gram-positive and Gram-negative bacteria under much lower concentrations.[63] In addition, LL-37 also exhibits the capability to induce calpain-mediated apoptosis through DNA fragmentation and mitochondrial depolarization in Jurkat cells as well as human oral squamous cell carcinoma cells.[64] Defensins (α- and β-defensins) are an expressed effector agent of the innate immune system of humans with broad antimicrobial activities.[65] Among them, α-defensins or named human neutrophil peptides (HNP-1, HNP-2 and HNP-3) that derive from the azurophilic granules of neutrophils could exist as dimers on cell membranes and show inhibitory activities against numerous cell lines, including human B-lymphoma cells, human oral squamous carcinoma cells, and MOT mouse teratocarcinoma cells.[66] In addition, bioactive peptides (GFHI, DFHING, FHG, and GLSDGEWQ) obtained from bovine meat-derived peptides exhibit cytotoxicity.[67] Among them, GFHI is most cytotoxic to the human breast cancer cell line (MCF-7) and could reduce the viability of the stomach adenocarcinoma cell line (AGS) in a concentration-dependent manner, whereas the peptide of GLSDGEWQ considerably prohibits the proliferation and growth of AGS cells. In addition, a novel anticancer bioactive peptide (ACPB-3) extracted from goat spleens or livers, has exhibited antiproliferative activities towards the human gastric cancer cell line (BGC-823) and gastric cancer stem cells (GCSCs).[68, 69]

Some bioactive peptides from aquatic animal sources, such as frogs, toads, fish, ascidians, mollusks, and other organisms have also been identified with potential anticancer activities.[70] For example, some amphibians, such as frogs and toads, can secrete mucus, which contains a wide range of antimicrobial peptides which show cytotoxicity towards human cancer cells.[71] China has a long history of using secretions from amphibians (e.g., frogs and toads) to prepare traditional Chinese medicines for multi-purpose therapeutic applications.[50] The well-studied ACPs from amphibian secretions are magainins, obtained from the skin of the African clawed frog *Xenopus laevis*, and exhibiting membranolytic properties.[72] Magainin 2, together with its potent synthetic analogues (magainins A, B, and G), can trigger a rapid death of haematopoietic and solid tumour cells via the formation of pores on cell membranes, but no cytotoxic activity was observed on normal human or murine fibroblast cell lines.[73] The hydrolytic products from dark tuna muscle have shown potential antiproliferative activities towards MCF-7 cells. Specifically, the fraction of peptides with molecular weights from 400–1400 Da from the digested products exhibits the strongest antiproliferative activity in cancer cells, because of the presence of two antiproliferative peptides, LPHVLTPEAGAT and PTAEGVYMVT.[74]

Milk and dairy products contain plenty of molecules that exhibit various bioactivities. Therefore, bioactive peptides prepared from milk and dairy products through enzyme-mediated digestion have been considered to be significant bioactive agents with anticancer activities. And plenty of reports have indicated the anticancer activities of bioactive peptides derived from milk protein. For instance, Roy and others discovered that bovine skim milk degraded by *Saccharomyces cerevisiae* showed an inhibitory effect on the proliferation of a human leukaemia cell line.[75] Lactoferrin is a glycoprotein with iron-binding properties isolated from the transferrin family and exhibits a variety of biofunctionalities, such as antibacterial, antiviral, anticancer, antiinflammatory, and immunomodulatory activities.[76] In addition, lactoferrin proteins treated by pepsin under acidic conditions could generate cationic peptides with obvious cytotoxic activities against both microorganisms and cancer cells via the mechanisms of cell cycle arrest, apoptosis, antiangiogenesis effects, antimetastasis effects, immune modulation and necrosis.[77] Thus, milk can not only supply essential proteins as nutrients in a normal daily diet but also have potentials for the preparation of ACPs for cancer prevention and management.[78] Therefore, the search for natural peptides from food sources with anticancer activities has increased in recent years. For example, the peptide of HVLSRAPR obtained from *Spirulina platensis* hydrolysates displayed cell selective and obvious cytotoxic activities towards HT-29 cancer cells but with little inhibitory effects on normal liver cell proliferation.[79] In addition, a tripeptide of WPP extracted from blood clam muscle exhibited strong inhibitory effects against PC-3, DU-145, H-1299 and HeLa cell lines.[80] Similarly, the hydrolysate of Soybean protein also contains many peptide segments such as Lunasin, RKQLQGVN,[81] GLTSK, LSGNK, GEGSGA, MPACGSS and MTEEY,[82] which can exert distinct antiproliferative actions on colorectal cancer HT-29 cells.

Venoms and toxins secreted by different animals are also composed of a large number of proteins or peptides, which were used as therapeutic agents in traditional medicine for centuries, and currently are explored for the discovery of novel ACPs.[83] Melittin is an amphiphilic peptide with 26 amino acid residues, which is obtained from the honeybee *Apis mellifera*, and exhibited inhibitory effects on the growth of different cancer cells *in vitro*, including astrocytoma, leukaemic, lung tumour, ovarian carcinoma, squamous carcinoma, glioma, hepatocellular carcinoma, osteosarcoma, prostate cancer and renal cancer cells.[84] In spite of its considerable cytotoxicity to a broad spectrum of tumour cells, melittin also exhibits toxicity towards normal cells. Thus, with the purpose of achieving optimal results, the therapeutic agent of melittin could be used through accurate and specific delivery to the targeted tumour areas. Crotamine, as the first venom-derived peptide polypeptide from South American rattle snake venom, is used as a natural cell-penetrating and antimicrobial peptide with pronounced antifungal activity.[85] Besides, crotamine also exhibits toxicity toward cancer cells from B16-F10 (murine melanoma cells), SK-Mel-28 (human melanoma cells), and Mia PaCa-2 (human pancreatic carcinoma cells) in a mouse model of melanoma.[86] Until now, more and more natural peptides with cationic, anionic or neutral properties have been identified and collected from various organisms, whose anticancer properties are summarised and presented in **Table 2**.[87]

Mechanism of Anticancer Peptides for Cancer Treatment

Unlike conventional anticancer chemotherapy drugs, which generally target specific biomolecules, most cationic ACPs interact with the membrane of cancer cells, resulting in cell lysis and death. Thus, ACPs provide the opportunity of developing therapeutics for cancer therapy with a new mode of action, which are complementary to conventional anticancer drugs, and to which cancer cells could not develop drug resistance. The mechanism by which ACPs perform their membrane-disruption role relies on a series of physicochemical properties, such as the sequence of peptide molecules, net positive charge, hydrophobicity, structural conformations (secondary structure, dynamics and orientation) in membranes, self-assembling, peptide concentrations, and membrane composition of cells.[54] Currently, several mechanisms of membrane disruption have been proposed to describe the activity of ACPs, including the carpet model, the barrel-stave model, and the toroidal-pore wormhole model (**Figure 5**).

The carpet model describes the association of ACPs with positive charges with phospholipids in the outer layer of the membranes with negative charges via electrostatic interactions, which leads to the parallel alignment of ACPs to the cell membrane, covering the cell in a carpet-like manner and without embedding them into the lipid bilayers.[102] But after peptide concentrations reach a threshold concentration, they change their molecular conformation by rotating themselves, inserting into the membrane, and forming micelle aggregates via hydrophobic interactions, resulting in membrane disintegration.

Table 2. Mechanism of some anticancer peptides from different origins for cancer treatment

No.	ACP	Cancer type	Mechanism	Molecular sequence	Reference
1	LL-37	Human oral squamous cell, carcinoma cells	Toroidal pore mechanism	LLGDFFRKSKEKIGKEFKRI VQRIKDFLRNLVPRTES	88
2	α-Defensins	Human myeloid leukaemia cell line (U937)	Cytolytic activity	ACYCRIPACIAGERRYGTCI YQGRLWAFCC	89
3	β-Defensin-3	HeLa, Jurkat and U937 cancer cell lines	Binding to cell membrane to cause cytolysis	GIINTLQKYYCRVRGGRCA VLSCLPKEEQIGKCSTRGRK CCRRKK	90
4	Bovine lactoferricin	Drug-resistant and drug-sensitive cancer cells	Cytolysis and immunogenicity	FKCRRWQWRMKKLGAP SITCVRRAF	91
5	Gomesin	Murine and human cancer cell lines along with melanoma and leukaemia	Carpet model for destroying the membrane	QCRRLCYKQRCVTYCRGR	92
6	Cecropin B1	NSCLC cell line	Tumour growth inhibition using pore formation and apoptosis	KWKIFKKIEKVGRNIRNG IIKAGPAVAVLGEAKAL	93
7	Magainin 2	Human lung cancer cells A59 and in	Formation of pores on cell membranes	GIGKFLHSAKKFGKAFVG EIMNS	94
8	Brevinin 2R	Breast adenocarcinoma MCF-7, and lung carcinoma A549 cell	Lysosomal death pathway and autophagy-like cell death	KLKNFAKGVAQSLLNKAS CKLSGQC	95
9	Bufforin IIb	Leukaemia, breast, prostate, and colon cancer	Mitochondrial apoptosis	TRSSRAGLQFPVGRVHRLL RK	96
10	Brevinvin	Lung cancer H460, melanoma cell, glioblastoma U251MG, colon cancer HCT116 cell lines	Penetrating into the lipidic bilayer causing cell death	FLPLAVSLAANFLPK LFCKI TKKC	97
11	Phylloseptin-PHa	Breast cancer cells MCF-7, breast epithelial cells MCF10A	Penetrating into the lipidic bilayer causing cell death	FLSLIPAAISAVSALANHF	98
12	Ranatuerin-2PLx	Prostate cancer cell PC-3	Cell apoptosis	GIMDTVKNAAKNLAGQLL DKLKCSITAC	99
13	Dermaseptins	Prostate cancer cell PC-3	Pore formation one the lipid bilayer	GLWSKIKEVGKEAAKAAAK AAGKAALGAVSEAV	100
14	Chrysophsin-1, -2 and -3	Human fibrosarcoma HT-1080, histiocytic lymphoma U937, and cervical carcinoma HeLa cell lines	Disrupt the plasma membrane	FFGWLIKGAIHAGKAIHG LIHRRRH	101
15	D-K6L9	Breast and prostate cancer cell lines	Reduce neovascularization	LKLLKKLLKKLLKLL	96

Note: Reprinted from Bakare et al.[87]

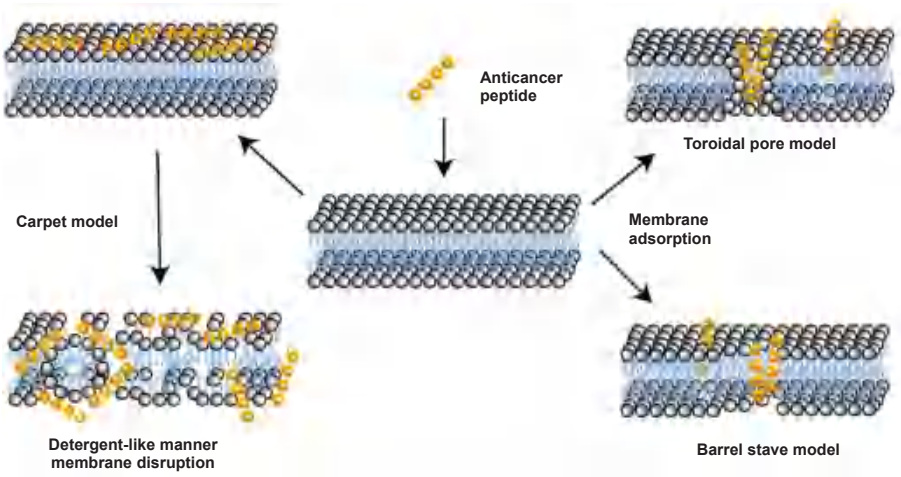

Figure 5. Schematic illustration of different mechanisms of anticancer peptides for cell entry.

With regard to the barrel-stave model, ACPs first attach on the surface of cell membrane via the physical interactions of the peptides with hydrophilic segments. Then the monomer peptide undergoes a structural change and aggregates together through supramolecular self-assembling to form transmembrane channels and stave-like structures within the lipid bilayer.[103] The molecular insertion of peptides generates a hydrophilic channel that expels the hydrophobic part of the bilayer. Once the formation of channel, more peptide molecules can enter and enlarge the channel's size. Furthermore, due to the physical interactions between ACPs and cancer cells, the integrity of cell membrane is also weakened. Currently, the only discovered ACP which kills cancer cells via the barrel-stave model is alamethicin.

The toroidal pore model describes a two-stage process of interactions of ACPs with cell membranes. Firstly, the peptide is inactive at low concentrations and aligns parallel to the membrane bilayer. And then it converts to the active form at certain concentrations, perpendicularly inserts into the membrane and irreversibly destabilises the bilayers via the formation of a toroidal-like pore structure.[104] The generated toroidal pore can allow for the entrance of more ACPs into the intracellular space of the cell. There are many examples of ACPs, such as cecropin A, protegrin-1 and magainin-2, that employ this mechanism to destabilise cell membranes.

Anticancer Peptides in Clinical Trials

Currently, there are a number of synthetic peptides and vaccines under clinical trials. This information could be found in the National Library of Medicine at the National Institutes of Health (**Table 3**).[17] For example, the cyclic undecapeptide of CIGB-300 (a peptide-based casein kinase 2 (CK-2) inhibitor) can inhibit CK-2-mediated phosphorylation, after fusing with the trans-acting activator of transcription (TAT) cell-penetrating peptide, resulting in apoptosis of cervical and non-small cell lung cancer cells.[105-107] Wilms' tumour 1 peptide vaccine exhibited high antitumour effects and safety on pediatric patients with a solid tumour, when administered with the adjuvant drug OK-432.[108] In addition, Wilms' tumour 1-pulsed dendritic cell vaccine was tested to treat patients with surgically resected pancreatic cancer under a phase I study.[109] The vaccine from a modified Wilms' tumour 1 (9-mer) peptide showed the potential to activate cytotoxic T-cells, after it was administered to treat patients with gynecological cancer.[110] After emulsification with Montanide ISA 51, the vaccine of LY6K-177 peptide was administered to patients with gastric cancer, and these patients showed high tolerance to the formulation in a phase I clinical trial.[111]

B-cell lymphocytic leukaemia and pancreatic cancer are associated with an increased level of telomerase activity.[112] The peptide vaccine of GV1001 was developed from the hTERT (EARPALLTSRLRFIPK), and tested in patients with non-resectable pancreatic cancer in phase I/II trials. Studies show that it was able to induce $CD4^+$ and $CD8^+$ T-cells, interact with professional antigen-presenting cells, and then engulf dead tumour tissue or cells.[113] Moreover, GV1001 also exhibited the potential to act as a candidate vaccine to treat the patients with B-cell chronic lymphocytic leukaemia, a telomerase-specific leukaemic cell line.[114]

The integration of the ACPs with other conventional drugs, such as such as cyclodepsipeptide plitidepsin and bevacizumab, has also been tested in refractory solid tumours and evaluated in phase I trials.[115] In addition, a short peptide, which can work as a luteinising hormone-releasing hormone (LHRH) agonist, was fused to cytotoxic analogs of LHRH to target cancer expressing receptors for LHRH. Based on the results of phase II clinical trial, the LHRH agonist displays anticancer activities in LHRH receptor-positive cancer types (human endometrial, ovarian and prostate cancer).[116] In recent years, a personalised peptide vaccine was created to work as a novel strategy for cancer treatment by boosting the immune response with specific peptides for each patient.[117] For example, 19 peptide mixtures selected from 31 personalised peptide vaccines were also assessed in a phase II clinical trial in patients with metastatic breast cancer. While other peptides of gp100:209-217 (210M)/Montanide™ ISA-51/Imiquimod and E39 peptide/granulocyte-macrophage colony-stimulating factor vaccine plus E39 booster have been approved by the U.S. Food and Drug Administration for treatment of high risk melanoma and ovarian cancer, respectively. In addition, the peptide of boronate bortezomib as a reversible 26S proteasome inhibitor, has been approved in clinical therapy for multiple myeloma therapy by degenerating several intracellular proteins.[118-120] Till now, various cancer vaccines based on ACPs or ACPs integrated with other adjuvants or drugs, have been developed and evaluated in clinical trials for safety, side effects and specificity for targeting cancer cells by activating immune responses. More ACP examples in clinical trials are summarised and presented in **Table 3**.

Summary and Future Perspective

As potential therapeutic agents for cancer therapy, ACPs have numerous advantages, but also have their inherent drawbacks, including low stability, easy degradation, potential toxicity, and low bioavailability, which may severely prohibit their clinical usage.[34] In recent years, different strategies have been taken to reconstruct or modify ACPs via chemical modification (e.g., cholesterol modification, phosphorylation, polyethylene glycol modification, glycosylation and palmitoylation) or replacement of natural amino acids with non-natural ones, with expected to retain their advantages while decreasing their shortcomings, thereby increasing their therapeutic efficiencies.[121] Besides, with the development of material chemistry and nanotechnology, various nanomaterials with unique optical, electronic, magnetic and photo-responsive properties have been used as a selective delivery system for tumour-targeted release of ACPs.[122] Furthermore, the combination of ACPs with other therapeutic modalities also holds great potentials to enhance therapeutic effects, decrease the toxicity and side effects, and prevent the development of drug resistance by cancer cells.[123] Till now, a large number of ACPs with anti-proliferative and apoptotic properties towards various cancer cell types, are evaluated in clinical trial or are already in the pre-clinical stage.[17]

Table 3. Lists of anticancer peptides in clinical trials

Phase	Biological peptides	Cancer type	Mechanisms
Early phase I	MUC-1 peptide vaccine	Breast cancer	Positive anti-MUC1 antibody responses
	HER-2/neu peptide vaccine	Breast cancer	Specific interferon-γ and IL-5 producing T-cell responses
	GAA/TT-peptide vaccine and poly-ICLC	Astrocytoma, oligoastrocytoma and glioma	GAA-specific T-cell responses
Phase I	Gag:267-274 peptide vaccine	Melanoma	Cytotoxic T-cell lymphocyte responses
	HPV16 E7 peptide-pulsed autologous DCs	Cervical cancer	Pulsed autologous DC immunotherapy
	LY6K, VEGFR1, VEGFR2	Esophageal cancer	Immune responses including LY6K, VEGFR1 and VEGFR2 specific T-cells
	Antiangiogenic peptide vaccine	Hepatocellular carcinoma	Cytotoxic T-cell lymphocyte responses
	HLA-A*0201 or HLA-A*0206-restricted URLC10 peptides	Non-small cell lung cancer	Cytotoxic T-cell lymphocyte responses, antigen cascade, regulatory T-cells, cancer antigens and human leukocyte antigen levels
Phase I/II	MAGE-3.A1 peptide and CpG 7909	Malignant melanoma	Cytotoxic T-cell lymphocyte responses
	VEGFR1-1084, VEGFR2-169	Pancreatic cancer	Cytotoxic T-cell lymphocyte responses
	HER-2/neu peptide vaccine	Breast cancer	Human epidermal growth factor receptor 2-specific T-cell response
Phase II	gp100:209-217(210M), HPV 16 E7:12-20	Melanoma	T-cell immunity
	WT1 126-134 peptide	Acute myeloid leukaemia	T-cell response
	G250 peptide	Metastatic renal cell carcinoma	Cytotoxic T-cell lymphocyte responses
Phase III	PR1 leukaemia peptide vaccine	Leukaemia	Immune response
Phase IV	Degarelix	Prostatic neoplasms	Binds to GnRH receptors

Note: Reprinted from Chiangjong et al.[17] DC: dendritic cell; GnRH: gonadotropin-releasing hormone; HER-2: human epidermal growth factor receptor; HPV: human papillomavirus; poly-ICLC: polyinosinic-polycytidylic acid stabilized with poly-L-lysine and carboxymethylcellulose; IL-5: interleukin-5; LY6K: lymphocyte antigen 6 family member K; MUC 1: transmembrane glycoprotein mucin 1; PR1: pathogenesis-related protein 1; URLC10: a peptide vaccine; VEGFR: vascular endothelial growth factor receptor.

Besides the significant progress in the identification of more ACPs from different natural resources, there are also developments of novel strategies for selective and targeting delivery of ACPs to cancer cells or regulating the fate of cancer cells via the process of enzyme-instructed self-assembly of peptides.[124, 125] Among them, enzyme-instructed self-assembly is promising to kill cancer cells with high specificity, relying on the specific activity of enzymes overexpressed by cancer cells to induce the formation of pericellular and intracellular peptide self-assemblies, which interrupted intercellular communications, blocked multiple cellular pathways, and prevented cell survival.[126, 127] Although enzyme-instructed self-assembly has exhibited numerous advantages for cancer therapy, such as high selectivity and minimal drug resistance, there is still much room for improving anticancer efficiency. Therefore, the continuous discovery of ACPs with optimised anticancer activities and development of advanced strategies with improved anticancer efficiency should offer an economically viable and therapeutically superior alternative to the current generation of chemotherapeutic drugs for cancer treatment.[128, 129]

Author contributions

Literature search and analysis, manuscript draft and figure preparation: YZ, CW, WZ and XL. All authors read and approved the final manuscript.

Financial support

This work was supported by the Key Laboratory of Polymeric Materials Design and Synthesis for Biomedical Function, Soochow University.

Acknowledgement

None.

Conflicts of interest statement

The authors declare no competing financial interest.

Editor note: Xinming Li is an Editorial Board member of *Biomaterials Translational*. He was blinded from reviewing or making decisions on the manuscript. The article was subject to the journal's standard procedures, with peer review handled independently of this Editorial Board member and his research group.

1. Poston, G. J. Global cancer surgery: the Lancet Oncology review. *Eur J Surg Oncol.* **2015**, *41*, 1559-1561.
2. Norouzi, P.; Mirmohammadi, M.; Houshdar Tehrani, M. H. Anticancer peptides mechanisms, simple and complex. *Chem Biol Interact.* **2022**, *368*, 110194.
3. Sung, H.; Ferlay, J.; Siegel, R. L.; Laversanne, M.; Soerjomataram, I.; Jemal, A.; Bray, F. Global Cancer Statistics 2020: GLOBOCAN estimates of incidence and mortality worldwide for 36 cancers in 185 countries. *CA Cancer J Clin.* **2021**, *71*, 209-249.
4. Hanahan, D.; Weinberg, R. A. The hallmarks of cancer. *Cell.* **2000**, *100*, 57-70.
5. Cai, Z.; Yin, Y.; Shen, C.; Wang, J.; Yin, X.; Chen, Z.; Zhou, Y.;

Zhang, B. Comparative effectiveness of preoperative, postoperative and perioperative treatments for resectable gastric cancer: A network meta-analysis of the literature from the past 20 years. *Surg Oncol.* **2018**, *27*, 563-574.

6. Yu, W. D.; Sun, G.; Li, J.; Xu, J.; Wang, X. Mechanisms and therapeutic potentials of cancer immunotherapy in combination with radiotherapy and/or chemotherapy. *Cancer Lett.* **2019**, *452*, 66-70.
7. Aljabery, F.; Shabo, I.; Gimm, O.; Jahnson, S.; Olsson, H. The expression profile of p14, p53 and p21 in tumour cells is associated with disease-specific survival and the outcome of postoperative chemotherapy treatment in muscle-invasive bladder cancer. *Urol Oncol.* **2018**, *36*, 530.e7-530.e18.
8. Rajalakshmi, M.; Suveena, S.; Vijayalakshmia, P.; Indu, S.; Roy, A.; Ludas, A. DaiCee: A database for anti-cancer compounds with targets and side effect profiles. *Bioinformation.* **2020**, *16*, 843-848.
9. Shimizu, C. Side effects of anticancer treatment and the needs for translational research on toxicity: a clinician's perspective. *Nihon Yakurigaku Zasshi.* **2015**, *146*, 72-75.
10. Pérez-Tomás, R. Multidrug resistance: retrospect and prospects in anti-cancer drug treatment. *Curr Med Chem.* **2006**, *13*, 1859-1876.
11. Hoekstra, R.; Verweij, J.; Eskens, F. A. Clinical trial design for target specific anticancer agents. *Invest New Drugs.* **2003**, *21*, 243-250.
12. Vulfovich, M.; Saba, N. Molecular biological design of novel antineoplastic therapies. *Expert Opin Investig Drugs.* **2004**, *13*, 577-607.
13. Wang, L.; Qu, L.; Lin, S.; Yang, Q.; Zhang, X.; Jin, L.; Dong, H.; Sun, D. Biological functions and applications of antimicrobial peptides. *Curr Protein Pept Sci.* **2022**, *23*, 226-247.
14. Hilchie, A. L.; Hoskin, D. W.; Power Coombs, M. R. Anticancer activities of natural and synthetic peptides. *Adv Exp Med Biol.* **2019**, *1117*, 131-147.
15. Soon, T. N.; Chia, A. Y. Y.; Yap, W. H.; Tang, Y. Q. Anticancer mechanisms of bioactive peptides. *Protein Pept Lett.* **2020**, *27*, 823-830.
16. Marqus, S.; Pirogova, E.; Piva, T. J. Evaluation of the use of therapeutic peptides for cancer treatment. *J Biomed Sci.* **2017**, *24*, 21.
17. Chiangjong, W.; Chutipongtanate, S.; Hongeng, S. Anticancer peptide: Physicochemical property, functional aspect and trend in clinical application (Review). *Int J Oncol.* **2020**, *57*, 678-696.
18. Vlieghe, P.; Lisowski, V.; Martinez, J.; Khrestchatisky, M. Synthetic therapeutic peptides: science and market. *Drug Discov Today.* **2010**, *15*, 40-56.
19. Thundimadathil, J. Cancer treatment using peptides: current therapies and future prospects. *J Amino Acids.* **2012**, *2012*, 967347.
20. Zhang, D.; He, Y.; Ye, Y.; Ma, Y.; Zhang, P.; Zhu, H.; Xu, N.; Liang, S. Little antimicrobial peptides with big therapeutic roles. *Protein Pept Lett.* **2019**, *26*, 564-578.
21. Juretić, D. Designed multifunctional peptides for intracellular targets. *Antibiotics (Basel).* **2022**, *11*, 1196.
22. Basith, S.; Manavalan, B.; Shin, T. H.; Lee, D. Y.; Lee, G. Evolution of machine learning algorithms in the prediction and design of anticancer peptides. *Curr Protein Pept Sci.* **2020**, *21*, 1242-1250.
23. Palomo, J. M. Solid-phase peptide synthesis: an overview focused on the preparation of biologically relevant peptides. *RSC Adv.* **2014**, *4*, 32658-32672.
24. Dai, Y.; Cai, X.; Shi, W.; Bi, X.; Su, X.; Pan, M.; Li, H.; Lin, H.; Huang, W.; Qian, H. Pro-apoptotic cationic host defense peptides rich in lysine or arginine to reverse drug resistance by disrupting tumor cell membrane. *Amino Acids.* **2017**, *49*, 1601-1610.
25. Navarro, S.; Aleu, J.; Jiménez, M.; Boix, E.; Cuchillo, C. M.; Nogués, M. V. The cytotoxicity of eosinophil cationic protein/ribonuclease 3 on eukaryotic cell lines takes place through its aggregation on the cell membrane. *Cell Mol Life Sci.* **2008**, *65*, 324-337.
26. Midoux, P.; Kichler, A.; Boutin, V.; Maurizot, J. C.; Monsigny, M. Membrane permeabilization and efficient gene transfer by a peptide containing several histidines. *Bioconjug Chem.* **1998**, *9*, 260-267.
27. Yamaguchi, Y.; Yamamoto, K.; Sato, Y.; Inoue, S.; Morinaga, T.; Hirano, E. Combination of aspartic acid and glutamic acid inhibits tumor cell proliferation. *Biomed Res.* **2016**, *37*, 153-159.
28. Oancea, E.; Teruel, M. N.; Quest, A. F.; Meyer, T. Green fluorescent protein (GFP)-tagged cysteine-rich domains from protein kinase C as fluorescent indicators for diacylglycerol signaling in living cells. *J Cell Biol.* **1998**, *140*, 485-498.
29. Shamova, O.; Orlov, D.; Stegemann, C.; Czihal, P.; Hoffmann, R.; Brogden, K.; Kolodkin, N.; Sakuta, G.; Tossi, A.; Sahl, H.-G.; Kokryakov, V.; Lehrer, R. I. ChBac3.4: a novel proline-rich antimicrobial peptide from goat leukocytes. *Int J Pept Res Ther.* **2009**, *15*, 31-42.
30. Dennison, S. R.; Whittaker, M.; Harris, F.; Phoenix, D. A. Anticancer alpha-helical peptides and structure/function relationships underpinning their interactions with tumour cell membranes. *Curr Protein Pept Sci.* **2006**, *7*, 487-499.
31. Kawaguchi, K.; Han, Q.; Li, S.; Tan, Y.; Igarashi, K.; Kiyuna, T.; Miyake, K.; Miyake, M.; Chmielowski, B.; Nelson, S. D.; Russell, T. A.; Dry, S. M.; Li, Y.; Singh, A. S.; Eckardt, M. A.; Unno, M.; Eilber, F. C.; Hoffman, R. M. Targeting methionine with oral recombinant methioninase (o-rMETase) arrests a patient-derived orthotopic xenograft (PDOX) model of BRAF-V600E mutant melanoma: implications for chronic clinical cancer therapy and prevention. *Cell Cycle.* **2018**, *17*, 356-361.
32. Ahmaditaba, M. A.; Houshdar Tehrani, M. H.; Zarghi, A.; Shahosseini, S.; Daraei, B. Design, synthesis and biological evaluation of novel peptide-like analogues as selective COX-2 inhibitors. *Iran J Pharm Res.* **2018**, *17*, 87-92.
33. Bhunia, D.; Mondal, P.; Das, G.; Saha, A.; Sengupta, P.; Jana, J.; Mohapatra, S.; Chatterjee, S.; Ghosh, S. Spatial position regulates power of tryptophan: discovery of a major-groove-specific nuclear-localizing, cell-penetrating tetrapeptide. *J Am Chem Soc.* **2018**, *140*, 1697-1714.
34. Hoskin, D. W.; Ramamoorthy, A. Studies on anticancer activities of antimicrobial peptides. *Biochim Biophys Acta.* **2008**, *1778*, 357-375.
35. Szlasa, W.; Zendran, I.; Zalesińska, A.; Tarek, M.; Kulbacka, J. Lipid composition of the cancer cell membrane. *J Bioenerg Biomembr.* **2020**, *52*, 321-342.
36. Schweizer, F. Cationic amphiphilic peptides with cancer-selective toxicity. *Eur J Pharmacol.* **2009**, *625*, 190-194.
37. Sok, M.; Sentjurc, M.; Schara, M. Membrane fluidity characteristics of human lung cancer. *Cancer Lett.* **1999**, *139*, 215-220.
38. Zwaal, R. F.; Schroit, A. J. Pathophysiologic implications of membrane phospholipid asymmetry in blood cells. *Blood.* **1997**, *89*, 1121-1132.
39. Mai, J. C.; Mi, Z.; Kim, S. H.; Ng, B.; Robbins, P. D. A proapoptotic peptide for the treatment of solid tumors. *Cancer Res.* **2001**, *61*, 7709-7712.
40. Li, H.; Kolluri, S. K.; Gu, J.; Dawson, M. I.; Cao, X.; Hobbs, P. D.; Lin, B.; Chen, G.; Lu, J.; Lin, F.; Xie, Z.; Fontana, J. A.; Reed, J. C.; Zhang, X. Cytochrome c release and apoptosis induced by mitochondrial targeting of nuclear orphan receptor TR3. *Science.* **2000**, *289*, 1159-1164.
41. Bouchet, S.; Tang, R.; Fava, F.; Legrand, O.; Bauvois, B. The CNGRC-GG-D(KLAKLAK)2 peptide induces a caspase-independent, Ca2+-

dependent death in human leukemic myeloid cells by targeting surface aminopeptidase N/CD13. *Oncotarget.* **2016**, *7*, 19445-19467.

42. Li, Y.; Yu, J. Research progress in structure-activity relationship of bioactive peptides. *J Med Food.* **2015**, *18*, 147-156.
43. Chalamaiah, M.; Yu, W.; Wu, J. Immunomodulatory and anticancer protein hydrolysates (peptides) from food proteins: a review. *Food Chem.* **2018**, *245*, 205-222.
44. Sharma, S. V. Melittin-induced hyperactivation of phospholipase A2 activity and calcium influx in ras-transformed cells. *Oncogene.* **1993**, *8*, 939-947.
45. Quintal-Bojórquez, N.; Segura-Campos, M. R. Bioactive peptides as therapeutic adjuvants for cancer. *Nutr Cancer.* **2021**, *73*, 1309-1321.
46. Lee, H. T.; Lee, C. C.; Yang, J. R.; Lai, J. Z.; Chang, K. Y. A large-scale structural classification of antimicrobial peptides. *Biomed Res Int.* **2015**, *2015*, 475062.
47. Libério, M. S.; Joanitti, G. A.; Fontes, W.; Castro, M. S. Anticancer peptides and proteins: a panoramic view. *Protein Pept Lett.* **2013**, *20*, 380-391.
48. Rothbard, J. B.; Jessop, T. C.; Lewis, R. S.; Murray, B. A.; Wender, P. A. Role of membrane potential and hydrogen bonding in the mechanism of translocation of guanidinium-rich peptides into cells. *J Am Chem Soc.* **2004**, *126*, 9506-9507.
49. Guidotti, G.; Brambilla, L.; Rossi, D. Cell-penetrating peptides: from basic research to clinics. *Trends Pharmacol Sci.* **2017**, *38*, 406-424.
50. Oelkrug, C.; Hartke, M.; Schubert, A. Mode of action of anticancer peptides (ACPs) from amphibian origin. *Anticancer Res.* **2015**, *35*, 635-643.
51. Gabernet, G.; Müller, A. T.; Hiss, J. A.; Schneider, G. Membranolytic anticancer peptides. *MedChemComm.* **2016**, *7*, 2232-2245.
52. Huang, Y. B.; Wang, X. F.; Wang, H. Y.; Liu, Y.; Chen, Y. Studies on mechanism of action of anticancer peptides by modulation of hydrophobicity within a defined structural framework. *Mol Cancer Ther.* **2011**, *10*, 416-426.
53. Lehrer, R. I.; Lichtenstein, A. K.; Ganz, T. Defensins: antimicrobial and cytotoxic peptides of mammalian cells. *Annu Rev Immunol.* **1993**, *11*, 105-128.
54. Kumar, P.; Kizhakkedathu, J. N.; Straus, S. K. Antimicrobial peptides: diversity, mechanism of action and strategies to improve the activity and biocompatibility in vivo. *Biomolecules.* **2018**, *8*, 4.
55. Veldhuizen, E. J.; Schneider, V. A.; Agustiandari, H.; van Dijk, A.; Tjeerdsma-van Bokhoven, J. L.; Bikker, F. J.; Haagsman, H. P. Antimicrobial and immunomodulatory activities of PR-39 derived peptides. *PLoS One.* **2014**, *9*, e95939.
56. Chan, Y. R.; Gallo, R. L. PR-39, a syndecan-inducing antimicrobial peptide, binds and affects p130(Cas). *J Biol Chem.* **1998**, *273*, 28978-28985.
57. Bae, S.; Oh, K.; Kim, H.; Kim, Y.; Kim, H. R.; Hwang, Y. I.; Lee, D. S.; Kang, J. S.; Lee, W. J. The effect of alloferon on the enhancement of NK cell cytotoxicity against cancer via the up-regulation of perforin/granzyme B secretion. *Immunobiology.* **2013**, *218*, 1026-1033.
58. Ramalho, S. D.; Pinto, M. E. F.; Ferreira, D.; Bolzani, V. S. Biologically active orbitides from the euphorbiaceae family. *Planta Med.* **2018**, *84*, 558-567.
59. Hu, E.; Wang, D.; Chen, J.; Tao, X. Novel cyclotides from Hedyotis diffusa induce apoptosis and inhibit proliferation and migration of prostate cancer cells. *Int J Clin Exp Med.* **2015**, *8*, 4059-4065.
60. Zhang, G.; Liu, S.; Liu, Y.; Wang, F.; Ren, J.; Gu, J.; Zhou, K.; Shan, B. A novel cyclic pentapeptide, H-10, inhibits B16 cancer cell growth and induces cell apoptosis. *Oncol Lett.* **2014**, *8*, 248-252.
61. Sable, R.; Parajuli, P.; Jois, S. Peptides, peptidomimetics, and polypeptides from marine sources: a wealth of natural sources for pharmaceutical applications. *Mar Drugs.* **2017**, *15*, 124.
62. Chakrabarti, S.; Guha, S.; Majumder, K. Food-derived bioactive peptides in human health: challenges and opportunities. *Nutrients.* **2018**, *10*, 1738.
63. Burton, M. F.; Steel, P. G. The chemistry and biology of LL-37. *Nat Prod Rep.* **2009**, *26*, 1572-1584.
64. Mader, J. S.; Mookherjee, N.; Hancock, R. E.; Bleackley, R. C. The human host defense peptide LL-37 induces apoptosis in a calpain- and apoptosis-inducing factor-dependent manner involving Bax activity. *Mol Cancer Res.* **2009**, *7*, 689-702.
65. Ganz, T.; Selsted, M. E.; Szklarek, D.; Harwig, S. S.; Daher, K.; Bainton, D. F.; Lehrer, R. I. Defensins. Natural peptide antibiotics of human neutrophils. *J Clin Invest.* **1985**, *76*, 1427-1435.
66. McKeown, S. T.; Lundy, F. T.; Nelson, J.; Lockhart, D.; Irwin, C. R.; Cowan, C. G.; Marley, J. J. The cytotoxic effects of human neutrophil peptide-1 (HNP1) and lactoferrin on oral squamous cell carcinoma (OSCC) in vitro. *Oral Oncol.* **2006**, *42*, 685-690.
67. Jang, A.; Jo, C.; Kang, K.-S.; Lee, M. Antimicrobial and human cancer cell cytotoxic effect of synthetic angiotensin-converting enzyme (ACE) inhibitory peptides. *Food Chem.* **2008**, *107*, 327-336.
68. Su, L.; Xu, G.; Shen, J.; Tuo, Y.; Zhang, X.; Jia, S.; Chen, Z.; Su, X. Anticancer bioactive peptide suppresses human gastric cancer growth through modulation of apoptosis and the cell cycle. *Oncol Rep.* **2010**, *23*, 3-9.
69. Yu, L.; Yang, L.; An, W.; Su, X. Anticancer bioactive peptide-3 inhibits human gastric cancer growth by suppressing gastric cancer stem cells. *J Cell Biochem.* **2014**, *115*, 697-711.
70. Suarez-Jimenez, G. M.; Burgos-Hernandez, A.; Ezquerra-Brauer, J. M. Bioactive peptides and depsipeptides with anticancer potential: sources from marine animals. *Mar Drugs.* **2012**, *10*, 963-986.
71. Conlon, J. M.; Mechkarska, M.; Lukic, M. L.; Flatt, P. R. Potential therapeutic applications of multifunctional host-defense peptides from frog skin as anti-cancer, anti-viral, immunomodulatory, and anti-diabetic agents. *Peptides.* **2014**, *57*, 67-77.
72. Kim, M. K.; Kang, N.; Ko, S. J.; Park, J.; Park, E.; Shin, D. W.; Kim, S. H.; Lee, S. A.; Lee, J. I.; Lee, S. H.; Ha, E. G.; Jeon, S. H.; Park, Y. Antibacterial and antibiofilm activity and mode of action of magainin 2 against drug-resistant acinetobacter baumannii. *Int J Mol Sci.* **2018**, *19*, 3041.
73. Lehmann, J.; Retz, M.; Sidhu, S. S.; Suttmann, H.; Sell, M.; Paulsen, F.; Harder, J.; Unteregger, G.; Stöckle, M. Antitumor activity of the antimicrobial peptide magainin II against bladder cancer cell lines. *Eur Urol.* **2006**, *50*, 141-147.
74. Hsu, K. C.; Li-Chan, E. C. Y.; Jao, C. L. Antiproliferative activity of peptides prepared from enzymatic hydrolysates of tuna dark muscle on human breast cancer cell line MCF-7. *Food Chem.* **2011**, *126*, 617-622.
75. Roy, M. K.; Watanabe, Y.; Tamai, Y. Induction of apoptosis in HL-60 cells by skimmed milk digested with a proteolytic enzyme from the yeast Saccharomyces cerevisiae. *J Biosci Bioeng.* **1999**, *88*, 426-432.
76. Steijns, J. M.; van Hooijdonk, A. C. Occurrence, structure, biochemical properties and technological characteristics of lactoferrin. *Br J Nutr.* **2000**, *84 Suppl 1*, S11-17.
77. Mader, J. S.; Salsman, J.; Conrad, D. M.; Hoskin, D. W. Bovine lactoferricin selectively induces apoptosis in human leukemia and carcinoma cell lines. *Mol Cancer Ther.* **2005**, *4*, 612-624.

78. Yin, C. M.; Wong, J. H.; Xia, J.; Ng, T. B. Studies on anticancer activities of lactoferrin and lactoferricin. *Curr Protein Pept Sci.* **2013**, *14*, 492-503.
79. Wang, Z.; Zhang, X. Isolation and identification of anti-proliferative peptides from Spirulina platensis using three-step hydrolysis. *J Sci Food Agric.* **2017**, *97*, 918-922.
80. Chi, C.-F.; Hu, F.-Y.; Wang, B.; Li, T.; Ding, G.-F. Antioxidant and anticancer peptides from the protein hydrolysate of blood clam (Tegillarca granosa) muscle. *J Funct Foods.* **2015**, *15*, 301-313.
81. Fernández-Tomé, S.; Sanchón, J.; Recio, I.; Hernández-Ledesma, B. Transepithelial transport of lunasin and derived peptides: Inhibitory effects on the gastrointestinal cancer cells viability. *J Food Compost Anal.* **2018**, *68*, 101-110.
82. Luna Vital, D. A.; González de Mejía, E.; Dia, V. P.; Loarca-Piña, G. Peptides in common bean fractions inhibit human colorectal cancer cells. *Food Chem.* **2014**, *157*, 347-355.
83. Soares, A. M.; Zuliani, J. P. Toxins of animal venoms and inhibitors: molecular and biotechnological tools useful to human and animal health. *Curr Top Med Chem.* **2019**, *19*, 1868-1871.
84. Havas, L. J. Effect of bee venom on colchicine-induced tumours. *Nature.* **1950**, *166*, 567-568.
85. Kerkis, I.; Hayashi, M. A.; Prieto da Silva, A. R.; Pereira, A.; De Sá Júnior, P. L.; Zaharenko, A. J.; Rádis-Baptista, G.; Kerkis, A.; Yamane, T. State of the art in the studies on crotamine, a cell penetrating peptide from South American rattlesnake. *Biomed Res Int.* **2014**, *2014*, 675985.
86. Pereira, A.; Kerkis, A.; Hayashi, M. A.; Pereira, A. S.; Silva, F. S.; Oliveira, E. B.; Prieto da Silva, A. R.; Yamane, T.; Rádis-Baptista, G.; Kerkis, I. Crotamine toxicity and efficacy in mouse models of melanoma. *Expert Opin Investig Drugs.* **2011**, *20*, 1189-1200.
87. Bakare, O. O.; Gokul, A.; Wu, R.; Niekerk, L. A.; Klein, A.; Keyster, M. Biomedical relevance of novel anticancer peptides in the sensitive treatment of cancer. *Biomolecules.* **2021**, *11*, 1120.
88. Aghazadeh, H.; Memariani, H.; Ranjbar, R.; Pooshang Bagheri, K. The activity and action mechanism of novel short selective LL-37-derived anticancer peptides against clinical isolates of Escherichia coli. *Chem Biol Drug Des.* **2019**, *93*, 75-83.
89. Fruitwala, S.; El-Naccache, D. W.; Chang, T. L. Multifaceted immune functions of human defensins and underlying mechanisms. *Semin Cell Dev Biol.* **2019**, *88*, 163-172.
90. Liu, S.; Zhou, L.; Li, J.; Suresh, A.; Verma, C.; Foo, Y. H.; Yap, E. P.; Tan, D. T.; Beuerman, R. W. Linear analogues of human beta-defensin 3: concepts for design of antimicrobial peptides with reduced cytotoxicity to mammalian cells. *ChemBioChem.* **2008**, *9*, 964-973.
91. Zweytick, D. LTX-315 - a promising novel antitumor peptide and immunotherapeutic agent. *Cell Stress.* **2019**, *3*, 328-329.
92. Jeyamogan, S.; Khan, N. A.; Sagathevan, K.; Siddiqui, R. Sera/organ lysates of selected animals living in polluted environments exhibit cytotoxicity against cancer cell lines. *Anticancer Agents Med Chem.* **2019**, *19*, 2251-2268.
93. Brady, D.; Grapputo, A.; Romoli, O.; Sandrelli, F. Insect cecropins, antimicrobial peptides with potential therapeutic applications. *Int J Mol Sci.* **2019**, *20*, 5862.
94. Pinto, I. B.; dos Santos Machado, L.; Meneguetti, B. T.; Nogueira, M. L.; Espínola Carvalho, C. M.; Roel, A. R.; Franco, O. L. Utilization of antimicrobial peptides, analogues and mimics in creating antimicrobial surfaces and bio-materials. *Biochem Eng J.* **2019**, *150*, 107237.
95. Li, B.; Lyu, P.; Xie, S.; Qin, H.; Pu, W.; Xu, H.; Chen, T.; Shaw, C.; Ge, L.; Kwok, H. F. LFB: A Novel Antimicrobial Brevinin-Like Peptide from the Skin Secretion of the Fujian Large Headed Frog, Limnonectes fujianensi. *Biomolecules.* **2019**, *9*, 242.
96. Zahedifard, F.; Lee, H.; No, J. H.; Salimi, M.; Seyed, N.; Asoodeh, A.; Rafati, S. Anti-leishmanial activity of Brevinin 2R and its Lauric acid conjugate type against L. major: In vitro mechanism of actions and in vivo treatment potentials. *PLoS Negl Trop Dis.* **2019**, *13*, e0007217.
97. Liu, Y.; Tavana, O.; Gu, W. p53 modifications: exquisite decorations of the powerful guardian. *J Mol Cell Biol.* **2019**, *11*, 564-577.
98. Chen, X.; Zhang, L.; Ma, C.; Zhang, Y.; Xi, X.; Wang, L.; Zhou, M.; Burrows, J. F.; Chen, T. A novel antimicrobial peptide, Ranatuerin-2PLx, showing therapeutic potential in inhibiting proliferation of cancer cells. *Biosci Rep.* **2018**, *38*, BSR20180710.
99. Tornesello, A. L.; Borrelli, A.; Buonaguro, L.; Buonaguro, F. M.; Tornesello, M. L. Antimicrobial peptides as anticancer agents: functional properties and biological activities. *Molecules.* **2020**, *25*, 2850.
100. Tripathi, A. K.; Kumari, T.; Harioudh, M. K.; Yadav, P. K.; Kathuria, M.; Shukla, P. K.; Mitra, K.; Ghosh, J. K. Identification of GXXXXG motif in Chrysophsin-1 and its implication in the design of analogs with cell-selective antimicrobial and anti-endotoxin activities. *Sci Rep.* **2017**, *7*, 3384.
101. Hansen, I.; Isaksson, J.; Poth, A. G.; Hansen, K.; Andersen, A. J. C.; Richard, C. S. M.; Blencke, H. M.; Stensvåg, K.; Craik, D. J.; Haug, T. Isolation and characterization of antimicrobial peptides with unusual disulfide connectivity from the colonial ascidian synoicum turgens. *Mar Drugs.* **2020**, *18*, 51.
102. Oren, Z.; Shai, Y. Mode of action of linear amphipathic alpha-helical antimicrobial peptides. *Biopolymers.* **1998**, *47*, 451-463.
103. Shai, Y. Mechanism of the binding, insertion and destabilization of phospholipid bilayer membranes by alpha-helical antimicrobial and cell non-selective membrane-lytic peptides. *Biochim Biophys Acta.* **1999**, *1462*, 55-70.
104. Matsuzaki, K.; Murase, O.; Fujii, N.; Miyajima, K. An antimicrobial peptide, magainin 2, induced rapid flip-flop of phospholipids coupled with pore formation and peptide translocation. *Biochemistry.* **1996**, *35*, 11361-11368.
105. Garay, H.; Espinosa, L. A.; Perera, Y.; Sánchez, A.; Diago, D.; Perea, S. E.; Besada, V.; Reyes, O.; González, L. J. Characterization of low-abundance species in the active pharmaceutical ingredient of CIGB-300: A clinical-grade anticancer synthetic peptide. *J Pept Sci.* **2018**, *24*, e3081.
106. Perea, S. E.; Reyes, O.; Baladron, I.; Perera, Y.; Farina, H.; Gil, J.; Rodriguez, A.; Bacardi, D.; Marcelo, J. L.; Cosme, K.; Cruz, M.; Valenzuela, C.; López-Saura, P. A.; Puchades, Y.; Serrano, J. M.; Mendoza, O.; Castellanos, L.; Sanchez, A.; Betancourt, L.; Besada, V.; Silva, R.; López, E.; Falcón, V.; Hernández, I.; Solares, M.; Santana, A.; Díaz, A.; Ramos, T.; López, C.; Ariosa, J.; González, L. J.; Garay, H.; Gómez, D.; Gómez, R.; Alonso, D. F.; Sigman, H.; Herrera, L.; Acevedo, B. CIGB-300, a novel proapoptotic peptide that impairs the CK2 phosphorylation and exhibits anticancer properties both in vitro and in vivo. *Mol Cell Biochem.* **2008**, *316*, 163-167.
107. Rodríguez-Ulloa, A.; Ramos, Y.; Gil, J.; Perera, Y.; Castellanos-Serra, L.; García, Y.; Betancourt, L.; Besada, V.; González, L. J.; Fernández-de-Cossio, J.; Sanchez, A.; Serrano, J. M.; Farina, H.; Alonso, D. F.; Acevedo, B. E.; Padrón, G.; Musacchio, A.; Perea, S. E. Proteomic profile regulated by the anticancer peptide CIGB-300 in non-small cell lung cancer (NSCLC) cells. *J Proteome Res.* **2010**, *9*, 5473-5483.
108. Hirabayashi, K.; Yanagisawa, R.; Saito, S.; Higuchi, Y.; Koya, T.; Sano, K.; Koido, S.; Okamoto, M.; Sugiyama, H.; Nakazawa, Y.; Shimodaira, S. Feasibility and immune response of WT1 peptide vaccination in

combination with OK-432 for paediatric solid tumors. *Anticancer Res.* **2018**, *38*, 2227-2234.

109. Yanagisawa, R.; Koizumi, T.; Koya, T.; Sano, K.; Koido, S.; Nagai, K.; Kobayashi, M.; Okamoto, M.; Sugiyama, H.; Shimodaira, S. WT1-pulsed dendritic cell vaccine combined with chemotherapy for resected pancreatic cancer in a phase I study. *Anticancer Res.* 2**018**, *38*, 2217-2225.
110. Ohno, S.; Takano, F.; Ohta, Y.; Kyo, S.; Myojo, S.; Dohi, S.; Sugiyama, H.; Ohta, T.; Inoue, M. Frequency of myeloid dendritic cells can predict the efficacy of Wilms' tumor 1 peptide vaccination. *Anticancer Res.* **2011**, *31*, 2447-2452.
111. Ishikawa, H.; Imano, M.; Shiraishi, O.; Yasuda, A.; Peng, Y. F.; Shinkai, M.; Yasuda, T.; Imamoto, H.; Shiozaki, H. Phase I clinical trial of vaccination with LY6K-derived peptide in patients with advanced gastric cancer. *Gastric Cancer.* **2014**, *17*, 173-180.
112. Vasef, M. A.; Ross, J. S.; Cohen, M. B. Telomerase activity in human solid tumors. Diagnostic utility and clinical applications. *Am J Clin Pathol.* **1999**, *112*, S68-75.
113. Bernhardt, S. L.; Gjertsen, M. K.; Trachsel, S.; Møller, M.; Eriksen, J. A.; Meo, M.; Buanes, T.; Gaudernack, G. Telomerase peptide vaccination of patients with non-resectable pancreatic cancer: A dose escalating phase I/II study. *Br J Cancer.* **2006**, *95*, 1474-1482.
114. Kokhaei, P.; Palma, M.; Hansson, L.; Osterborg, A.; Mellstedt, H.; Choudhury, A. Telomerase (hTERT 611-626) serves as a tumor antigen in B-cell chronic lymphocytic leukemia and generates spontaneously antileukemic, cytotoxic T cells. *Exp Hematol.* **2007**, *35*, 297-304.
115. Aspeslagh, S.; Awada, A.; A, S. M. P.; Aftimos, P.; Bahleda, R.; Varga, A.; Soria, J. C. Phase I dose-escalation study of plitidepsin in combination with bevacizumab in patients with refractory solid tumors. *Anticancer Drugs.* **2016**, *27*, 1021-1027.
116. Engel, J. B.; Tinneberg, H. R.; Rick, F. G.; Berkes, E.; Schally, A. V. Targeting of peptide cytotoxins to LHRH receptors for treatment of cancer. *Curr Drug Targets.* **2016**, *17*, 488-494.
117. Noguchi, M.; Matsumoto, K.; Uemura, H.; Arai, G.; Eto, M.; Naito, S.; Ohyama, C.; Nasu, Y.; Tanaka, M.; Moriya, F.; Suekane, S.; Matsueda, S.; Komatsu, N.; Sasada, T.; Yamada, A.; Kakuma, T.; Itoh, K. An open-label, randomized phase II trial of personalized peptide vaccination in patients with bladder cancer that progressed after platinum-based chemotherapy. *Clin Cancer Res.* **2016**, *22*, 54-60.
118. Brown, T. A.; Byrd, K.; Vreeland, T. J.; Clifton, G. T.; Jackson, D. O.; Hale, D. F.; Herbert, G. S.; Myers, J. W.; Greene, J. M.; Berry, J. S.; Martin, J.; Elkas, J. C.; Conrads, T. P.; Darcy, K. M.; Hamilton, C. A.; Maxwel, G. L.; Peoples, G. E. Final analysis of a phase I/IIa trial of the folate-binding protein-derived E39 peptide vaccine to prevent recurrence in ovarian and endometrial cancer patients. *Cancer Med.* **2019**, *8*, 4678-4687.
119. Schwartzentruber, D. J.; Lawson, D. H.; Richards, J. M.; Conry, R. M.; Miller, D. M.; Treisman, J.; Gailani, F.; Riley, L.; Conlon, K.; Pockaj, B.; Kendra, K. L.; White, R. L.; Gonzalez, R.; Kuzel, T. M.; Curti, B.; Leming, P. D.; Whitman, E. D.; Balkissoon, J.; Reintgen, D. S.; Kaufman, H.; Marincola, F. M.; Merino, M. J.; Rosenberg, S. A.; Choyke, P.; Vena, D.; Hwu, P. gp100 peptide vaccine and interleukin-2 in patients with advanced melanoma. *N Engl J Med.* **2011**, *364*, 2119-2127.
120. Mikecin, A. M.; Walker, L. R.; Kuna, M.; Raucher, D. Thermally targeted p21 peptide enhances bortezomib cytotoxicity in androgen-independent prostate cancer cell lines. *Anticancer Drugs.* **2014**, *25*, 189-199.
121. Xie, M.; Liu, D.; Yang, Y. Anti-cancer peptides: classification, mechanism of action, reconstruction and modification. *Open Biol.* **2020**, *10*, 200004.
122. Hu, X.; Liu, S. Recent advances towards the fabrication and biomedical applications of responsive polymeric assemblies and nanoparticle hybrid superstructures. *Dalton Trans.* **2015**, *44*, 3904-3922.
123. Hwang, J. S.; Kim, S. G.; Shin, T. H.; Jang, Y. E.; Kwon, D. H.; Lee, G. Development of anticancer peptides using artificial intelligence and combinational therapy for cancer therapeutics. *Pharmaceutics.* **2022**, *14*, 997.
124. Regberg, J.; Srimanee, A.; Langel, U. Applications of cell-penetrating peptides for tumor targeting and future cancer therapies. *Pharmaceuticals (Basel).* **2012**, *5*, 991-1007.
125. Chatzisideri, T.; Leonidis, G.; Sarli, V. Cancer-targeted delivery systems based on peptides. *Future Med Chem.* **2018**, *10*, 2201-2226.
126. Kim, B. J.; Xu, B. Enzyme-instructed self-assembly for cancer therapy and imaging. *Bioconjug Chem.* **2020**, *31*, 492-500.
127. Shi, J.; Xu, B. Nanoscale assemblies of small molecules control the fate of cells. *Nano Today.* **2015**, *10*, 615-630.
128. Liu, X.; Wu, F.; Ji, Y.; Yin, L. Recent advances in anti-cancer protein/peptide delivery. *Bioconjug Chem.* **2019**, *30*, 305-324.
129. Conibear, A. C.; Schmid, A.; Kamalov, M.; Becker, C. F. W.; Bello, C. Recent advances in peptide-based approaches for cancer treatment. *Curr Med Chem.* **2020**, *27*, 1174-1205.

Received: November 17, 2022
Revised: February 2, 2023
Accepted: March 10, 2023
Available online: March 28, 2023

Mechanical environment for *in vitro* cartilage tissue engineering assisted by *in silico* models

Rob Jess[1,2,#], *Tao Ling*[3,#,†], *Yi Xiong*[3,*], *Chris J. Wright*[1], *Feihu Zhao*[1,2,*]

Key Words:
cartilage tissue engineering; *in silico* modelling; mechanical stimulation; mechanobiology

From the Contents

ABSTRACT

Mechanobiological study of chondrogenic cells and multipotent stem cells for articular cartilage tissue engineering (CTE) has been widely explored. The mechanical stimulation in terms of wall shear stress, hydrostatic pressure and mechanical strain has been applied in CTE in vitro. It has been found that the mechanical stimulation at a certain range can accelerate the chondrogenesis and articular cartilage tissue regeneration. This review explicitly focuses on the study of the influence of the mechanical environment on proliferation and extracellular matrix production of chondrocytes in vitro for CTE. The multidisciplinary approaches used in previous studies and the need for in silico methods to be used in parallel with in vitro methods are also discussed. The information from this review is expected to direct facial CTE research, in which mechanobiology has not been widely explored yet.

***Corresponding authors:**
Feihu Zhao,
feihu.zhao@swansea.ac.uk;
Yi Xiong,
xiongy3@sustech.edu.cn.

#Author equally.

†Present Addresses:
Department of Computing, Hong Kong Polytechnic University, Hong Kong Special Administrative Region, China

http://doi.org/10.12336/biomatertransl.2023.01.004

How to cite this article:
Jess, R.; Ling, T.; Xiong, Y.; Wright, C. J.; Zhao, F. Mechanical environment for *in vitro* cartilage tissue engineering assisted by *in silico* models. *Biomater Transl.* **2023**, *4*(1), 18-26.

Introduction

Current optimal management in the reconstruction of facial cartilage involves the use of autograft, allograft, or xenograft chondrocyte sources, which present the difficulties of donor site morbidity, transplant rejection, and low source availability.[1] Cartilage tissue engineering (CTE) provides a promising solution, which involves the seeding of multipotent stem cells, chondrogenic progenitor cells, or chondrocytes onto porous scaffolds.[2] This method is followed by the expansion of culture volume and the generation of neo-synthesised extracellular matrix (ECM) prior to implantation.[3] Cartilage tissue growth within the scaffolds is a complex process with multiple mechanical, biochemical, and genetic factors influencing chondrogenesis, further complicated by the temporality of the process. If the cell/tissue culture time can be shortened, patients who have facial cartilage damage can receive the implants at an appropriate time. Therefore, there is a demand to accelerate the chondrogenesis as well as proliferation and ECM production of chondrocytes during cell culturing for facial CTE.

Different *in vitro* studies used different cell types, for example, some have used mesenchymal stem cells,[3,4] and others used primary chondrocytes,[5,6] for CTE. The majority of these studies have found that the mechanical environment can influence differentiation, proliferation, and ECM production of primary chondrocytes and mesenchymal stem cells in articular CTE experiments.[7] Mechanobiology for facial CTE has not been extensively investigated yet. The mechanical environment influences CTE in both static and dynamic culture conditions. For static culture condition, the mechanical factors that can influence the chondrocytes' behaviours are stiffness of materials used for housing the cells.[8] For dynamic culture condition, mechanical factors that influence the chondrocyte behaviours include fluid-induced wall shear stress (WSS), hydrostatic pressure and mechanical strain.[7] These mechanical stimulation processes are applied to cells using bioreactors such as perfusion bioreactors, spinner flasks and mechanical compression bioreactors. Computational studies have demonstrated that the scaffold geometric features such as porosity, pore size and pore shape also influence these mechanical stimulations of cells within three-dimensional (3D) scaffolds.[9]

Thus, one of the promising strategies for guiding cellular behaviour is to tune the scaffold geometric features and scaffold materials mechanical properties.[10] Recent advances in scaffold design and manufacturing such as 3D printing have permitted the precise control of scaffold geometric features including porosities, pore size and curvature, as well as mechanical properties such as stiffness.[11] Critically, the field of CTE has now reached a juncture, in which the combination of predefined, quantifiable mechanical forces is possible. However, optimising these parameters in conjunction to enhance the cellular behaviours (such as chondrogenic differentiation, proliferation and ECM production) presents a challenge due to the high cost associated with the trial-and-error *in vitro*/*in vivo* experiments. With the emergence of *in silico* (computational) tissue engineering, it may help reduce, refine and replace some of the *in vitro*/*in vivo* experiments. Therefore, a multidisciplinary approach is essential using *in silico* methods to determine the optimum scaffold geometric features and mechanical properties for both static and dynamic cell culture conditions; and/or bioreactor loading condition for dynamic cell culture.[12]

This review will explicitly focus on the study of the influence of mechanical environment on proliferation and matrix production of chondrocytes *in vitro* for CTE. As chondrocytes mechanobiology has been more widely investigated for articular CTE than that for facial CTE, we will discuss the literature mostly based on the articular CTE in this review. The use of *in silico* approaches to model the intricate mechanical stimulation for refining *in vitro* tissue engineering studies is also discussed. Due to the similar requirements for articular CTE and facial CTE (e.g., accelerated chondrogenesis, proliferation and ECM production), the knowledge of mechanobiology for articular CTE can be extrapolated for facial CTE studies. Consequently, future research is suggested for the facial CTE field.

Static Culturing Condition

Effect of substrate stiffness on tissue growth

Cells exert forces on the material to which they adhere, and also receive mechanical feedback from these surfaces, even under static culturing conditions.[13] Through mechanotransduction, this mechanical feedback influences the adhesion strength and cytoskeletal architecture of the cells, and thereby influences the cellular behaviours. It has been shown that the stiffness of the substrate material affects chondrocyte behaviours such as proliferation and ECM production.[14] The material stiffness is sensed via molecular pathway (such as Rac1), which modulates S-phase entry and control cell proliferation.[15, 16] Therefore, changing the substrate material stiffness will influence the modular pathway, and consequently influence cell proliferation. Also, cells grown on stiff substrates with different stiffnesses generate different amounts of F-actin, different spread, and display varying yes-associated protein/transcriptional co-activator with PDZ-binding motif in the nucleus, which in turn, affects the cell proliferation.[17] **Table 1** summarises previous *in vitro* studies that demonstrated the substrate material stiffness dependent phenomena of chondrocytes.[5, 18-23]

In silico models for tissue engineering under static condition

In this section, the *in silico* models for modelling the cell mechanobiological behaviour in tissue engineering based on the cell-material interaction are discussed. *In silico* modelling is usually used for simulating the cell behaviours on substrates in static culturing conditions (**Figure 1A**). The aim is to evaluate and optimise the material in terms of the properties (such as mechanical properties). This can help direct the *in vitro* work and avoid excessive trial-and-error for *in vitro* experiments.

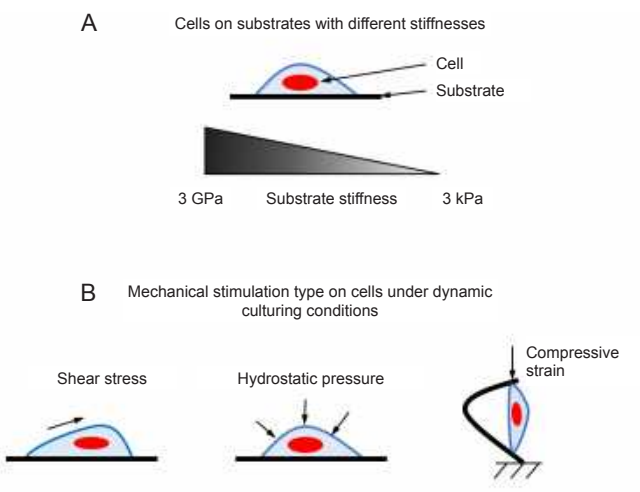

Figure 1. (A) In static culturing condition, cells are cultured on substrates with different stiffnesses. (B) Different types of mechanical stimulations have been applied to cells in dynamic culturing conditions.

1 Department of Biomedical Engineering, Faculty of Science and Engineering, Swansea University, Swansea, UK; 2 Zienkiewicz Institute for Modelling, Data and AI, Swansea University, Swansea, UK; 3 School of System Design and Intelligent Manufacturing, Southern University of Science and Technology, Shenzhen, Guangdong Province, China

Table 1. Chondrocytes respond to substrates with different stiffness in cell culturing

Chondrocytes resource	Substrate material & stiffness	Biological responses	Reference
Porcine	Hydrogel: (i) 3.7 kPa (ii) 53 kPa	• Type I and II collagen: no difference • Cell number and ECM amount: (i) > (ii)	5
Sheep	Hydrogel: (i) 5 kPa (ii) 10 kPa (iii) 20 kPa	• Aggrecan, Col2a1, and Sox9 levels: (i) > (ii) or (iii) • Organisation of actin cytoskeleton (co-related to loss of chondrocyte phenotype): (i) < (ii) or (iii)	18
Bovine	Hydrogel: (i) 3.8 kPa (ii) 17.1 kPa (iii) 29.9 kPa	• Round cell morphology and decreased actin cytoskeletal organisation: (iii) > (ii) > (i) • sGAG/DNA, Col2a1 and aggrecan expressions: (iii) > (ii) > (i)	19
Bovine	Hydrogel: (i) 1 kPa (ii) 15 kPa (iii) 30 kPa	• sGAG and type II collagen expressions: (iii) > (ii) > (i)	20
Murine	Type II collagen-coated PAM: 0.2 – 1.1 MPa	• Proteoglycan deposition, and *Sox9*, *Col2a1*, and aggrecan mRNA expressions are greatest under the substrate stiffness of 0.5 MPa • mRNA level: no difference	21
Bovine	PAM gel coated with type I collagen: (i) 4 kPa (ii) 10 kPa (iii) 40 kPa (iv) 100 kPa	• Differentiated chondrocyte phenotype: (i) > (ii) – (iv) • Type II collagen and aggrecan genes: (i) > (ii) – (iv) • Type I collagen: (i) < (ii) – (iv)	22
Human	(i) PDMS: 4.8 MPa (ii) PS: 2.9 GPa	• Sox9 and type II collagen expressions: (i) > (ii) • Proliferation: no difference	23

Note: Col2a1: type II collagen alpha-1; ECM: extracellular matrix; PAM: polyacrylamide; PDMS: polydimethylsiloxane; PS: polystyrene; sGAG: sulphated glycosaminoglycans; SOX9: SRY-box transcription factor 9.

The mechanical interaction between the substrate material and cells is via focal adhesions that connect intracellular actin bundles and the extracellular substrate: F-actin and myosin generate and transmit forces.[24] Therefore, currently, some *in silico* models of single cell mechanics focus on modelling the force generation and transmission within sub-cellular components such as stress fibres (SFs) and focal adhesions, and the corresponding remodelling of the SFs. These *in silico* models aim to predict the cellular behaviours that are influenced by the substrate stiffness. Most of the cell mechanics models have employed a coupled thermodynamics and mechanics approach for studying single cell behaviour.[24-27] For SF, it consists of three phenomena: SF formation is triggered by an activation signal; reduction in fibre tension leads to fibre dissociation; and the contractile behaviour of SFs is similar to muscle mechanics.[24] This chemo-mechanical behaviour of SF is commonly modelled by a simplified Hill-like equation as described[28] (Equation 1):

$$\frac{\sigma}{\sigma_o} = \begin{cases} 0 & \frac{\dot{\varepsilon}}{\dot{\varepsilon_o}} < -\frac{\eta}{k_v} \\ 1 + \frac{k_v}{\eta}\left(\frac{\dot{\varepsilon}}{\dot{\varepsilon_o}}\right) & -\frac{\eta}{k_v} \le \frac{\dot{\varepsilon}}{\dot{\varepsilon_o}} \le 0 \\ 1 & \frac{\dot{\varepsilon}}{\dot{\varepsilon_o}} > 0 \end{cases} \quad (1)$$

where η $(0 \le \eta \le 1)$ is a nondimensional biochemical state parameter for characterising the recruitment of actin and myosin in an SF bundle; nondimensional constant $\bar{k}_v$ is the fractional reduction in fibre stress upon increasing the shortening rate by $\dot{\varepsilon_o}$; $\dot{\varepsilon}$ is the axial fibre strain rate.

For focal adhesion, its formation is modelled by a mechano-chemical model,[29, 30] which mathematically describes the relationship between the chemical potential, mechanical energy and integrins concentration.

Scaling up groups of cells (rather than single cell), some other *in silico* models have simulated the cellular activities that are influenced by substrate stiffness for CTE application using an agent-based modelling approach.[31, 32] These *in silico* models can be applied to tuning the 3D scaffold mechanical properties such as stiffness for CTE application.

Dynamic Culturing Condition

To study the cell physiology and pathology, mechanical stimulation needs to be applied to cells in CTE experiments *in vitro* with dynamic culturing conditions. The methods of mechanical stimulation that can influence chondrocyte growth are dynamic compression, shear forces, and hydrostatic forces as illustrated in **Figure 1B**. Dynamic culturing conditions have the potential to support higher cell populations than static conditions,[33] induce chondrogenic differentiation of mesenchymal stem cells, and enhance the production of the cartilage-specific ECM.[34] The mechanical stimulation is considered as a driving factor for regulating the calcium ions (Ca^{2+}) entry, primarily through voltage-operated calcium channels, transient receptor potential channels, and purinergic receptors.[35] In addition to the growth factors, such as: transforming growth factor-β, insulin-like growth factor, and bone morphogenetic protein-2, -4, -7, Ca^{2+} is needed to

regulate the cell functions (e.g., synthesis of ECM components) during chondrogenic process.[35, 36] In the following sub-sections, different types of mechanical stimulation for CTE are discussed.

Effect of dynamic compression on cartilaginous tissue growth

To replicate the *in vivo* environment of cyclical compressive loading induced by physical activity (such as walking or running), dynamic compression in the form of uniaxial cyclical loading force, has been applied to the tissue culture with a specific and quantifiable frequency, amplitude, and total duration.[37-39]

In many *in vitro* CTE studies, mechanical stimulation has been applied to cell-laden hydrogels to stimulate cells. Many studies have found that continuous compressive loading yields superior biological and mechanical properties of constructs. For instance, Nebelung et al.[37] utilised human osteoarthritic chondrocytes that were seeded into type I collagen hydrogels at a density of 2×10^5 cells/mL in a compression bioreactor system applying a compressive stimulation of 10% loading at a frequency of 0.3 Hz for 28 days. They found that type II collagen and proteoglycan production was significantly increased relative to unstimulated controls, as well as gene expression of type I collagen, type II collagen and matrix metalloproteinase-13. Mechanically stimulated constructs demonstrated higher values of elastic stiffness.[37] This phenomenon was also observed by Sawatjui et al.[40] who used scaffolds made from silk fibroin with gelatine/chondroitin sulfate/hyaluronate in a ratio of 2:1 for culturing articular chondrocytes under dynamic (10% strain, 1 Hz, for 1 hour/d) and static compression for 2 weeks. In addition to upregulated biological expression including type II collagen and aggrecan under dynamic condition, the resultant stiffness of tissue-scaffold struts was higher under dynamic condition.[40] Another study by Grogan et al.[41] sought to establish if there was a potentiating effect of perfusion and dynamic compression in the chondrogenicity of articular chondrocytes embedded in 2% alginate. Constructs were placed in a control static culture, a bioreactor for perfusion alone (at 100 mL/min) and a bioreactor for perfusion and dynamic compression (of 20% strain at 0.5 Hz, for 1 hour each day). *Col2a1* mRNA expression levels were significantly raised in both bioreactors relative to the control at days 7 and 14. However, there were no significant differences in gene expression between the two bioreactor protocols at day 7 or 14, suggesting that dynamic compression did not further promote chondrogenicity relative to perfusion alone.[41]

Some other studies used porous biomaterial scaffolds for housing the cells in CTE *in vitro* experiments. For example, Sawatjui et al.[40] assessed the response of healthy human articular chondrocytes seeded on 3D PEGT/PBT constructs to dynamic compression (5% strain at 0.1 Hz for 6 cycles of 2 hours duration over 3 days). It was found that glycosaminoglycan (GAG) synthesis, accumulation, and release all significantly increased with dynamic compression relative to control scaffolds, but this increase was heavily dependent on the baseline GAG/DNA ratio of the samples.[40] This suggested that the donor tissue characteristics before mechanical stimulation were important factors in determining response.

Some recent studies applied mechanical compression loading to the cartilage explant in bioreactors.[39, 42, 43] Engstrøm et al.[39] found that compressive loading alters cartilage tissue turnover and enforces the need to include mechanical loading in a translation *ex vivo* cartilage model. In another study, a bone-cartilage explant was investigated under the physiologically-relevant compression.[43] It was found that the physiological loading rapidly activated markers of ECM synthesis and tissue homeostasis via the anabolic transforming growth factor-β/Smad3 pathway, whereas supra-physiological compression induces an initial remodelling response for inhibiting tissue degeneration.[43]

Effect of wall shear stress on cartilaginous tissue growth

WSS is a force tangential to the cell wall. It can be induced by direct solid-on-solid stimulation (contact shear) or through hydrodynamic forces (fluid shear). Contact shear is present physiologically as cartilage rubs against cartilage with the rotating movements of joints. This can be recreated *in vitro* using bioreactors, which maintain pre-determined contact shear frequencies and amplitudes. Fluid-induced shear may be present physiologically as synovial fluid, nutrients and wastes transfer across the face of chondrocytes. This has been simulated by *in vitro* experiments using the bioreactors, such as rotating-wall, perfusion and spinner flask bioreactors.[44]

One of the first studies of the impact of contact shear on cartilage tissue chondrogenesis studied bovine chondrocytes cultured in disks on polysulfone chambers.[45] The disks were exposed to shear strain amplitudes ranging from 1–3% and frequencies of 0.01–1.0 Hz for 24 hours in total, in order to determine the optimal conditions for proteoglycan and protein synthesis. Results indicated that there were no significant differences in proteoglycan or protein synthesis across these ranges, with a 25% and 50% increase respectively relative to static controls.45 A following study assessed the impact of long-term shear strain on bovine chondrocytes cultured on a porous calcium polyphosphate substrate.[46] In 4-week cell culturing experiments, the chondrocytes were exposed to a range of amplitudes and durations of shear strain, and the optimum condition of 2% shear strain amplitude at a frequency of 1 Hz for 400 cycles on alternate days was found. Under this optimum condition, after 1 week, collagen production had increased by 23% whilst proteoglycan production had increased by 20% relative to unstimulated controls. After 4 weeks, there was substantially more tissue grown (1.85 *vs.* 1.58 mg dry weight) and improved mechanical properties (load bearing capacity increased three-fold, stiffness increased 6-fold) relative to unstimulated controls.

Another study examining the influence of contact shear on human chondrocytes was conducted by Shahin and Doran.38 Healthy human foetal chondrocytes were isolated, then seeded onto polyglycolic acid-alginate scaffolds. These constructs were placed within the bioreactor and exposed to a combined compression and shear loading at a strain amplitude of 2.2%

(frequency = 0.05 Hz) for 10 minutes each day for 2.5 weeks. Results demonstrated a 2.1-fold increase in the construct's dry weight and a 2.0-fold increase in cell number relative to static control. There were also significant increases in GAG, total collagen, and type II collagen concentrations relative to the non-stimulated control.

Some other *in vitro* CTE studies also applied fluid shear stress on chondrocytes in the experiments. For example, Gooch et al.[47] determined the effect of fluid shear on ECM production of bovine calf chondrocytes. In this study, chondrocytes were seeded into polyglycolic acid disc-shaped scaffolds which were placed in spinner flasks and subjected to different angular velocities (0, 80, 120, and 160 r/min). It was found that scaffolds stimulated by fluid shear exhibited higher levels of collagen and generated and released more GAG relative to static scaffolds, with no significant variations between these intensities of angular velocities. Another study used human articular chondrocytes; it was found that fluid shear of 1.6 Pa applied using a cone viscometer altered chondrocyte morphology over a period of 48–72 hours.[48] The research observed that chondrocytes began to elongate and align in the direction of the fluid shear, and GAG synthesis increased 2-fold.[48] In another chondrocyte mechanobiological study, human articular chondrocytes were used, and exposed to fluid shear stress via a rotating-wall-vessel (rotating speed = 6 – 8 r/min).[49] Akmal et al.[49] found that GAG and hydroxyproline synthesis alongside type II collagen were significantly increased, compared to a static culturing condition.

Effect of hydrostatic forces on cartilaginous tissue growth

Hydrostatic forces can be defined as the forces exerted on the cell as a result of fluid pressure, either static or dynamic. One of the early studies in this field exposed primary bovine chondrocytes in a monolayer to 10 MPa of hydrostatic pressure for 4 hours.[6] In one group of cell culturing experiments, dynamic pressure with the frequency of 1 Hz was applied, while the other group was under static culturing condition. Results demonstrated that while static pressure had no effect on aggrecan or type II collagen mRNA levels, intermittent pressure increased these expressions by 31% and 36% respectively. Static pressure increased GAG synthesis by 32%, but intermittent pressure increased synthesis by 65%.[6] Additional studies of primary bovine chondrocytes suggested that intermittent pressures of 5–15 MPa promoted ECM production whereas continuous higher pressures of 20–50 MPa resulted in decreases.[50]

Studying human osteoarthritic chondrocytes cultured on type I and III collagen membranes, Scherer et al.51 found that biosynthetic activity was increased with dynamic hydrostatic pressure of 0.2 MPa following a loading regime of 30 minutes on and 2 minutes off. Furthermore, Ikenoue et al.[52] studied the impact of different regimes of intermittent hydrostatic pressure on normal human chondrocytes cultured in monolayer. In this study, cell culturing was carried out under hydrostatic pressures of 1, 5, and 10 MPa at 1 Hz for 4 hours per day. Aggrecan and type II collagen mRNA levels were analysed on days 1 and 4 and compared to unloaded cultures. Aggrecan signals increased by a non-significant amount, 30%, and 50% at 1, 5 and 10 MPa respectively on day 1, and increased by 40%, 80%, and 90% respectively on day 4. Type II collagen production was more sensitive to duration of exposure to dynamic hydrostatic pressure, and significant upregulation of mRNA signal was only found on day 4, with increases of 20%, 60%, and 70% for intermittent pressures of 1, 5, and 10 MPa respectively. This study provided clear evidence that separate markers of chondrogenesis may be influenced differently by hydrostatic pressure regime variations.[52]

In 2012, Correia et al.[53] used human nasal chondrocytes for studying the influence of hydrostatic pressure on chondrogenesis as evidenced by gene expression of aggrecan, type II collagen, and Sox9 as well as immunostaining of cartilage ECM. Chondrocytes were encapsulated in gellan gum hydrogels, cultured over a period of 3 weeks, and exposed to three stimulation regimes: (i) pulsatile hydrostatic pressure of 0.1–0.4 MPa at 0.1 Hz for 3 hours a day, 5 days a week; (ii) steady hydrostatic pressure at 0.4 MPa for 3 hours a day, 5 days a week; (iii) static culturing. It was found that the pulsatile regime induced an increase in the deposition of type II collagen and GAG relative to the steady hydrostatic pressure and static culturing conditions. Furthermore, the expression of type II collagen and *Sox9* genes were significantly greater than the steady and static controls.[53] In 2017, Nazempour et al.50 utilised a novel bioreactor system to simultaneously apply shear stress (0.02 Pa) and oscillating hydrostatic pressure (4 MPa at 0.5 Hz) to bovine articular chondrocytes in culture on agarose scaffolds for 21 days. They found that GAG and total collagen secretions were increased more significantly under a combination of shear stress and oscillating hydrostatic pressure together than that under either static condition or shear stress.[50]

In silico modelling for tissue engineering under dynamic condition

Bioreactors have been used for applying mechanical stimulation as their operation and physical environment can be accurately controlled, giving a comprehensive understanding of the forces acting upon the cells. *In silico* approaches have been used to calculate cell stimulation under dynamic conditions and/or determine the loading conditions of bioreactors. Such an approach has the potential to greatly reduce the environmental impact of the research by cutting down on unnecessary, flawed, or problematic experiments, allowing for a more informed approach.

For bioreactors that apply a deformation to the scaffold, compression or stretching, the finite element method can be used to calculate the local strains. It is assumed that the cells are subjected to the strain magnitude at the location of the scaffold that they are attached to.[54]

For bioreactors that use medium flow with induced WSS for cellular stimulation, the computational fluid dynamics (CFD) approach has been used to analyse the generated fluid velocity and WSS.[44, 55] In cell culturing experiments using 3D porous scaffolds, it was found that the scaffold porosity, pore size and pore shape have a distinct influence on the resultant WSS acting on cells within bioreactors.[9] To quantify the flow velocity and WSS on cells within scaffolds, and/or to determine the loading

conditions of bioreactors, in most circumstances, the CFD models were based on empty scaffolds for WSS calculation at the scaffold surfaces. This was under the assumption that the WSS at the scaffold surfaces was a good representation of the WSS sensed by the cells that attach to the scaffold surfaces. This assumption is well met in the initial situation in cell culturing experiments where the cell morphology is flat once they are attached to the scaffold surfaces. A major limitation of these *in silico* models is their failure to consider the cells and developing tissue within scaffolds. As mentioned above, this is reasonable at the start of the experiment when the cells initially attach to the scaffold surface. However, as the cells grow and proliferate they produce ECM, and this will lead to a change in the scaffolds porosity and the surface morphology. Consequently, the fluid flow and WSS can dramatically change.[56, 57]

To account for the change in scaffold porosity, some *in silico* models included a tissue growth model based on a modified level set method that considered the influence of scaffold structs curvature κ and cellular WSS τ (Equations 2 and 3). Guyot et al.[58, 59] simulated the dynamic process of neo-tissue growth V_G based on this model:

$$V_G = \begin{cases} -A \cdot \kappa \cdot f(\tau)\ \kappa > 0 \\ 0\ \kappa \le 0 \end{cases} \quad (2)$$

$$f(\tau) = \begin{cases} 0.5 + \frac{0.5\tau}{a_1}\ 0 \le \tau \le a_1 \\ 1\ a_2 \le \tau \le a_1 \\ \frac{\tau - a_3}{a_2 - a_3}\ a_2 \le \tau \le a_3 \\ 0\ \tau \ge a_3 \end{cases} \quad (3)$$

where, a_1 and a_2 are the minimal and maximal shear stress enhancing neo-tissue formation (a_1 = 10 mPa, a_2 = 30 mPa) and a_3 the critical shear stress (50 mPa).[58]

Some other studies have defined that the tissue growth function V_G is governed by both the nutrient concentration C and the WSS as Equation 4:[60, 61]

$$V_G = \frac{k_M \cdot C}{k_M + C} \cdot f(\tau) \quad (4)$$

wherein, k_M is the maximum cell growth rate, k_S is the saturation coefficient of nutrient concentration (e.g., k_M = 5.8 × 10^{-6} g/cm^3/s, k_S = 2.3 × 10^{-3} g/cm^3 for CTE application), a_1 and a_2 are the minimal and maximal shear stresses for enhancing tissue formation (e.g., a_1 = 100 mPa, a_2 = 600 mPa for cartilaginous tissue formation) and a_3 the critical shear stress value (e.g., a_3 = 1000 mPa for cartilaginous tissue formation). In Equation 5, the WSS τ is calculated from the CFD model, and the nutrient concentration C is calculated from nutrient the diffusion-convection model, which moreover is coupled with the CFD model for the fluid velocity in convection term:

$$f(\tau) = \begin{cases} 0.6 + 4\tau\ 0 \le \tau \le a_1 \\ 1\ a_1 \le \tau \le a_2 \\ 2.5(1 - \tau)\ a_2 \le \tau \le a_3 \\ 0\ \tau \ge a_3 \end{cases} \quad (5)$$

Some tissue engineering experiments used mechanical compression to the scaffold in the bioreactor for applying mechanical stimulation (mechanical strain) on cells.[62] Previous *in silico* models have simulated the cell differentiation, proliferation, migration and apoptosis of cells within scaffolds under mechanical compression:[63, 64]

$$\frac{\partial n_i}{\partial t} = D_h \cdot \nabla^2 n_i + f(p) \cdot \nabla n_i + f^{PR}(S) \cdot n_i - f^{D}(S) \cdot n_i - f^{A}(S) \cdot n_i \quad (6)$$

where, S is the mechanical stimuli that depend on the octahedral shear strain and interstitial fluid velocity inside neo-tissue; ni was the cell densities of different cell phenotypes i, e.g., multipotent stem cells, and chondrocytes.; D_h is the cell migration rate; $f(p)$ is a function of fluid pressure (p); $f^{PR}(S)$, $f^{D}(S)$ and $f^{A}(S)$ are the mechanical stimuli (S)-related cell proliferation, differentiation and apoptosis rates, respectively. This *in silico* model for predicting cellular activities under mechanical compression was not developed explicitly for facial CTE. However, the model can be applied for CTE when the parameters, such as Dh, $f^{PR}(S)$, $f^{D}(S)$ and $f^{A}(S)$ are tuned to fit the context of facial CTE.

After further development and adaption of the *in silico* models for the application of CTE, these *in silico* models may help in optimising the experiment conditions for facial CTE, avoiding too high cost in terms of time and finance caused by excessive trial-and-error experiments.

Conclusion and Outlook

Using a combination of *in vitro* and *in silico* approaches can elucidate and optimise the micro-mechanical environment of chondrocytes for CTE. Although big progress has been made in the mechanobiology of chondrocytes for articular CTE, it is still a marginal area in facial CTE. Another limitation of this review is that the current *in silico* models are not developed explicitly for facial CTE. However, similar types of mechanical stimulation/environment are considered in the *in silico* models in this review. For future applications in facial CTE, the parameters in the models will need to be adapted. Therefore, the authors expect that the information from this review can inform and guide the mechanobiology study for facial CTE. The following suggestions are made for future facial cartilage CTE studies:

- Replicate the mechanical stimulation types in cell culturing experiments for facial cartilage CTE using different bioreactors for perfusion, mechanical compression, and hydrostatic pressure. Thus, finding the optimal level of mechanical stimulation for specific purposes such as accelerating chondrocytes proliferation in facial CTE;
- Tune the mechanical properties of biomaterials for guiding the cell behaviours for facial cartilage regeneration, e.g., stiffness of cross-linked hydrogel for 3D bioprinting and stiffness of scaffold struts;
- If using scaffold-based techniques combined with bioreactors for dynamic cell culturing, scaffold porous geometric features such as porosity, pore size and pore shape can be designed for tuning the mechanical environment applied to cells for facial CTE.

To investigate the above issues based on *in vitro* experiments, numerous trial-and-error experiments will be needed, leading to high costs in terms of time and finance. Moreover,

without computing, quantitative data, e.g., for mechanical stimulation, scaffold geometries and mechanical properties of biomaterial, are difficult to obtain from *in vitro* experiments. With the validated *in silico* models, it is expected to (i) replace some of trail-and-error *in vitro* experiments for finding the optimal conditions for CTE; (ii) provide the precise values of parameters that need to be assessed. Therefore, these studies are suggested to be conducted using *in silico* – assisted *in vitro* investigation for generating rigorous and comprehensive understanding, meanwhile saving the cost of excessive trial-and-error *in vitro* experiments.

Author contributions

RJ and TL equally contributed to this narrative review, and drafted this review. RJ, TL, YX and FZ participated in the plan and design of this review. YX, CW and FZ read and edited the paper. All authors approved the final version of the manuscript.

Financial support

This work was financial supported by the EPSRC – IAA Research Impact Fund, (No. RIF202/RIR1035-109) and Royal Society Research Grant (No. RGS\R2\212280).

Acknowledgement

None.

Conflicts of interest statement

None.

1. Jovic, T. H.; Jessop, Z. M.; Al-Sabah, A.; Whitaker, I. S. 12 - The clinical need for 3D printed tissue in reconstructive surgery. In *3D bioprinting for reconstructive surgery*, Thomas, D. J.; Jessop, Z. M.; Whitaker, I. S., Eds.; Woodhead Publishing: 2018; pp 235-244.
2. Francis, S. L.; Di Bella, C.; Wallace, G. G.; Choong, P. F. M. Cartilage tissue engineering using stem cells and bioprinting technology-barriers to clinical translation. *Front Surg.* **2018**, *5*, 70.
3. Kessler, M. W.; Grande, D. A. Tissue engineering and cartilage. *Organogenesis.* **2008**, *4*, 28-32.
4. Fahy, N.; Alini, M.; Stoddart, M. J. Mechanical stimulation of mesenchymal stem cells: Implications for cartilage tissue engineering. *J Orthop Res.* **2018**, *36*, 52-63.
5. Schuh, E.; Hofmann, S.; Stok, K.; Notbohm, H.; Müller, R.; Rotter, N. Chondrocyte redifferentiation in 3D: the effect of adhesion site density and substrate elasticity. *J Biomed Mater Res A.* **2012**, *100*, 38-47.
6. Smith, R. L.; Rusk, S. F.; Ellison, B. E.; Wessells, P.; Tsuchiya, K.; Carter, D. R.; Caler, W. E.; Sandell, L. J.; Schurman, D. J. In vitro stimulation of articular chondrocyte mRNA and extracellular matrix synthesis by hydrostatic pressure. *J Orthop Res.* **1996**, *14*, 53-60.
7. O'Conor, C. J.; Case, N.; Guilak, F. Mechanical regulation of chondrogenesis. *Stem Cell Res Ther.* **2013**, *4*, 61.
8. Ghasemi-Mobarakeh, L.; Prabhakaran, M. P.; Tian, L.; Shamirzaei-Jeshvaghani, E.; Dehghani, L.; Ramakrishna, S. Structural properties of scaffolds: Crucial parameters towards stem cells differentiation. *World J Stem Cells.* **2015**, *7*, 728-744.
9. Zhao, F.; Vaughan, T. J.; McNamara, L. M. Quantification of fluid shear stress in bone tissue engineering scaffolds with spherical and cubical pore architectures. *Biomech Model Mechanobiol.* **2016**, *15*, 561-577.
10. O'Brien, F. J. Biomaterials & scaffolds for tissue engineering. *Mater Today.* **2011**, *14*, 88-95.
11. Irawan, V.; Sung, T. C.; Higuchi, A.; Ikoma, T. Collagen scaffolds in cartilage tissue engineering and relevant approaches for future development. *Tissue Eng Regen Med.* **2018**, *15*, 673-697.
12. Zhao, F.; van Rietbergen, B.; Ito, K.; Hofmann, S. Flow rates in perfusion bioreactors to maximise mineralisation in bone tissue engineering in vitro. *J Biomech.* **2018**, *79*, 232-237.
13. Breuls, R. G.; Jiya, T. U.; Smit, T. H. Scaffold stiffness influences cell behavior: opportunities for skeletal tissue engineering. *Open Orthop J.* **2008**, *2*, 103-109.
14. Olivares-Navarrete, R.; Lee, E. M.; Smith, K.; Hyzy, S. L.; Doroudi, M.; Williams, J. K.; Gall, K.; Boyan, B. D.; Schwartz, Z. Substrate stiffness controls osteoblastic and chondrocytic differentiation of mesenchymal stem cells without exogenous stimuli. *PLoS One.* **2017**, *12*, e0170312.
15. Selig, M.; Lauer, J. C.; Hart, M. L.; Rolauffs, B. Mechanotransduction and stiffness-sensing: mechanisms and opportunities to control multiple molecular aspects of cell phenotype as a design cornerstone of cell-instructive biomaterials for articular cartilage repair. *Int J Mol Sci.* **2020**, *21*, 5399.
16. Jiang, C.; Sun, Z. M.; Zhu, D. C.; Guo, Q.; Xu, J. J.; Lin, J. H.; Chen, Z. X.; Wu, Y. S. Inhibition of Rac1 activity by NSC23766 prevents cartilage endplate degeneration via Wnt/β-catenin pathway. *J Cell Mol Med.* **2020**, *24*, 3582-3592.
17. Dobrokhotov, O.; Samsonov, M.; Sokabe, M.; Hirata, H. Mechanoregulation and pathology of YAP/TAZ via Hippo and non-Hippo mechanisms. *Clin Transl Med.* **2018**, *7*, 23.
18. Sanz-Ramos, P.; Mora, G.; Vicente-Pascual, M.; Ochoa, I.; Alcaine, C.; Moreno, R.; Doblaré, M.; Izal-Azcárate, I. Response of sheep chondrocytes to changes in substrate stiffness from 2 to 20 Pa: effect of cell passaging. *Connect Tissue Res.* **2013**, *54*, 159-166.
19. Li, X.; Chen, S.; Li, J.; Wang, X.; Zhang, J.; Kawazoe, N.; Chen, G. 3D culture of chondrocytes in gelatin hydrogels with different stiffness. *Polymers (Basel).* **2016**, *8*, 269.
20. Bachmann, B.; Spitz, S.; Schädl, B.; Teuschl, A. H.; Redl, H.; Nürnberger, S.; Ertl, P. Stiffness matters: fine-tuned hydrogel elasticity alters chondrogenic redifferentiation. *Front Bioeng Biotechnol.* **2020**, *8*, 373.
21. Allen, J. L.; Cooke, M. E.; Alliston, T. ECM stiffness primes the TGFβ pathway to promote chondrocyte differentiation. *Mol Biol Cell.* **2012**, *23*, 3731-3742.
22. Schuh, E.; Kramer, J.; Rohwedel, J.; Notbohm, H.; Müller, R.; Gutsmann, T.; Rotter, N. Effect of matrix elasticity on the maintenance of the chondrogenic phenotype. *Tissue Eng Part A.* **2010**, *16*, 1281-1290.
23. Bergholt, N. L.; Foss, M.; Saeed, A.; Gadegaard, N.; Lysdahl, H.; Lind, M.; Foldager, C. B. Surface chemistry, substrate, and topography guide the behavior of human articular chondrocytes cultured in vitro. *J Biomed Mater Res A.* **2018**, *106*, 2805-2816.
24. Ronan, W.; Deshpande, V. S.; McMeeking, R. M.; McGarry, J. P. Cellular contractility and substrate elasticity: a numerical investigation of the actin cytoskeleton and cell adhesion. *Biomech Model Mechanobiol.* **2014**, *13*, 417-435.
25. McEvoy, E.; Deshpande, V. S.; McGarry, P. Free energy analysis of cell spreading. *J Mech Behav Biomed Mater.* **2017**, *74*, 283-295.
26. Ristori, T.; Vigliotti, A.; Baaijens, F. P. T.; Loerakker, S.; Deshpande, V. S. Prediction of cell alignment on cyclically strained grooved substrates. *Biophys J.* **2016**, *111*, 2274-2285.
27. Ristori, T.; Notermans, T. M. W.; Foolen, J.; Kurniawan, N. A.;

Bouten, C. V. C.; Baaijens, F. P. T.; Loerakker, S. Modelling the combined effects of collagen and cyclic strain on cellular orientation in collagenous tissues. *Sci Rep.* **2018**, *8*, 8518.
28. Deshpande, V. S.; McMeeking, R. M.; Evans, A. G. A bio-chemo-mechanical model for cell contractility. *Proc Natl Acad Sci U S A.* **2006**, *103*, 14015-14020.
29. Ronan, W.; Pathak, A.; Deshpande, V. S.; McMeeking, R. M.; McGarry, J. P. Simulation of the mechanical response of cells on micropost substrates. *J Biomech Eng.* **2013**, *135*, 101012.
30. Deshpande, V. S.; Mrksich, M.; McMeeking, R. M.; Evans, A. G. A bio-mechanical model for coupling cell contractility with focal adhesion formation. *J Mech Phys Solids.* **2008**, *56*, 1484-1510.
31. O'Reilly, A.; Kelly, D. J. A computational model of osteochondral defect repair following implantation of stem cell-laden multiphase scaffolds. *Tissue Eng Part A.* **2017**, *23*, 30-42.
32. Burke, D. P.; Kelly, D. J. Substrate stiffness and oxygen as regulators of stem cell differentiation during skeletal tissue regeneration: a mechanobiological model. *PLoS One.* **2012**, *7*, e40737.
33. Guo, T.; Yu, L.; Lim, C. G.; Goodley, A. S.; Xiao, X.; Placone, J. K.; Ferlin, K. M.; Nguyen, B. N.; Hsieh, A. H.; Fisher, J. P. Effect of dynamic culture and periodic compression on human mesenchymal stem cell proliferation and chondrogenesis. *Ann Biomed Eng.* **2016**, *44*, 2103-2113.
34. Hwang, N. S.; Zhang, C.; Hwang, Y. S.; Varghese, S. Mesenchymal stem cell differentiation and roles in regenerative medicine. *Wiley Interdiscip Rev Syst Biol Med.* **2009**, *1*, 97-106.
35. Ravalli, S.; Szychlinska, M. A.; Lauretta, G.; Musumeci, G. New insights on mechanical stimulation of mesenchymal stem cells for cartilage regeneration. *Appl Sci.* **2020**, *10*, 2927.
36. Ouyang, X.; Xie, Y.; Wang, G. Mechanical stimulation promotes the proliferation and the cartilage phenotype of mesenchymal stem cells and chondrocytes co-cultured in vitro. *Biomed Pharmacother.* **2019**, *117*, 109146.
37. Nebelung, S.; Gavenis, K.; Rath, B.; Tingart, M.; Ladenburger, A.; Stoffel, M.; Zhou, B.; Mueller-Rath, R. Continuous cyclic compressive loading modulates biological and mechanical properties of collagen hydrogels seeded with human chondrocytes. *Biorheology.* **2011**, *48*, 247-261.
38. Shahin, K.; Doran, P. M. Tissue engineering of cartilage using a mechanobioreactor exerting simultaneous mechanical shear and compression to simulate the rolling action of articular joints. *Biotechnol Bioeng.* **2012**, *109*, 1060-1073.
39. Engstrøm, A.; Gillesberg, F. S.; Bay Jensen, A. C.; Karsdal, M. A.; Thudium, C. S. Dynamic compression inhibits cytokine-mediated type II collagen degradation. *Osteoarthr Cartil Open.* **2022**, *4*, 100292.
40. Sawatjui, N.; Limpaiboon, T.; Schrobback, K.; Klein, T. Biomimetic scaffolds and dynamic compression enhance the properties of chondrocyte- and MSC-based tissue-engineered cartilage. *J Tissue Eng Regen Med.* **2018**, *12*, 1220-1229.
41. Grogan, S. P.; Sovani, S.; Pauli, C.; Chen, J.; Hartmann, A.; Colwell, C. W., Jr.; Lotz, M. K.; D'Lima, D. D. Effects of perfusion and dynamic loading on human neocartilage formation in alginate hydrogels. *Tissue Eng Part A.* **2012**, *18*, 1784-1792.
42. Engstrøm, A.; Gillesberg, F. S.; Groen, S. S.; Frederiksen, P.; Bay-Jensen, A. C.; Karsdal, M. A.; Thudium, C. S. Intermittent dynamic compression confers anabolic effects in articular cartilage. *Appl Sci.* **2021**, *11*, 7469.
43. Capuana, E.; Marino, D.; Di Gesù, R.; La Carrubba, V.; Brucato, V.; Tuan, R. S.; Gottardi, R. A high-throughput mechanical activator for cartilage engineering enables rapid screening of in vitro response of tissue models to physiological and supra-physiological loads. *Cells Tissues Organs.* **2022**, *211*, 670-688.
44. Vetsch, J. R.; Betts, D. C.; Müller, R.; Hofmann, S. Flow velocity-driven differentiation of human mesenchymal stromal cells in silk fibroin scaffolds: A combined experimental and computational approach. *PLoS One.* **2017**, *12*, e0180781.
45. Jin, M.; Frank, E. H.; Quinn, T. M.; Hunziker, E. B.; Grodzinsky, A. J. Tissue shear deformation stimulates proteoglycan and protein biosynthesis in bovine cartilage explants. *Arch Biochem Biophys.* **2001**, *395*, 41-48.
46. Waldman, S. D.; Spiteri, C. G.; Grynpas, M. D.; Pilliar, R. M.; Kandel, R. A. Long-term intermittent shear deformation improves the quality of cartilaginous tissue formed in vitro. *J Orthop Res.* **2003**, *21*, 590-596.
47. Gooch, K. J.; Kwon, J. H.; Blunk, T.; Langer, R.; Freed, L. E.; Vunjak-Novakovic, G. Effects of mixing intensity on tissue-engineered cartilage. *Biotechnol Bioeng.* **2001**, *72*, 402-407.
48. Smith, R. L.; Donlon, B. S.; Gupta, M. K.; Mohtai, M.; Das, P.; Carter, D. R.; Cooke, J.; Gibbons, G.; Hutchinson, N.; Schurman, D. J. Effects of fluid-induced shear on articular chondrocyte morphology and metabolism in vitro. *J Orthop Res.* **1995**, *13*, 824-831.
49. Akmal, M.; Anand, A.; Anand, B.; Wiseman, M.; Goodship, A. E.; Bentley, G. The culture of articular chondrocytes in hydrogel constructs within a bioreactor enhances cell proliferation and matrix synthesis. *J Bone Joint Surg Br.* **2006**, *88*, 544-553.
50. Nazempour, A.; Quisenberry, C. R.; Abu-Lail, N. I.; Van Wie, B. J. Combined effects of oscillating hydrostatic pressure, perfusion and encapsulation in a novel bioreactor for enhancing extracellular matrix synthesis by bovine chondrocytes. *Cell Tissue Res.* **2017**, *370*, 179-193.
51. Scherer, K.; Schünke, M.; Sellckau, R.; Hassenpflug, J.; Kurz, B. The influence of oxygen and hydrostatic pressure on articular chondrocytes and adherent bone marrow cells in vitro. *Biorheology.* **2004**, *41*, 323-333.
52. Ikenoue, T.; Trindade, M. C.; Lee, M. S.; Lin, E. Y.; Schurman, D. J.; Goodman, S. B.; Smith, R. L. Mechanoregulation of human articular chondrocyte aggrecan and type II collagen expression by intermittent hydrostatic pressure in vitro. *J Orthop Res.* **2003**, *21*, 110-116.
53. Correia, C.; Pereira, A. L.; Duarte, A. R.; Frias, A. M.; Pedro, A. J.; Oliveira, J. T.; Sousa, R. A.; Reis, R. L. Dynamic culturing of cartilage tissue: the significance of hydrostatic pressure. *Tissue Eng Part A.* **2012**, *18*, 1979-1991.
54. Olivares, A. L.; Marsal, E.; Planell, J. A.; Lacroix, D. Finite element study of scaffold architecture design and culture conditions for tissue engineering. *Biomaterials.* **2009**, *30*, 6142-6149.
55. Melke, J.; Zhao, F.; van Rietbergen, B.; Ito, K.; Hofmann, S. Localisation of mineralised tissue in a complex spinner flask environment correlates with predicted wall shear stress level localisation. *Eur Cell Mater.* **2018**, *36*, 57-68.
56. Zhao, F.; Lacroix, D.; Ito, K.; van Rietbergen, B.; Hofmann, S. Changes in scaffold porosity during bone tissue engineering in perfusion bioreactors considerably affect cellular mechanical stimulation for mineralization. *Bone Rep.* **2020**, *12*, 100265.
57. Papantoniou, I.; Guyot, Y.; Sonnaert, M.; Kerckhofs, G.; Luyten, F. P.; Geris, L.; Schrooten, J. Spatial optimization in perfusion bioreactors improves bone tissue-engineered construct quality attributes. *Biotechnol Bioeng.* **2014**, *111*, 2560-2570.
58. Guyot, Y.; Papantoniou, I.; Luyten, F. P.; Geris, L. Coupling curvature-dependent and shear stress-stimulated neotissue growth in dynamic

bioreactor cultures: a 3D computational model of a complete scaffold. *Biomech Model Mechanobiol.* **2016**, *15*, 169-180.

59. Guyot, Y.; Luyten, F. P.; Schrooten, J.; Papantoniou, I.; Geris, L. A three-dimensional computational fluid dynamics model of shear stress distribution during neotissue growth in a perfusion bioreactor. *Biotechnol Bioeng.* **2015**, *112*, 2591-2600.
60. Shakhawath Hossain, M.; Bergstrom, D. J.; Chen, X. B. A mathematical model and computational framework for three-dimensional chondrocyte cell growth in a porous tissue scaffold placed inside a bi-directional flow perfusion bioreactor. *Biotechnol Bioeng.* **2015**, *112*, 2601-2610.
61. Nava, M. M.; Raimondi, M. T.; Pietrabissa, R. A multiphysics 3D model of tissue growth under interstitial perfusion in a tissue-engineering bioreactor. *Biomech Model Mechanobiol.* **2013**, *12*, 1169-1179.
62. Brunelli, M.; Perrault, C. M.; Lacroix, D. Short bursts of cyclic mechanical compression modulate tissue formation in a 3D hybrid scaffold. *J Mech Behav Biomed Mater.* **2017**, *71*, 165-174.
63. Zhao, F.; Mc Garrigle, M. J.; Vaughan, T. J.; McNamara, L. M. In silico study of bone tissue regeneration in an idealised porous hydrogel scaffold using a mechano-regulation algorithm. *Biomech Model Mechanobiol.* **2018**, *17*, 5-18.
64. Wang, L.; Shi, Q.; Cai, Y.; Chen, Q.; Guo, X.; Li, Z. Mechanical-chemical coupled modeling of bone regeneration within a biodegradable polymer scaffold loaded with VEGF. *Biomech Model Mechanobiol.* **2020**, *19*, 2285-2306.

Received: December 27, 2022
Revised: January 17, 2023
Accepted: February 27, 2023
Available online: March 28, 2023

Biomaterials Translational

Mechanically conditioned cell sheets cultured on thermo-responsive surfaces promote bone regeneration

Gen Wang[#], Zhangqin Yuan[#], Li Yu[#], Yingkang Yu, Pinghui Zhou, Genglei Chu, Huan Wang, Qianping Guo, Caihong Zhu, Fengxuan Han, Song Chen[*], Bin Li[*]

Key Words:
cell sheet; ECM production; mechanical loading; osteogenesis; PNIPAAm

From the Contents

ABSTRACT

Cell sheet-based scaffold-free technology holds promise for tissue engineering applications and has been extensively explored during the past decades. However, efficient harvest and handling of cell sheets remain challenging, including insufficient extracellular matrix content and poor mechanical strength. Mechanical loading has been widely used to enhance extracellular matrix production in a variety of cell types. However, currently, there are no effective ways to apply mechanical loading to cell sheets. In this study, we prepared thermo-responsive elastomer substrates by grafting poly(N-isopropyl acrylamide) (PNIPAAm) to poly(dimethylsiloxane) (PDMS) surfaces. The effect of PNIPAAm grafting yields on cell behaviours was investigated to optimize surfaces suitable for cell sheet culturing and harvesting. Subsequently, MC3T3-E1 cells were cultured on the PDMS-g-PNIPAAm substrates under mechanical stimulation by cyclically stretching the substrates. Upon maturation, the cell sheets were harvested by lowering the temperature. We found that the extracellular matrix content and thickness of cell sheet were markedly elevated upon appropriate mechanical conditioning. Reverse transcription quantitative polymerase chain reaction and Western blot analyses further confirmed that the expression of osteogenic-specific genes and major matrix components were up-regulated. After implantation into the critical-sized calvarial defects of mice, the mechanically conditioned cell sheets significantly promoted new bone formation. Findings from this study reveal that thermo-responsive elastomer, together with mechanical conditioning, can potentially be applied to prepare high-quality cell sheets for bone tissue engineering.

http://doi.org/10.12336/biomatertransl.2023.01.005

How to cite this article:
Wang, G.; Yuan, Z.; Yu, L.; Yu, Y.; Zhou, P.; Chu, G.; Wang, H.; Guo, Q.; Zhu, C.; Han, F.; Chen, S.; Li, B. Mechanically conditioned cell sheets cultured on thermo-responsive surfaces promote bone regeneration. *Biomater Transl.* **2023**, *4*(1), 27-40.

Introduction

Bone tissue engineering aims to repair or replace impaired tissues by establishing three-dimensional complex with reconstructed shape, structure and/or functions mimicking those of original tissues.[1] Currently, typical protocols of bone tissue engineering involve *in vitro* seeding and culturing cells on designed scaffolds, followed by transplanting the engineered three-dimensional tissues into defect sites to restore the original tissues.[2, 3] Although many tissues have been successfully regenerated,[4-7] including eyes,[8] skin,[9, 10] cartilage,[11, 12] liver,[13, 14] heart[15] and muscle,[16, 17] the widespread application of tissue engineering is limited by the undesired side effects, including inflammation caused by the degradation of scaffolds, internal cell necrosis due to insufficient nutrient supply, and mismatch of cell proliferation and scaffold degradation.[18-20]

To meet these challenges, scaffold-free cell sheet engineering has been developed.[21] This approach overcomes a series of barriers within conventional tissue engineering,[22] including insufficient cell adhesion rate, potential inflammation, immune

response and reduced biological activity caused by scaffold materials.[23, 24] By now, functional cell sheets have been utilised to facilitate the regeneration of many soft tissues, including periodontal ligament,[25] blood vessels,[26] cornea[27] and myocardium.[28] To prepare the cell sheets, desired cells were cultured on a substrate to form a tissue-like sheet consisting of cells and their associated extracellular matrix (ECM), which were then harvested, assembled and transplanted. Traditionally, enzymes such as trypsin have been used to harvest cells from culture dishes. However, the hydrolysis process can impair different cell surface receptors, transporters and ECM.[29] In contrast to the harmful enzymatic treatment, recovering from the surface of thermally responsive polymers can retain the structure and function of cell sheets. Currently, substrates (e.g. tissue culture dish) functionalised with thermal responsive poly(N-isopropyl acrylamide) (PNIPAAm) were widely used for cell sheets culturing.[30-32] Above its low critical solution temperature (around 32°C), PNIPAAm is slightly hydrophobic and can support cell adherence, spreading and proliferation. While it becomes hydrophilic below its low critical solution temperature, forming a hydration layer between PNIPAAm and the cultured cells. Therefore, cell sheets cultured on PNIPAAm-functionalised substrates can be easily and integrally harvested by lowering the temperature, without disturbing cell-cell contact and association between cells and ECM.[33]

Although cell sheet culturing and harvesting have been greatly improved by utilizing temperature-sensitive polymers as the substrates, applying cell sheets to the repairing of hard tissues is rarely reported due to insufficient ECM content and poor mechanical strength.[34, 35] Recently, mechanical stimulation has been reported to play a key role in cell growth.[36-38] Numerous studies have shown that mechanical stimulation can regulate the behaviour of various cells, such as differentiation of stem cells,[39, 40] anabolic and biosynthetic activity of chondrocytes,[41, 42] progression of osteoarthritis[43] and osteogenic differentiation of human bone marrow-derived mesenchymal stem cells.[44] Appropriate loading and stimulation mimicking the internal cellular micro-environment have been demonstrated to promote cell proliferation, myofiber organization,[45-47] generation of ECM,[46] gene expression and bone formation.[48, 49] In addition, cyclic mechanical strain enhances the function and development of engineered tissues by improving the production of collagen and elastin.[50] Moreover, the mechanical properties of engineered tissues can also be improved by culturing under mechanical stimulation.[43] Therefore, cell sheets with enhanced thickness and mechanical properties obtained through appropriate cyclic mechanical stimulation possess great potential for bone tissue engineering applications.

In this study, we developed elastic and stretchable poly(dimethylsiloxane) (PDMS) substrates with grafted PNIPAAm surface for intact cell sheet harvesting, and appropriate mechanical stimulation was applied to obtain cell sheets with enhanced thickness and mechanical properties (**Figure 1**). Specifically, thermo-responsive elastomer substrates treated with surface O_2-plasma-ultraviolet (UV)-initiated polymerization were used as supporting substrates to culture cell sheets. Mechanical stimulation was further applied to the substrates to enhance the ECM production and osteogenic differentiation of cell sheets before they were subsequently implanted to the mouse calvarial defect sites. This technique can be applied to potential scaffold-free bone tissue engineering applications.

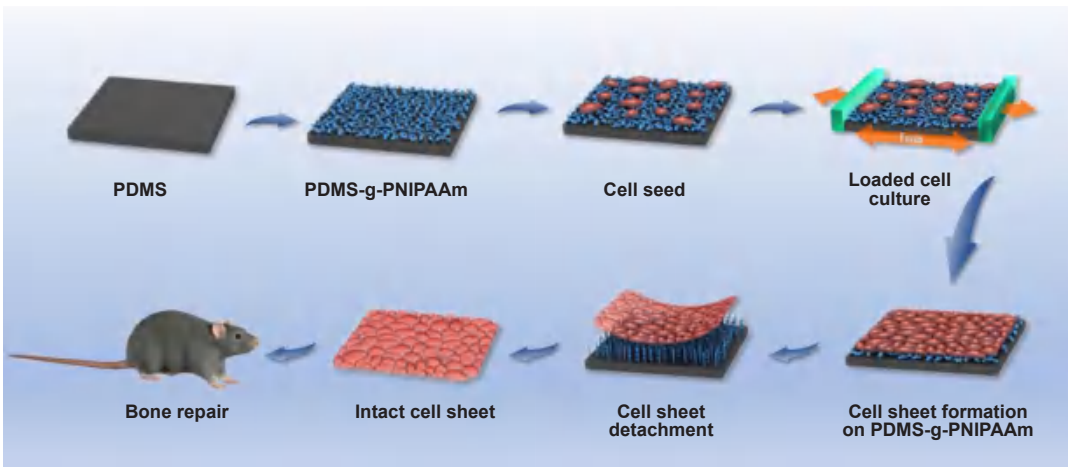

Figure 1. Schematic illustration of the preparation of cell sheets under mechanical stimulation and its implantation in a mouse calvarial defect model. Cells were cultured on the PDMS-g-PNIPAAm and then fixed in a loaded cell culture apparatus and subjected to cyclic mechanical stimulation to promote cell sheet formation. The harvested cell sheet was implanted into a calvarial defect of mouse for enhanced bone repair. PDMS-g-PNIPAAm: grafting polymerization of poly(N-isopropyl acrylamide) to poly(dimethylsiloxane).

***Corresponding authors:** Bin Li, binli@suda.edu.cn; Song Chen, chensong@suda.edu.cn.

#Author equally.

Orthopedic Institute, Department of Orthopaedic Surgery, The First Affiliated Hospital, Suzhou Medical College, Soochow University, Suzhou, Jiangsu Province, China

Methods

Preparation of thermo-responsive elastomer substrates

N-isopropyl acrylamide (NIPAAm) was purchased from J&K Scientific Ltd. (Beijing, China) and used as received PDMS (Dow Corning, Midland, MI, USA) substrates (1.5 mm thickness or specifically mentioned in the text) were prepared based on manufacturer's instruction. Briefly, PDMS precursor was mixed with curing agent (Dow Corning) with 10:1 ratio by weight, then degassed and cured in a polytetrafluoroethylene mold at 60°C overnight.

Cured PDMS substrates were fully rinsed with acetone (Yonghua Chemical Co., Ltd., Suzhou, China) and dried in vacuum oven (Shanghai Jing Hong Laboratory Instrument Co., Ltd., Shanghai, China) before grafting. The cleaned PDMS substrates were modified with oxygen plasma for 2 minutes, formed by a plasma cleaner (PDC-MG, Chengdu Mingheng Science&Thechnology Co., Ltd., Chengdu, China), to generate peroxide groups on PDMS substrates. Then the substrates were immediately immersed into NIPAAm aqueous solution with desired concentration and irradiated with UV lamp (500 W) to generate radicals to initiate grafting polymerization of PNIPAAm on PDMS substrates (PDMS-g-PNIPAAm). After 30 minutes, the substrates were cleaned with ultrapure water and dried with the blower. In this study, the polymerization was conducted with NIPAAm concentrations of 0.05 M, 0.1 M and 0.2 M to fabricate PDMS-g-PNIPAAm substrates with low, medium and high grafting yields, respectively (PDMS signify non-grafted PDMS substrate; gPDMS-L, gPDMS-M and gPDMS-H signify PDMS-g-PNIPAAm substrate with low, medium and high grafting yield, respectively).

Attenuated total reflectance Fourier transform infrared spectroscopy analysis

PDMS-g-PNIPAAm surfaces were analysed using attenuated total reflectance Fourier transform infrared spectroscopy (Thermo Fisher Scientific, Waltham, MA, USA) in a wave number range of 650–4000 cm^{-1}. Thirty-six scans were performed for each sample and OMNIC 8.2 software (Thermo Fisher Scientific) was used to process the data. The absorbance ratio between the height of peaks at 1650 cm^{-1} (PNIPAAm amide I) and 2962 cm^{-1} (PDMS methyl absorbance) was calculated to determine the relative grafting yield, as previously described.[51]

PDMS-g-PNIPAAm morphology observation

PDMS-g-PNIPAAm substrate with different grafting yields and pristine PDMS substrates were examined with a scanning electron microscope (SEM; Quanata250, FEI Company, Hillsboro, OR, USA). SEM imaging was performed with an acceleration voltage determined by smart SEM software (XT microscope Server, FEI Company). For analysis of the chemical composition on the substrates, energy dispersion spectrum (AMETEK, San Diego, CA, USA) was also performed. Atomic force microscopy (AFM; Bruker BioSpin, Billerica, MA, USA) imaging was conducted to analyze the surface morphology and surface roughness. AFM images were acquired by tapping mode in air with silicone tip cantilevers with imaging size of 10 μm × 10 μm scans at a scan rate of 0.2 Hz. The roughness of the samples was reported as root-mean-square roughness values.

Contact angle measurements

Sessile drop method[52, 53] was used to analyze the static water contact angles on PDMS-g-PNIPAAm and pristine PDMS substrates using a KRUSS DSA25 contact angle equipment (KRÜSS, Hamburg, Germany). The substrates were rinsed with a large amount of 75% ethanol and dried in vacuum drying chamber before testing. ImageJ v1.8.0 software (National Institutes of Health, Bethesda, MD, USA)[54] was applied to determine contact angles.

To study the thermal responsiveness of PDMS-g-PNIPAAm samples, the water contact angles were measured in a temperature-controlled environmental chamber. Contact angles were taken at 4°C and 37°C. The chamber temperature was first equilibrated for 10 minutes and then a drop of water was dropped on the samples to measure the water contact angle. The values of contact angle were tested in at least three areas for each sample.

Cell sheet culture

Mouse pre-osteoblast cells (MC3T3-E1, subclone 14, RRID: CVCL_0409) were bought from Cell Bank (Chinese Academy of Sciences, Shanghai, China) and cultured in alpha-minimum essential medium (HyClone, Logan, UT, USA) supplemented with 10% fetal bovine serum (HyClone) at 37°C and under a humidified 5% CO_2 atmosphere. The medium was replaced once every 2 days.

For cell sheet culturing, PDMS-g-PNIPAAm samples were first soaked in 75% ethanol for 2.5 hours and then exposed to fume hood ultraviolet light for 30 minutes. After sterilization, the samples were repeatedly cleaned with phosphate buffered saline (PBS) and coated with fibronectin by soaking in 20 μg/mL fibronectin (F8141-1MG, Sigma, St. Louis, MO, USA) in PBS overnight. The PDMS-g-PNIPAAm substrates were then placed in a PDMS cell culture dish fabricated according to our customised mold of similar cube box that was 6.0 cm in length, 3.0 cm wide and 2.0 cm high. MC3T3-E1 cells were inoculated on each substrate with a density of 360,000 cells (20,000 cells/cm^2). After the cells were passaged at 50% confluence, a group of samples was fixed in loaded cell culture system (Suzhou Haomian Precision Technology Co., Ltd., Suzhou, China) and further cultured under the loaded condition (loaded) for 3 days, while other samples were continuingly cultured under original static condition (static). A loaded cell culture system was utilised to apply dynamic mechanical stimulation to the cultured cell sheets by stretching the cell-attached elastic substrates cyclically. In this study, we applied uniaxial loading with 5% strain at a frequency of 0.5 Hz for 4 hours/day on cell sheets, according to previous studies.[55, 56] Cells under static condition were defined as the control group.

Cell proliferation assay

Cell counting kit-8 (NCM Biotech, Suzhou, China) was utilised to analyse the proliferation of MC3T3-E1 cells cultured on PDMS-g-PNIPAAm substrate with the highest grafting yield after mechanical stimulation. Cells were cultured under both loaded and static conditions. After 1, 2, 3, 4 and 5 days, Cell

counting kit-8 was performed according to the instructions. The absorbance was measured spectrophotometrically using a microplate reader (BioTek, Winooski, VT, USA) at wavelength of 450 nm.

Cell morphology observation

Cytoskeleton staining was applied to observe the morphology of cells cultured under different culture conditions. After culturing for 1, 3 and 5 days, MC3T3-E1 cells were fixed in 4% paraformaldehyde at 37°C for 30 minutes. The samples were then stained for actin with phalloidin (1:250, Cat# 40735ES75, Yeasen Biotechnology, Shanghai, China) and stained for nuclei with 4′,6-diamidino-2-phenylindole (1:1000, Beyotime, Shanghai, China). After staining, images of cytoskeleton staining were visualised via fluorescence microscopy (Zeiss Axiovert 200, Carl Zeiss Inc., Thornwood, NY, USA).

The same way was also performed after cell sheet detachment for observing the morphology change after detachment.

Cell sheet harvesting

After 7 days of culturing, cell sheets were detached from the substrate and harvested by lowering the temperature from 37°C to 4°C in 10 minutes to initiate a thermal responsive change of PNIPAAm and detachment of cell sheets. The processes of cell sheet detachment and morphology change during detachment were imaged using a Nikon TMS inverted microscope (Japan) and recorded by a computer.

Cell viability in the cell sheet was determined using the live/dead viability cytotoxicity kit (C16702, Yeasen Biotechnology). After detachment, cell sheets were rinsed with PBS. The resultant cell sheets were incubated in the staining solution (2 μL Calcein-AM and 8 μL ethidium homodimer-1 in 2 mL PBS) for 1 hour. Fluorescence microscopy was used to image the cell sheets after detachment.

Determination of the extracellular matrix production

Measurement of total proteins and DNA content of cell sheets was used to determine the ECM production. Briefly, cell sheets under different culture conditions were collected for extracting protein and DNA, respectively, after mechanical stimulation. Total proteins were extracted from cell sheets under different culture conditions using a tissue or cell total protein extraction kit (Sangon Biotech, Shanghai, China) according to the manufacturer's protocol. These proteins were quantified using a bicinchoninic acid protein assay kit (Beyotime). What's more, a cell/tissue DNA kit was used for DNA extraction (Yeasen Biotechnology) and concentration was measured using NanoDrop 2000 spectrophotometers (Thermo Fisher Scientific).

Evaluation of cell sheets thickness

The thickness of cell sheets under different culture conditions was evaluated via section staining imaging and SEM imaging. The cell sheets were fixed in 4% paraformaldehyde for 30 minutes at room temperature and then dehydrated at 10%, 30%, 50%, 70%, 85%, 90%, and 100% alcohol for 10 minutes each time subsequently. The cell sheets were embedded in paraffin for hematoxylin and eosin (H&E) and Masson staining (Solarbio, Beijing, China), respectively. After staining, the cell sheet sections were imaged using a bright field microscope (Carl Zeiss Inc.). The images were analysed using ImageJ to determine the thickness of cell sheets. Each image of cell sheet section was measured at 200 points, and at least three samples per each test were taken for statistical analysis.

For SEM, after fixation and dehydration, the cell sheets were dried using a critical point dryer (Cat# CPD030, Leica, Wetzlar, Germany). The samples were then sputter coated with gold for 30 seconds using an Ion Sputter (SC7620, Quorum Technologies, Lewes, UK).

Reverse transcription quantitative polymerase chain reaction

Reverse transcription quantitative polymerase chain reaction was tested to study the gene expression of type I collagen (Col I), Runt-related transcription factor 2 (Runx2) and osteopontin (OPN) from MC3T3-E1 cells that were cultured under different conditions. Total RNA was extracted using TRIzol reagent (Invitrogen, Carlsbad, CA, USA). Complementary DNA was synthesised from 1 μg of total RNA using IScript™ cDNA synthesis kit (Bio-Rad, Hercules, CA, USA). The housekeeping gene β-actin was used as an internal control and the relative changes in mRNA levels were analysed by the $2^{-\Delta\Delta CT}$ method. Sequences of primers for the target genes are listed in **Table 1**.[57]

Table 1. Primers sequences used for reverse transcription quantitative polymerase chain reaction

Gene	Forward (5′–3′)	Reverse (5′–3′)
Col I	CCT AGC AAC ATG CCA ATC TTT ACA	TTG TCC ACG CGG TCC TCT
Runx2	CCA ACC CAC GAA TGC ACT ATC	TAG TGA GTG GTG GCG GAC ATA C
OPN	TGA GAC TGG CAG TGG TTT GC	CCA CTT TCA CCG GGA GAC A
β-Actin	TTC AAC ACC CCA GCC ATG T	GTG GTA CGA CCA GAG GCA TAC A

Note: Col I: type I collagen; OPN: osteopontin; Runx2: Runt-related transcription factor 2.

Western blot analysis

Western blotting was applied to quantify protein expression. Briefly, cells were rinsed with PBS and then lysed in extraction buffer and phenylmethylsulfonyl fluoride. Cell extracts were centrifuged at 4°C for 10 minutes, and the supernatants were then collected. The protein concentration of cells was measured using bicinchoninic acid protein quantification kit (Beyotime). The same amounts of the samples were separated using 10% sodium dodecyl sulfate-polyacrylamide gel electrophoresis (Beyotime), and then transferred to

nitrocellulose membranes (Beyotime). The membranes were blocked with 5% skim milk, using PBS with 0.05% Tween-20 for 2 hours. The membranes were then probed successively with Col I, Runx2, OPN and β-actin at 4°C overnight. The membranes were washed and then incubated with the respective horseradish peroxidase-conjugated secondary antibodies (LI-COR, Lincoln, NE, USA) for 1 hour at room temperature. Proteins were detected by autoradiography (Bio-Rad). The primary antibodies used in this study are listed in **Table 2**.

Table 2. Antibodies for western blot analyses

Antibody	Species	Concentration	Catalog number	RRID number	Source
Col I	Mouse	1:1000	ab6308	AB_305411	Abcam, Cambridge, UK
Runx2	Rabbit	1:1000	ab76956	AB_156595	Abcam, Cambridge, UK
OPN	Rabbit	1:1000	ab63856	AB_1524127	Abcam, Cambridge, UK
β-Actin	Mouse	1:1000	ab8226	AB_306371	Abcam, Cambridge, UK
Goat anti-rabbit horseradish peroxidase secondary antibody	Goat	1:10000	926-80011	AB_2721264	LI-COR, Lincoln, NE, USA
Goat anti-mouse horseradish peroxidase secondary antibody	Goat	1:10000	926-80010	AB_2721263	LI-COR, Lincoln, NE, USA

Note: Col I: type I collagen; OPN: osteopontin; Runx2: Runt-related transcription factor 2.

In vivo experiments

All procedures followed the National Research Council's Guide for the Care and Use of Laboratory Animals[58] and were approved by the Institutional Animal Care and Use Committee of Soochow University (ECSU-201700041) on August 1, 2017. Twenty-four male C57BL/6J mice (specific-pathogen-free level, 8 weeks old, 250 ± 5 g, Hangzhou Ziyuan Experimental Animal Technology Co., Ltd., license No. SCXK (Zhe) 2019-0004) were randomly divided into three groups (each group included eight samples). After mice were anaesthetized, a 4 mm diameter drill was then used to penetrate the left side of the entire calvarial to create defects. After filling the defect with cell sheets, the skin was tightly sutured. The skull samples were harvested at 4 and 8 weeks and fixed by 4% paraformaldehyde for 24 hours. The fixed mouse calvarial samples were analysed using a micro-computed tomography system (SkyScan 1176, SkyScan, Aartselaar, Belgium) at a voltage of 50 kV and an electric current of 50 μA. Three-dimensional reconstruction was performed using Mimics 15.0 software (Bruker BioSpin, Billerica, MA, USA) and calculating bone volume/tissue volume by using CTAn v1.12 software (Bruker BioSpin). All samples were immersed in decalcifying solution and the solution was changed every day for 2 weeks. These skull tissues were dehydrated with graded dehydration and embedded in paraffin before being sectioned into 6-μm thick slices. After deparaffinised and rehydrated, the slices were stained with H&E staining kits according to manufacturer's instructions.

Statistical analysis

All data are expressed as the mean ± standard deviation (SD). Statistical analyses were performed by SPSS software (24.0, IBM Corp., Armonk, NY, USA) to determine the statistically significant differences among different groups. Statistical analyses including Student's *t*-test and one-way analysis of variance followed by Tukey's *post hoc* analysis were performed for two-group and multi-group comparisons, respectively. A significant difference was defined as a value of $P < 0.05$.

Results

Fabrication of PDMS-g-PNIPAAm substrates

PDMS-g-PNIPAAm substrates with different grafting yields were prepared by UV-initiated polymerization. This method is facile and the grafting yield of PNIPAAm can be easily controlled by adjusting the parameters like monomer concentration, UV radiation time, and temperature (**Additional Figure 1**). The surface morphology of PDMS-g-PNIPAAm substrate with different grafting yields was analysed using SEM and AFM (**Figure 2**). In general, the roughness of the surface increased after the modification. As shown in **Figure 2A** and **Additional Figure 2**, the pristine PDMS surface was clean and smooth, and the energy dispersion spectrum spectra revealed the peaks of carbon, oxygen and silicon. In comparison, the surfaces of PDMS, gPDMS-L, gPDMS-M and gPDMS-H substrate all showed uneven and wrinkled structures, and the structures became more evident with higher grafting yields. The gPDMS-H substrate showed the most wrinkled surface. The energy dispersion spectrum spectra showed nitrogen elements in addition to carbon, oxygen and silicon, demonstrating the successful grafting of PNIPAAm on the PDMS substrate. In addition, the SEM image of the cross section of the substrate (**Figure 2B**) showed that there was a clear thin layer of grafted PNIPAAm on the PDMS-g-PNIPAAm substrate, and the thickness increased with the increase of graft yields.

The surface morphology and roughness of the substrates were also analysed using AFM (**Figure 2C**). It was apparent that the PDMS-g-PNIPAAm substrate with higher grafting yield showed more uneven and corrugated structures. The surface roughness of PDMS, gPDMS-L, gPDMS-M and gPDMS-H substrate was measured to be 23.9 nm, 102 nm and 273 nm, respectively, which were evidently higher than 7.07 nm of pristine PDMS substrate.

Attenuated total reflectance Fourier transform infrared spectroscopy results showed the characteristic structures of the PDMS-g-PNIPAAm substrate with different grafting yields. As shown in **Figure 2D**, attenuated total reflectance

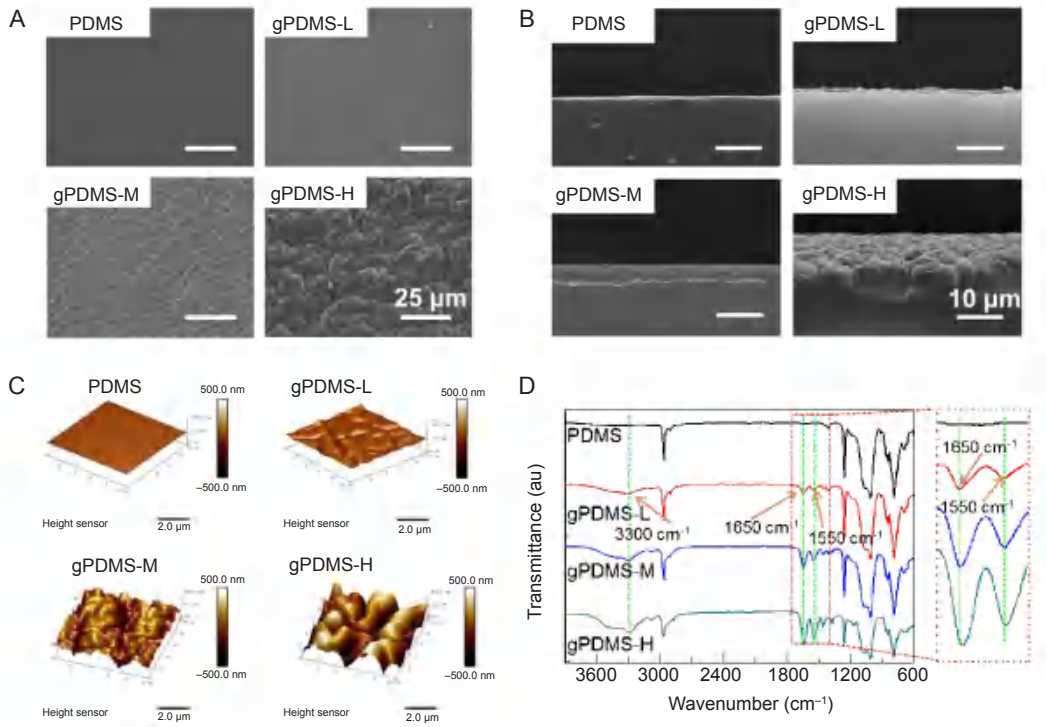

Figure 2. Microstructure of non-grafted PDMS substrate and PDMS-g-PNIPAAm substrate with different grafting yields. (A–D) SEM images (A), SEM images of the cross section (B), AFM images (C), and ATR-FTIR spectra (D) of the surfaces of PDMS, gPDMS-L, gPDMS-M and gPDMS-H substrates ($n \geq 3$). Scale bars: 25 μm (A), 10 μm (B), 2.5 μm (C). gPDMS-L, gPDMS-M and gPDMS-H indicate PDMS-g-PNIPAAm substrate with low, medium and high grafting yield, respectively. AFM: atomic force microscopy; ATR-FTIR: attenuated total reflectance Fourier transform infrared spectroscopy; au: arbitrary unit; PDMS: poly(N-isopropyl acrylamide); PDMS-g-PNIPAAm: grafting polymerization of poly(N-isopropyl acrylamide) to poly(dimethylsiloxane); SEM: scanning electron microscope.

Fourier transform infrared spectroscopy spectra of PDMS-g-PNIPAAm substrate with different grafting yields all revealed the presence of two new strong absorbance peaks at 1550 cm^{-1} and 1650 cm^{-1}. The former can be assigned to the C=O stretching vibration of an amide group, while the latter to N–H deforming vibration of the amide group. Also, a broad peak appears at ~3300 cm^{-1} that can be attributed to the N–H stretching vibration.[31, 59] These results demonstrated that the PNIPAAm has been successfully grafted on the surface of PDMS substrate. Moreover, it was observed that the height of peaks at 1550 cm^{-1}, 1650 cm^{-1} and 3300 cm^{-1} increased in accordance with increasing grafting yields, indicating more PNIPAAm was grafted on PDMS substrates with higher monomer concentration during polymerization.

The detachment of cell sheets from PDMS-g-PNIPAAm substrates

The MC3T3-E1 cells were cultured at 37°C and detached at 4°C, therefore, the water contact angles of PDMS-g-PNIPAAm substrates were measured at 4°C and 37°C to evaluate their thermal response. The PDMS was hydrophobic, with water contact angles around 110° at 4°C and 37°C (**Figure 3A** and **B**). With PNIPAAm grafted, the PDMS-g-PNIPAAm substrates showed lower water contact angles (70°) than pristine PDMS at 37°C and the contact angles significantly decreased from 70° (hydrophobic) to 50° (hydrophilic) when lowering the temperature to 4°C. For PDMS-g-PNIPAAm substrates with high grafting yield, the most significant change of contact angle was observed, indicating their most evident thermal responsiveness, which makes them the most suitable for cell sheet detachment.

Subsequently, the detachment of cell sheets from PDMS-g-PNIPAAm substrate with different grafting yields was investigated (**Figure 3C**). The cell sheets began to detach by folding gradually from the edge of the substrate to the intermediate region, and continued to take place over time. The grafting facilitates the detachment of the cell sheets, as shown in **Figure 3C**, the substrate with the highest grafting yield detached much faster in comparison to other groups. The cell sheet on the PDMS-g-PNIPAAm substrate with the highest grafting yield finally migrated out of the view of microscope after 18 minutes. Then cell sheet was utterly detached and intact cell sheet could be obtained after 30 minutes. By contrast, the cell sheet remained firmly attached to PDMS substrate throughout the process. For PDMS-g-PNIPAAm substrates with low and medium grafting yields, effective detachment of cell sheets was not observed and intact cell sheets could not be harvested. The results indicated that the PDMS-g-PNIPAAm substrates with high grafting yield are most suitable for cell sheet detachment, therefore are selected for the following studies.

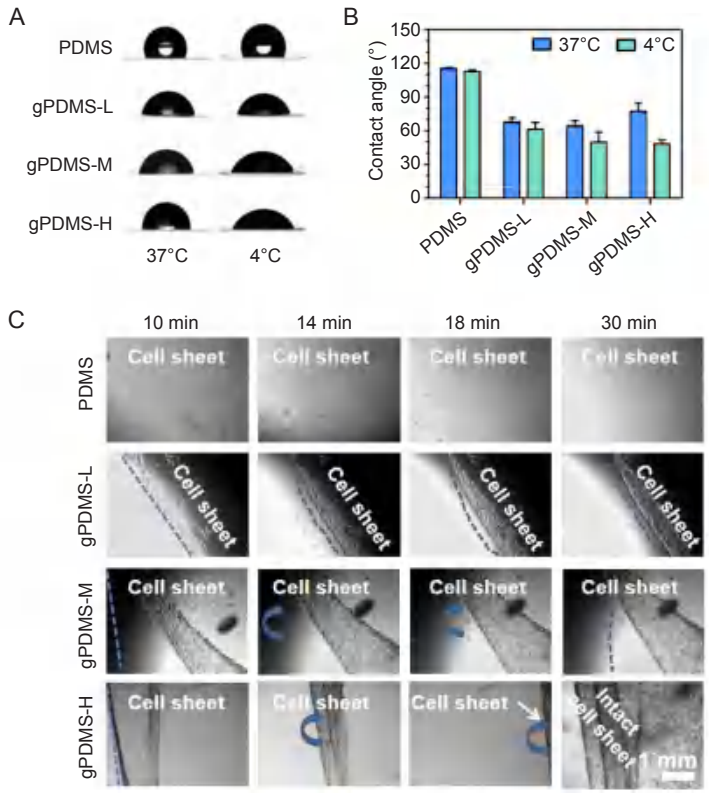

Figure 3. Temperature sensitivity of PDMS-g-PNIPAAm substrates. (A, B) The images of water contact angle (A) and water contact angle measured (B) on PDMS, gPDMS-L, gPDMS-M and gPDMS-H substrates with different grafting yields at 37°C and 4°C. Data are expressed as the mean ± SD ($n \geq 3$). (C) Detachment of cell sheets from the PDMS, gPDMS-L, gPDMS-M and gPDMS-H substrates after incubating at 4°C for 10, 14, 18 and 30 minutes. Blue dotted lines indicate the dividing line between the adhesion area and the detachment area of the cell sheet. Blue arrows indicate the direction of the detachment of the cell sheet. Scale bar: 1 mm . gPDMS-L, gPDMS-M and gPDMS-H indicate PDMS-g-PNIPAAm substrate with low, medium and high grafting yield, respectively. PDMS: poly(N-isopropyl acrylamide); PDMS-g-PNIPAAm: grafting polymerization of poly(N-isopropyl acrylamide) to poly(dimethylsiloxane).

Cell sheets culture under mechanical conditioning

MC3T3-E1 cells were cultured on PDMS-g-PNIPAAm substrates with high grafting yield to study the effect of mechanical stimulation on cell growth. **Figure 4A** showed the cell proliferation results at 1, 2, 3, 4, 5, 6 and 7 days obtained by cell counting kit-8 assay. Compared with the static group, the group with mechanical stimulation demonstrated higher optical density values, indicating enhanced proliferation under loaded condition. Cytoskeletal staining images showed that cells were able to adhere and proliferate well under both static and loaded conditions (**Figure 4B**).

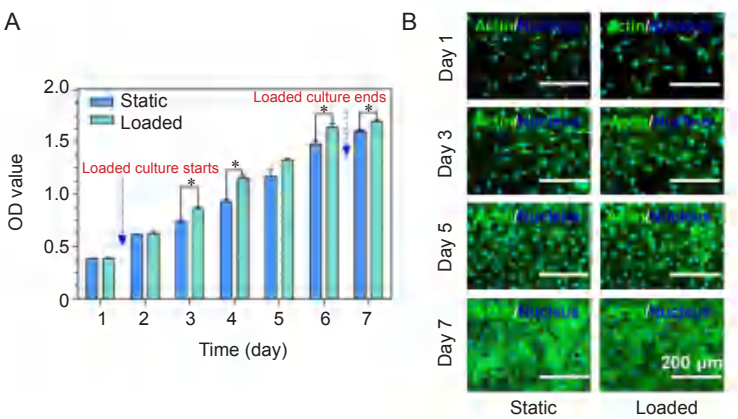

Figure 4. Loaded culture of cell sheets. (A) Cell proliferation under static or loaded conditions. Data are expressed as the mean ± SD ($n = 3$). *$P < 0.05$ (Student's *t*-test). (B) F-actin staining (green) of MC3T3-E1 cells under static or loaded conditions. Scale bars: 200 μm. OD: optical density.

The detachment of cell sheets after loaded culture

After mechanical stimulation, cell sheet detachment in both groups was studied. Intact cell sheets could be harvested in loaded group by lowering the temperature from 37°C to 4°C (**Figure 5A**). With the increase of time, the cell sheet gradually detached from the surface. The complete detachment time of the cell sheet in loaded group was slightly longer (~45 minutes) than that of static group, which might be attributed to enhanced thickness and strength due to mechanical stimulation. Cytoskeletal staining images showed the morphologies of cell sheets, before and after detachment. Before detachment, cells adhered to the substrate with flat and spread shape, and mutual extrusion were found to overlap (**Figure 5B**). Upon detachment, the shape of cells changed to spherical or ovoid due to loss of adhesion sites. Live/dead staining was conducted to study the cell viability (**Figure 5C**). The images showed that nearly all cells were dyed green both before and after detachment, indicating the viability of cells after detachment.

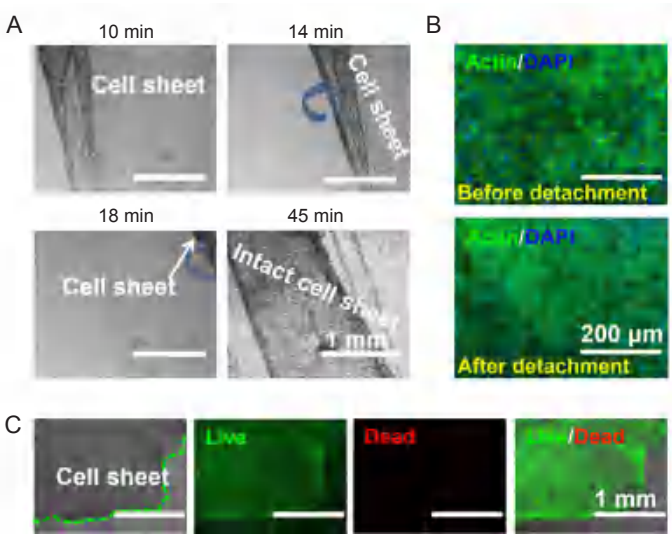

Figure 5. Cell sheets detachment after mechanical stimulation (n = 3). (A) Detachment of cell sheets from the PDMS-g-PNIPAAm surface of high grafting yield after incubation at 4°C for 10, 14, 18 and 45 minutes. Blue arrows indicate the direction of the detachment of the cell sheet. (B) F-actin staining (green) of cell sheets before and after detachment. (C) Live/dead staining of cell sheets after detachment. The cell sheets were cultured under loaded condition to confluence. Green dotted lines indicate the dividing line between the cell sheet and the blank area. Scale bars: 1 mm (A, C), 200 μm (B). PDMS-g-PNIPAAm: grafting polymerization of poly(N-isopropyl acrylamide) to poly(dimethylsiloxane).

Effect of mechanical stimulation on ECM production of cell sheets

To determine if mechanical stimulation can promote ECM production, we characterised the thickness of the cell sheets cultured under static and loaded conditions. Cytoskeleton staining images showed that cells were uniformly dispersed within the cell sheet under both static and loaded conditions (**Figure 6A**), and no significant difference was observed between the groups. Under H&E staining, the thickness of cell sheets in loaded group is significantly larger than static group (**Figure 6B** and **C**). Masson staining revealed that the thickness of cell sheets under loaded condition was thicker than that under static condition (**Additional Figure 3**). The same result can also be observed in the SEM images. Furthermore, cell sheets obtained from loaded group showed more cell-to-cell junction and ECM content than static group (**Figure 6D**). Moreover, the ratio between total protein and total DNA of loaded group was also higher than static group, suggesting more ECM content density in loaded group (**Figure 6E–G**).

Effect of mechanical stimulation on osteogenic differentiation

The expression of osteogenic-specific genes (*Col I*, *Runx2*, and *OPN*) in cell sheets was examined using reverse transcription quantitative polymerase chain reaction (**Figure 7A–C**). The results showed that at 3 days, the expression of *Col I* and *Runx2* was higher in the loaded group than the static group, while the expression of *OPN* has no difference. The reason is that *Col I* and *Runx2* are mainly expressed during early osteogenesis, while *OPN* is generally expressed during late osteogenesis.[60] After culturing for 7 days, all the genes were expressed more in the loaded group. Western blot analysis further confirmed that the production of Col I, Runx2 and OPN proteins was significantly higher in the loaded group at 7 days (**Figure 7D**).

***In vivo* bone formation capacity**

The critical calvarial defect is used to evaluate *in vivo* bone formation capacity of cell sheets after mechanical stimulation. After implantation for 4 weeks and 8 weeks, new bone formation is analysed by micro-CT and H&E staining (**Figure 8**). At 4 weeks, as shown in the micro-CT results (**Figure 8A** and **B**), loaded group exhibited better bone formation ability with higher bone volume/tissue volume value in comparison to control and static groups. At 8 weeks, notable new bone formation was observed in the loaded group. In contrast, less new bone tissue was observed at the peripheral part of the

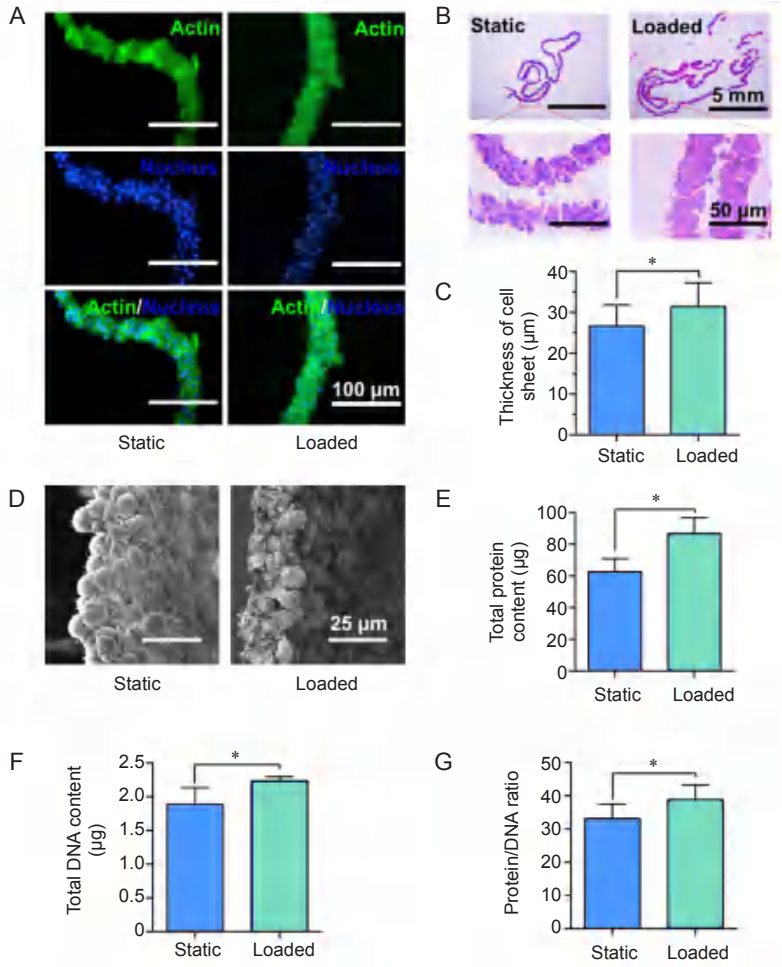

Figure 6. Thickness of cell sheets and extracellular matrix production under static and loaded conditions. (A, B) Cytoskeleton staining images (A) and hematoxylin and eosin staining images (B) of cell sheet sections. (C) Statistical analysis of the cell sheet thickness. (D–G) Scanning electron microscope images (D), the total protein contents (E), the total DNA contents (F) and the content ratio of protein to DNA of cell sheets (G) after culturing for 7 days. Scale bars: 100 μm (A), 5 mm (B upper), 50 μm (B lower), 25 μm (C). Data are expressed as the mean ± SD (n = 3). *P < 0.05 (Student's t-test).

defects in static and control groups (**Figure 8A**). Moreover, the loaded group showed the highest bone volume/tissue volume value (**Figure 8B**). H&E staining showed that the loaded group had much more new bone formation than the control group and the group with cell sheets alone (**Figure 8C**). The most obvious calcium deposition was observed in the loaded group at 8 weeks, and the newly formed bone in this group began to grow from the periphery to the middle.

Discussion

As a scaffold-free method, cell sheet engineering provides a promising approach to bone tissue engineering by avoiding scaffold-associated issues like insufficient cell adhesion, probable immune rejection and so on. Generally, the most widely used substrate for cell sheet culturing is rigid culture dish grafted with thermal responsive PNIPAAm and the intact cell sheet is harvested by lowering the temperature. However, except for integrity, thickness, toughness and abundant ECM are important for the application of cell sheets as well. Therefore, in this study, we aim to introduce mechanical stimulation to promote ECM production and bone formation potential of cell sheets.

At present, the most established technology for the preparation of PNIPAAm thermosensitive surface is based on the polymerization initiated by electron beam.[29] However, electron beam irradiation requires expensive equipment. Hence, as an alternative to electron beam radiation, UV radiation was widely used to graft PNIPAAm onto surfaces.[61] Most cell sheets were currently cultivated on solely PNIPAAm-grafted cell culture dishes. Additional treatments are required in terms of different targeted tissues. E.g., patterned surfaces are developed in order to generate heterotypic tissues,[62] and in order to generate more ECM, mechanical stimulation is applied.[63] However, conventional substrates are generally stiff and unstretchable, elastic and stretchable PDMS substrates are admirable to apply mechanical stimulation. The stiffness can also influence cell mechanobiological behaviours, such as cell adhesion, proliferation, and differentiation.[64] In a previous study, elastic PDMS substrates have been grafted with thermal

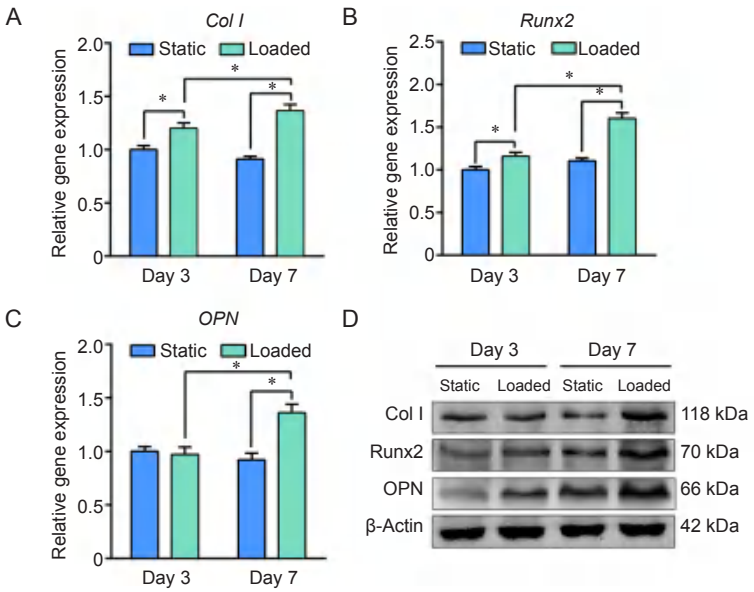

Figure 7. Effect of mechanical stimulation on the osteogenesis of MC3T3-E1 cells. (A–C) Gene expression of type I collagen (*Col I*), Runt-related transcription factor 2 (*Runx2*) and osteopontin (*OPN*) using β-actin as housekeeping gene and the static group as control. Data are expressed as the mean ± SD ($n = 3$). *$P < 0.05$ (Student's *t*-test). (D) Western blot analysis of Col I, Runx2 and OPN protein expression.

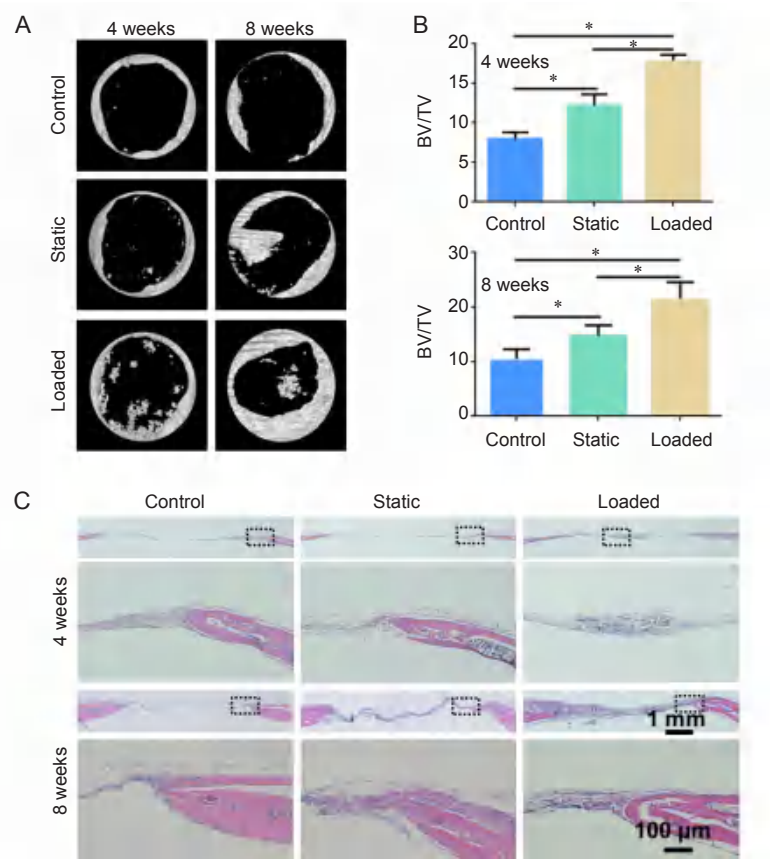

Figure 8. Bone formation of cell sheets in the calvarial defects of mice at 4 and 8 weeks, respectively. (A) Three-dimensional reconstruction images. (B) BV/TV at 4 and 8 weeks. Data are expressed as the mean ± SD ($n = 4$). *$P < 0.05$ (one-way analysis of variance followed by Tukey's *post hoc* analysis). (C) Overview and magnified images of the sections stained with hematoxylin and eosin. Scale bars: 1 mm, 100 μm (enlarged images). BV/TV: bone volume/tissue volume.

responsive PNIPAAm by adsorption of photo-initiator and subsequent initiation of grafting polymerization by UV radiation.[65] In this study, PDMS-g-PNIPAAm was prepared by UV-initiated polymerization. The results showed that PDMS-g-PNIPAAm substrates changed from 70° to 50° when the temperature lowered from above 37°C to 4°C (**Figure 3A** and **B**), and the more significant change was found for the substrate with the highest grafting yield, due to more PNIPAAm on the substrates, which makes them the most suitable for cell sheet detachment.

The surface properties of substrates were reported to significantly affect the cell behaviours. For example, fibroblasts spread and proliferate better on PDMS with lower PNIPAAm-grafted yield when treated with gelatin coating, while osteoblasts and mesenchymal stem cells proliferate better on surfaces with higher grafting yields and no gelatin coating.[65, 66] The PNIPAAm-grafted yield was also shown to affect cell detachment.[65] Therefore, cell behaviour on different PDMS-g-PNIPAAm substrates was studied by culturing MC3T3-E1 cells on the substrates. For all the substrates, we found cells could attach and proliferate well on all the substrates without significant differences. However, cell sheets showed different detachment behaviour on PDMS-g-PNIPAAm substrates. For the ones with high grafting yield, the cell sheets could easily detach from the substrate and remain intact after detachment (**Figure 3C**). As mentioned above, substrates with high grafting yield are more sensitive to temperature and more helpful for cell detachment. Our results are in agreement with previous reports on the impacts of grafting yields of PNIPAAm on the detachment behaviour of cell sheets.[67] Therefore, in the following studies, we used the substrates with high grafting yields for their favourable cell detachment behaviour.

Except for the integrity of cell sheets, thickness, toughness and abundant ECM is also important for bone repair. Recently, numerous studies demonstrated the critical impacts of mechanical loading on cell-ECM interactions and ECM formation, in addition to the chemical composition and structure of ECM.[68] Therefore, we hypothesised that cell sheets with enhanced ECM content and strength could be achieved by applying dynamic mechanical stimulation during culturing. The elasticity of PDMS-g-PNIPAAm substrates allows dynamic mechanical stimulation by cyclic stretching of the elastic substrates during cell sheet culturing. Previous work in our laboratory showed that mechanical stretching with the condition of 5% strength, 0.5 Hz, and 4 hours/day, could promote the secretion of ECM and expression of osteogenic-specific genes. The results showed the enhanced thickness for the cell sheets cultured under loaded condition than static condition (**Figure 6A–C** and **Additional Figure 3**). Furthermore, cell sheets cultured under loaded condition seemed to show more cell-to-cell junction and denser ECM (**Figure 6D**). The total protein weight of cell sheet cultured under loaded condition was much higher than static condition (**Figure 6E**). These results indicate that more ECM was formed in the cell sheets after mechanical stimulation. This is in accordance with previous report,[68] showing appropriate mechanical stimulation significantly promotes cell proliferation and ECM secretion.

Several studies have indicated that the expression of various genes in cells could be regulated by applying mechanical stimulations.[43, 49] With hydrostatic pressure and uniaxial compression, MSCs showed enhanced chondrogenic expression, while application of tensile strain enhanced osteogenic expression.[44] The effects of cyclic mechanical stretching on osteogenic differentiation of human intraoral MSCs and expression of osteogenic genes in MC3T3-E1 osteoblasts cells were investigated. The results show that mechanical stimulation can significantly increase osteogenic gene expression and bone formation.[69] In this study, a significant up-regulation of the osteogenic differentiation markers genes *Col I*, *Runx2*, and *OPN* was observed in cell sheets cultured under mechanical stimulation, compared with that cultured under static conditions (**Figure 7**). The higher expression levels of Col I and OPN indicate a higher level of calcification stage. Even single mechanical stimulation up-regulated osteogenic transcription factor Runx2, both in the reverse transcription quantitative polymerase chain reaction and western blot. This over-expression of the transcription factor in mechanically stimulated groups provides evidence that stimulation by cyclic strain promoted MC3T3-E1 differentiation. It has also reported that dynamic stretching of the substrate can cause fluid-induced wall shear stress on cells,[70, 71] which could influence osteogenesis.[72] From our point of view, there might be some wall shear stress at a low level, but the major effect of mechanical-induced osteogenesis is due to mechanical strain. Finally, *in vivo* experiment further indicated the cell sheets prepared under mechanical stimulation had superior bone formation capacity as well (**Figure 8**). In all, we showed that cyclic mechanical stimulation could significantly up-regulate the expression of osteogenic genes, *Col I*, *Runx2*, and *OPN*, and thereby stimulate the differentiation of MC3T3-E1 and further bone formation. Compared to other scaffolds, our scaffold-free cell sheets not only avoid the inflammation caused by degradation of scaffolds and mismatch of cell proliferation, but also generate abundant ECM by applying mechanical stimulation to cells. This study indicates the great potential of mechanically conditioned cell sheets to be used as synthetic bone graft substitutes. The effects of different types and magnitude of the forces on the cell sheets preparation need to be further investigated.

In this study, we successfully prepared a thermal responsive and elastic PDMS-g-PNIPAAm substrate by grafting PNIPAAm on elastomeric using O_2-plasma-UV initiated graft polymerization, to study the effects of cyclic mechanical stimulation on cell sheets engineering. MC3T3-E1 cells proliferated well on PDMS-g-PNIPAAm substrates, and intact cell sheets could be easily harvested by lowering the temperature from PDMS-g-PNIPAAm substrates with the highest grafting yield. Cell culture experiment demonstrated that the thickness and the ECM content of cell sheets were remarkably enhanced with mechanical stimulation, and the expression of osteogenic genes and bone formation were significantly promoted. This provides a feasible and facile approach to enhance the properties of engineered cell sheets, and can be further applied with cell sheet engineering techniques for potential scaffold-free tissue engineering applications.

Author contributions

BL and SC conceived and designed the study; GW, ZY, LY, YY, PZ, GC, HW, QG, CZ, and FH performed the experiments and data analysis; GW, ZY, LY, SC and BL wrote the manuscript with input from all coauthors. All authors have read and approved the final version of the manuscript.

Financial support

This work was financial supported bythe National Natural Science Foundation of China (No. 81925027), and the Priority Academic Program Development of Jiangsu Higher Education Institutions.

Acknowledgement

None.

Conflicts of interest statement

The authors declare that no competing interests exist.

Editor note: Bin Li is an Editorial Board member of *Biomaterials Translational*. He was blinded from reviewing or making decisions on the manuscript. The article was subject to the journal's standard procedures, with peer review handled independently of this Editorial Board member and his research group.

Additional files

Additional Figure 1: Effect of NIPAAm monomer concentration, polymerization temperature, polymerization time and distance from UV source on grafting yield of PDMS-g-PNIPAAm surface.

Additional Figure 2: Energy dispersion spectrum of PDMS, gPDMS-L, gPDMS-M and gPDMS-H substrates.

Additional Figure 3: Masson staining of cell sheet cross-sections and thickness distribution of cell sheet obtained under static or loaded conditions.

1. Green, J. J.; Elisseeff, J. H. Mimicking biological functionality with polymers for biomedical applications. *Nature*. **2016**, *540*, 386-394.
2. Triffitt, J. T.; Wang, Q. Application of stem cells in translational medicine. *Biomater Transl*. **2021**, *2*, 285-286.
3. Steijvers, E.; Ghei, A.; Xia, Z. Manufacturing artificial bone allografts: a perspective. *Biomater Transl*. **2022**, *3*, 65-80.
4. Han, F.; Hu, Y.; Li, J.; Gong, J.; Guo, Q.; Zhu, C.; Zhu, X.; Yang, H.; Li, B. In situ silk fibroin-mediated crystal formation of octacalcium phosphate and its application in bone repair. *Mater Sci Eng C Mater Biol Appl*. **2019**, *95*, 1-10.
5. Burg, K. J.; Porter, S.; Kellam, J. F. Biomaterial developments for bone tissue engineering. *Biomaterials*. **2000**, *21*, 2347-2359.
6. Zhang, K.; Wang, S.; Zhou, C.; Cheng, L.; Gao, X.; Xie, X.; Sun, J.; Wang, H.; Weir, M. D.; Reynolds, M. A.; Zhang, N.; Bai, Y.; Xu, H. H. K. Advanced smart biomaterials and constructs for hard tissue engineering and regeneration. *Bone Res*. **2018**, *6*, 31.
7. Xu, Y.; Peng, J.; Richards, G.; Lu, S.; Eglin, D. Optimization of electrospray fabrication of stem cell-embedded alginate-gelatin microspheres and their assembly in 3D-printed poly(ε-caprolactone) scaffold for cartilage tissue engineering. *J Orthop Translat*. **2019**, *18*, 128-141.
8. Rafat, M.; Li, F.; Fagerholm, P.; Lagali, N. S.; Watsky, M. A.; Munger, R.; Matsuura, T.; Griffith, M. PEG-stabilized carbodiimide crosslinked collagen-chitosan hydrogels for corneal tissue engineering. *Biomaterials*. **2008**, *29*, 3960-3972.
9. Kumbar, S. G.; Nukavarapu, S. P.; James, R.; Nair, L. S.; Laurencin, C. T. Electrospun poly(lactic acid-co-glycolic acid) scaffolds for skin tissue engineering. *Biomaterials*. **2008**, *29*, 4100-4107.
10. Chouhan, D.; Mandal, B. B. Silk biomaterials in wound healing and skin regeneration therapeutics: from bench to bedside. *Acta Biomater*. **2020**, *103*, 24-51.
11. Xuan, H.; Hu, H.; Geng, C.; Song, J.; Shen, Y.; Lei, D.; Guan, Q.; Zhao, S.; You, Z. Biofunctionalized chondrogenic shape-memory ternary scaffolds for efficient cell-free cartilage regeneration. *Acta Biomater*. **2020**, *105*, 97-110.
12. Castilho, M.; Mouser, V.; Chen, M.; Malda, J.; Ito, K. Bi-layered micro-fibre reinforced hydrogels for articular cartilage regeneration. *Acta Biomater*. **2019**, *95*, 297-306.
13. Bhatia, S. N.; Underhill, G. H.; Zaret, K. S.; Fox, I. J. Cell and tissue engineering for liver disease. *Sci Transl Med*. **2014**, *6*, 245sr242.
14. Sabetkish, S.; Kajbafzadeh, A. M.; Sabetkish, N.; Khorramirouz, R.; Akbarzadeh, A.; Seyedian, S. L.; Pasalar, P.; Orangian, S.; Beigi, R. S.; Aryan, Z.; Akbari, H.; Tavangar, S. M. Whole-organ tissue engineering: decellularization and recellularization of three-dimensional matrix liver scaffolds. *J Biomed Mater Res A*. **2015**, *103*, 1498-1508.
15. Shimizu, T.; Yamato, M.; Kikuchi, A.; Okano, T. Cell sheet engineering for myocardial tissue reconstruction. *Biomaterials*. **2003**, *24*, 2309-2316.
16. Qazi, T. H.; Mooney, D. J.; Pumberger, M.; Geissler, S.; Duda, G. N. Biomaterials based strategies for skeletal muscle tissue engineering: existing technologies and future trends. *Biomaterials*. **2015**, *53*, 502-521.
17. Pedde, R. D.; Mirani, B.; Navaei, A.; Styan, T.; Wong, S.; Mehrali, M.; Thakur, A.; Mohtaram, N. K.; Bayati, A.; Dolatshahi-Pirouz, A.; Nikkhah, M.; Willerth, S. M.; Akbari, M. Emerging biofabrication strategies for engineering complex tissue constructs. *Adv Mater*. **2017**, *29*, 1606061.
18. Yang, J.; Yamato, M.; Kohno, C.; Nishimoto, A.; Sekine, H.; Fukai, F.; Okano, T. Cell sheet engineering: recreating tissues without biodegradable scaffolds. *Biomaterials*. **2005**, *26*, 6415-6422.
19. Yamato, M.; Okano, T. Cell sheet engineering. *Mater Today*. **2004**, *7*, 42-47.
20. Xu, X.; Song, J. Segmental long bone regeneration guided by degradable synthetic polymeric scaffolds. *Biomater Transl*. **2020**, *1*, 33-45.
21. McMurray, R. J.; Gadegaard, N.; Tsimbouri, P. M.; Burgess, K. V.; McNamara, L. E.; Tare, R.; Murawski, K.; Kingham, E.; Oreffo, R. O.; Dalby, M. J. Nanoscale surfaces for the long-term maintenance of mesenchymal stem cell phenotype and multipotency. *Nat Mater*. **2011**, *10*, 637-644.
22. Kelm, J. M.; Fussenegger, M. Scaffold-free cell delivery for use in regenerative medicine. *Adv Drug Deliv Rev*. **2010**, *62*, 753-764.
23. Badylak, S. F.; Gilbert, T. W. Immune response to biologic scaffold materials. *Semin Immunol*. **2008**, *20*, 109-116.
24. Anderson, J. M.; Rodriguez, A.; Chang, D. T. Foreign body reaction to biomaterials. *Semin Immunol*. **2008**, *20*, 86-100.
25. Akizuki, T.; Oda, S.; Komaki, M.; Tsuchioka, H.; Kawakatsu, N.; Kikuchi, A.; Yamato, M.; Okano, T.; Ishikawa, I. Application of periodontal ligament cell sheet for periodontal regeneration: a pilot study in beagle dogs. *J Periodontal Res*. **2005**, *40*, 245-251.
26. L'Heureux, N.; Dusserre, N.; Konig, G.; Victor, B.; Keire, P.; Wight, T. N.; Chronos, N. A.; Kyles, A. E.; Gregory, C. R.; Hoyt, G.; Robbins, R. C.; McAllister, T. N. Human tissue-engineered blood vessels for adult arterial revascularization. *Nat Med*. **2006**, *12*, 361-365.
27. Nishida, K.; Yamato, M.; Hayashida, Y.; Watanabe, K.; Maeda, N.; Watanabe, H.; Yamamoto, K.; Nagai, S.; Kikuchi, A.; Tano, Y.; Okano, T. Functional bioengineered corneal epithelial sheet grafts from corneal stem cells expanded ex vivo on a temperature-responsive cell culture surface. *Transplantation*. **2004**, *77*, 379-385.
28. Matsuura, K.; Masuda, S.; Haraguchi, Y.; Yasuda, N.; Shimizu, T.; Hagiwara, N.; Zandstra, P. W.; Okano, T. Creation of mouse embryonic stem cell-derived cardiac cell sheets. *Biomaterials*. **2011**, *32*, 7355-7362.

29. Doberenz, F.; Zeng, K.; Willems, C.; Zhang, K.; Groth, T. Thermoresponsive polymers and their biomedical application in tissue engineering - a review. *J Mater Chem B.* **2020**, *8*, 607-628.
30. Yamato, M.; Utsumi, M.; Kushida, A.; Konno, C.; Kikuchi, A.; Okano, T. Thermo-responsive culture dishes allow the intact harvest of multilayered keratinocyte sheets without dispase by reducing temperature. *Tissue Eng.* **2001**, *7*, 473-480.
31. Lin, J. B.; Isenberg, B. C.; Shen, Y.; Schorsch, K.; Sazonova, O. V.; Wong, J. Y. Thermo-responsive poly(N-isopropylacrylamide) grafted onto microtextured poly(dimethylsiloxane) for aligned cell sheet engineering. *Colloids Surf B Biointerfaces.* **2012**, *99*, 108-115.
32. Yu, Q.; Zhang, Y.; Chen, H.; Zhou, F.; Wu, Z.; Huang, H.; Brash, J. L. Protein adsorption and cell adhesion/detachment behavior on dual-responsive silicon surfaces modified with poly(N-isopropylacrylamide)-block-polystyrene copolymer. *Langmuir.* **2010**, *26*, 8582-8588.
33. Kushida, A.; Yamato, M.; Konno, C.; Kikuchi, A.; Sakurai, Y.; Okano, T. Decrease in culture temperature releases monolayer endothelial cell sheets together with deposited fibronectin matrix from temperature-responsive culture surfaces. *J Biomed Mater Res.* **1999**, *45*, 355-362.
34. Hamdi, H.; Furuta, A.; Bellamy, V.; Bel, A.; Puymirat, E.; Peyrard, S.; Agbulut, O.; Menasché, P. Cell delivery: intramyocardial injections or epicardial deposition? A head-to-head comparison. *Ann Thorac Surg.* **2009**, *87*, 1196-1203.
35. Shimizu, T.; Sekine, H.; Yang, J.; Isoi, Y.; Yamato, M.; Kikuchi, A.; Kobayashi, E.; Okano, T. Polysurgery of cell sheet grafts overcomes diffusion limits to produce thick, vascularized myocardial tissues. *FASEB J.* **2006**, *20*, 708-710.
36. Liu, Y.; Wang, L.; Li, S.; Zhang, T.; Chen, C.; Hu, J.; Sun, D.; Lu, H. Mechanical stimulation improves rotator cuff tendon-bone healing via activating IL-4/JAK/STAT signaling pathway mediated macrophage M2 polarization. *J Orthop Translat.* **2022**, *37*, 78-88.
37. Lin, C. Y.; Song, X.; Seaman, K.; You, L. Microfluidic co-culture platforms for studying osteocyte regulation of other cell types under dynamic mechanical stimulation. *Curr Osteoporos Rep.* **2022**, *20*, 478-492.
38. Zhang, J.; Hao, X.; Chi, R.; Qi, J.; Xu, T. Moderate mechanical stress suppresses the IL-1β-induced chondrocyte apoptosis by regulating mitochondrial dynamics. *J Cell Physiol.* **2021**, *236*, 7504-7515.
39. Lee, H. P.; Gu, L.; Mooney, D. J.; Levenston, M. E.; Chaudhuri, O. Mechanical confinement regulates cartilage matrix formation by chondrocytes. *Nat Mater.* **2017**, *16*, 1243-1251.
40. Wang, T.; Chen, P.; Chen, L.; Zhou, Y.; Wang, A.; Zheng, Q.; Mitchell, C. A.; Leys, T.; Tuan, R. S.; Zheng, M. H. Reduction of mechanical loading in tendons induces heterotopic ossification and activation of the β-catenin signaling pathway. *J Orthop Translat.* **2021**, *29*, 42-50.
41. Guilak, F. Biomechanical factors in osteoarthritis. *Best Pract Res Clin Rheumatol.* **2011**, *25*, 815-823.
42. Ni, R.; Guo, X. E.; Yan, C.; Wen, C. Hemodynamic stress shapes subchondral bone in osteoarthritis: An emerging hypothesis. *J Orthop Translat.* **2022**, *32*, 85-90.
43. Gauvin, R.; Parenteau-Bareil, R.; Larouche, D.; Marcoux, H.; Bisson, F.; Bonnet, A.; Auger, F. A.; Bolduc, S.; Germain, L. Dynamic mechanical stimulations induce anisotropy and improve the tensile properties of engineered tissues produced without exogenous scaffolding. *Acta Biomater.* **2011**, *7*, 3294-3301.
44. Dai, Z. Q.; Wang, R.; Ling, S. K.; Wan, Y. M.; Li, Y. H. Simulated microgravity inhibits the proliferation and osteogenesis of rat bone marrow mesenchymal stem cells. *Cell Prolif.* **2007**, *40*, 671-684.
45. Vandenburgh, H. H. Dynamic mechanical orientation of skeletal myofibers in vitro. *Dev Biol.* **1982**, *93*, 438-443.
46. Vandenburgh, H. H.; Swasdison, S.; Karlisch, P. Computer-aided mechanogenesis of skeletal muscle organs from single cells in vitro. *FASEB J.* **1991**, *5*, 2860-2867.
47. Collinsworth, A. M.; Torgan, C. E.; Nagda, S. N.; Rajalingam, R. J.; Kraus, W. E.; Truskey, G. A. Orientation and length of mammalian skeletal myocytes in response to a unidirectional stretch. *Cell Tissue Res.* **2000**, *302*, 243-251.
48. Hu, B.; El Haj, A. J.; Dobson, J. Receptor-targeted, magneto-mechanical stimulation of osteogenic differentiation of human bone marrow-derived mesenchymal stem cells. *Int J Mol Sci.* **2013**, *14*, 19276-19293.
49. Lambert, C. A.; Colige, A. C.; Munaut, C.; Lapière, C. M.; Nusgens, B. V. Distinct pathways in the over-expression of matrix metalloproteinases in human fibroblasts by relaxation of mechanical tension. *Matrix Biol.* **2001**, *20*, 397-408.
50. Gilbert, T. W.; Stewart-Akers, A. M.; Sydeski, J.; Nguyen, T. D.; Badylak, S. F.; Woo, S. L. Gene expression by fibroblasts seeded on small intestinal submucosa and subjected to cyclic stretching. *Tissue Eng.* **2007**, *13*, 1313-1323.
51. Ducouret, C.; Petersohn, E.; Betz, N.; Le Moel, A. Fourier transform infrared analysis of heavy ion grafting of poly(vinylidene fluoride). *Spectrochim Acta A Mol Biomol Spectrosc.* **1995**, *51*, 567-572.
52. Ponomar, M.; Krasnyuk, E.; Butylskii, D.; Nikonenko, V.; Wang, Y.; Jiang, C.; Xu, T.; Pismenskaya, N. Sessile drop method: critical analysis and optimization for measuring the contact angle of an ion-exchange membrane surface. *Membranes (Basel).* **2022**, *12*, 765.
53. Huhtamäki, T.; Tian, X.; Korhonen, J. T.; Ras, R. H. A. Surface-wetting characterization using contact-angle measurements. *Nat Protoc.* **2018**, *13*, 1521-1538.
54. Schneider, C. A.; Rasband, W. S.; Eliceiri, K. W. NIH Image to ImageJ: 25 years of image analysis. *Nat Methods.* **2012**, *9*, 671-675.
55. Yu, L.; Cai, Y.; Wang, H.; Pan, L.; Li, J.; Chen, S.; Liu, Z.; Han, F.; Li, B. Biomimetic bone regeneration using angle-ply collagen membrane-supported cell sheets subjected to mechanical conditioning. *Acta Biomater.* **2020**, *112*, 75-86.
56. Zhang, W.; Wang, H.; Yuan, Z.; Chu, G.; Sun, H.; Yu, Z.; Liang, H.; Liu, T.; Zhou, F.; Li, B. Moderate mechanical stimulation rescues degenerative annulus fibrosus by suppressing caveolin-1 mediated pro-inflammatory signaling pathway. *Int J Biol Sci.* **2021**, *17*, 1395-1412.
57. Livak, K. J.; Schmittgen, T. D. Analysis of relative gene expression data using real-time quantitative PCR and the 2(-Delta Delta C(T)) method. *Methods.* **2001**, *25*, 402-408.
58. National Research Council. Guide for the Care and Use of Laboratory Animals, 8th edition. National Academies Press: Washington, DC, USA, 2011.
59. Liu, L.; Sheardown, H. Glucose permeable poly (dimethyl siloxane) poly (N-isopropyl acrylamide) interpenetrating networks as ophthalmic biomaterials. *Biomaterials.* **2005**, *26*, 233-244.
60. Huang, X.; Das, R.; Patel, A.; Nguyen, T. D. Physical stimulations for bone and cartilage regeneration. *Regen Eng Transl Med.* **2018**, *4*, 216-237.
61. Sugiura, S.; Imano, W.; Takagi, T.; Sakai, K.; Kanamori, T. Thermoresponsive protein adsorption of poly(N-isopropylacrylamide)-modified streptavidin on polydimethylsiloxane microchannel surfaces. *Biosens Bioelectron.* **2009**, *24*, 1135-1140.
62. Rim, N. G.; Yih, A.; Hsi, P.; Wang, Y.; Zhang, Y.; Wong, J. Y. Micropatterned cell sheets as structural building blocks for biomimetic vascular patches. *Biomaterials.* **2018**, *181*, 126-139.
63. Kessler, D.; Dethlefsen, S.; Haase, I.; Plomann, M.; Hirche, F.; Krieg, T.;

Eckes, B. Fibroblasts in mechanically stressed collagen lattices assume a "synthetic" phenotype. *J Biol Chem.* **2001**, *276*, 36575-36585.
64. Zhang, W.; Chu, G.; Wang, H.; Chen, S.; Li, B.; Han, F. Effects of matrix stiffness on the differentiation of multipotent stem cells. *Curr Stem Cell Res Ther.* **2020**, *15*, 449-461.
65. Ma, D.; Chen, H.; Shi, D.; Li, Z.; Wang, J. Preparation and characterization of thermo-responsive PDMS surfaces grafted with poly(N-isopropylacrylamide) by benzophenone-initiated photopolymerization. *J Colloid Interface Sci.* **2009**, *332*, 85-90.
66. Shi, D.; Ma, D.; Dong, F.; Zong, C.; Liu, L.; Shen, D.; Yuan, W.; Tong, X.; Chen, H.; Wang, J. Proliferation and multi-differentiation potentials of human mesenchymal stem cells on thermoresponsive PDMS surfaces grafted with PNIPAAm. *Biosci Rep.* **2009**, *30*, 149-158.
67. Nagase, K.; Yamato, M.; Kanazawa, H.; Okano, T. Poly(N-isopropylacrylamide)-based thermoresponsive surfaces provide new types of biomedical applications. *Biomaterials.* **2018**, *153*, 27-48.
68. Humphrey, J. D.; Dufresne, E. R.; Schwartz, M. A. Mechanotransduction and extracellular matrix homeostasis. *Nat Rev Mol Cell Biol.* **2014**, *15*, 802-812.
69. Hao, J.; Zhang, Y.; Jing, D.; Shen, Y.; Tang, G.; Huang, S.; Zhao, Z. Mechanobiology of mesenchymal stem cells: Perspective into mechanical induction of MSC fate. *Acta Biomater.* **2015**, *20*, 1-9.
70. Kreutzer, J.; Viehrig, M.; Pölönen, R. P.; Zhao, F.; Ojala, M.; Aalto-Setälä, K.; Kallio, P. Pneumatic unidirectional cell stretching device for mechanobiological studies of cardiomyocytes. *Biomech Model Mechanobiol.* **2020**, *19*, 291-303.
71. Thompson, M. S.; Abercrombie, S. R.; Ott, C. E.; Bieler, F. H.; Duda, G. N.; Ventikos, Y. Quantification and significance of fluid shear stress field in biaxial cell stretching device. *Biomech Model Mechanobiol.* **2011**, *10*, 559-564.
72. Wittkowske, C.; Reilly, G. C.; Lacroix, D.; Perrault, C. M. In vitro bone cell models: impact of fluid shear stress on bone formation. *Front Bioeng Biotechnol.* **2016**, *4*, 87.

Received: November 24, 2022
Revised: January 14, 2023
Accepted: February 17, 2023
Available online: March 28, 2023

Biomaterials Translational

Systematic evaluation of three porcine-derived collagen membranes for guided bone regeneration

Andrew Tai[1,2,#], Euphemie Landao-Bassonga[1,2,#], Ziming Chen[1,#], Minh Tran[3], Brent Allan[1,3,4], Rui Ruan[1], Dax Calder[3], Mithran Goonewardene[3], Hien Ngo[3], Ming Hao Zheng[1,2,]*

Key Words:
barrier membrane; collagen membrane; dental implant; guided bone regeneration; immunogen

From the Contents

ABSTRACT

Guided bone regeneration is one of the most common surgical treatment modalities performed when an additional alveolar bone is required to stabilize dental implants in partially and fully edentulous patients. The addition of a barrier membrane prevents non-osteogenic tissue invasion into the bone cavity, which is key to the success of guided bone regeneration. Barrier membranes can be broadly classified as non-resorbable or resorbable. In contrast to non-resorbable membranes, resorbable barrier membranes do not require a second surgical procedure for membrane removal. Commercially available resorbable barrier membranes are either synthetically manufactured or derived from xenogeneic collagen. Although collagen barrier membranes have become increasingly popular amongst clinicians, largely due to their superior handling qualities compared to other commercially available barrier membranes, there have been no studies to date that have compared commercially available porcine-derived collagen membranes with respect to surface topography, collagen fibril structure, physical barrier property, and immunogenic composition. This study evaluated three commercially available non-crosslinked porcine-derived collagen membranes (Striate+™, Bio-Gide® and Creos™ Xenoprotect). Scanning electron microscopy revealed similar collagen fibril distribution on both the rough and smooth sides of the membranes as well as the similar diameters of collagen fibrils. However, D-periodicity of the fibrillar collagen is significantly different among the membranes, with Striate+™ membrane having the closest D-periodicity to native collagen I. This suggests that there is less deformation of collagen during manufacturing process. All collagen membranes showed superior barrier property evidenced by blocking 0.2–16.4 μm beads passing through the membranes. To examine the immunogenic agents in these membranes, we examined the membranes for the presence of DNA and alpha-gal by immunohistochemistry. No alpha-gal or DNA was detected in any membranes. However, using a more sensitive detection method (real-time polymerase chain reaction), a relatively strong DNA signal was detected in Bio-Gide® membrane, but not Striate+™ and Creos™ Xenoprotect membranes. Our study concluded that these membranes are similar but not identical, probably due to the different ages and sources of porcine tissues, as well as different manufacturing processes. We recommend further studies to understand the clinical implications of these findings.

***Corresponding author:**
Ming Hao Zheng, minghao.zheng@uwa.edu.au.

#Author equally.

http://doi.org/10.12336/biomatertransl.2023.01.006

How to cite this article:
Tai, A.; Landao-Bassonga, E.; Chen, Z.; Tran, M.; Allan, B.; Ruan, R.; Calder, D.; Goonewardene, M. H.; Ngo, H.; Zheng, M. H. Systematic evaluation of three porcine-derived collagen membranes for guided bone regeneration. *Biomater Transl.* **2023**, *4*(1), 41-50.

Introduction

Osseointegrated dental implants have revolutionized the field of dentistry for the treatment of edentulism. In instances where there is insufficient alveolar bone to provide initial stabilization of a dental implant, additional bone regeneration is required before placing an implant. Guided bone regeneration (GBR) is the most common and effective strategy to provide sufficient bone for the osseointegration of dental implants into the alveolar bone. Dahlin et al.[1] in 1988 first described GBR, based on the

hypothesis that different cells have differential migration rates toward the wound during healing. Initially, a cell-occlusive polytetrafluoroethylene or Teflon™ (DuPont) membrane was utilized, fibroblasts and other soft connective tissue cells were prevented from populating the wound area.[2] Since then, the use of a barrier membrane to exclude non-osteogenic tissue has become the gold standard for GBR, since rapidly proliferating epithelium and connective tissue interfere with the regeneration of bone surrounding the dental implants.

Natural and synthetic barrier membranes have been developed for GBR.[2-4] Natural barrier membranes are comprised of collagen or chitosan, whereas synthetic barrier membranes are made of aliphatic polyesters, primarily polytetrafluoroethylene, polylactic acid or poly-glycolic acid. Natural barrier membranes, in particular collagen membranes, are popular for GBR as their overall advantages include biocompatibility and are resorbable, which avoids a second surgery for membrane removal.[3] Natural membranes that are currently used for GBR and derived from porcine sources include Striate+™, Bio-Gide® and Creos™ Xenoprotect, all of which are not cross-linked and manufactured using different protocols.

Collagen is a natural polymer that has been used in medical application for the last 100 years. There are seven types of fibrillar collagens (types I, II, III, V, XI, XXIV and XXVII), which are characterised by the repeating amino acid motif $(Gly\text{-}X\text{-}Y)_n$, with proline and 4-hydroxyproline amino acids commonly detected at the X and Y positions respectively.[5-8] The glycine residue is important for the stabilization of collagen. The tropocollagen molecules form triple helices by hydrogen bond formation between molecules and form a triple helix rod approximately 300 nm long and 1.5 nm in diameter.[9] Collagen fibrils are assembled from collagen rods from 50 to a few hundred nanometers in diameter depending on the types and number of collagen helix rods.

The D-periodicity of collagen fibrils is measured from overlap and gap regions between self-assembled collagen molecules. The D-periodicity of collagen fibrils is 67 nm, predicted by the Hodge-Petruska model[5, 9-11] and vadalited in different tissues[12] Non-fibrillar collagens are also rich in glycine, proline and hydroxyproline, but the helical region is short or interrupted. They contribute to the formation of extracellular matrix's network, e.g., basement membrane. The commercially available porcine-derived membranes for GBR are mainly composed of fibrillar collagen types I and III. Processing of porcine-derived membranes can alter the D-periodicity of collagen fibrils.[13, 14] Alteration of the D-periodicity may affect the susceptibility to degradation mediated by collagenase which is present in saliva.[15, 16]

Implantation of xenogenic materials can cause acute immunological responses. A severe response could lead to poor bone regeneration affecting the osseointegration of dental implants. Common antigens in porcine barrier membranes are galactose-α-1,3-galactose (alpha-gal, α-gal)) and DNA.α-gal is a sugar molecule present in meat, including pork, beef and lamb. The enzyme α-1,3-galactosyltransferase is crucial for the synthesis of α-gal, but is only inactivated in humans and primates. Anti-α-gal antibodies (IgA, IgG, IgE and IgM), have been identified in humans and are responsible for triggering immune responses against porcine xenotransplants.[17] On the other hand, xenogeneic DNA, originating from the nucleus and mitochondria of the source tissue, can also trigger an immune reaction. Removal of DNA and α-gal in the manufacturing process is a key step for producing high quality animal or allogenic derived collagen devices.[18]

In this study, we examined the biological and physical barrier characteristics of three collagen membranes used for GBR that are all porcine-derived. Given the difference in the breed and age of animals as well as manufacturing processes, we hypothesized that there will be differences in the surface topology, diameter and D-periodicity of collagen fibrils, and α-gal and DNA content among these membranes. Our study has provided detailed analyses of the three porcine-derived collagen membranes - Creos™ Xenoprotect, Bio-Gide® and Striate+™ - and identified their similarities and differences, which we speculate may have clinical relevance with respect to the early wound healing events required for optimal peri-implant bone regeneration.

Methods

Collagen membranes

Three types of commercially-available porcine-derived collagen membranes: (1) Striate+™ manufactured by Orthocell Ltd., Perth, Western Australia, Australia (30 mm × 40 mm), (2) Bio-Gide® manufactured by Geistlich Pharma, Wolhusen, Switzerland (30 mm × 40 mm) and (3) Creos™ Xenoprotect manufactured by Matricel GmbH, Herzogenrath, Germany (30 mm × 40 mm) were used in this study. Raw materials are porcine mesentery as positive controls for heamatoxylin and eosin staining and real-time polymerase chain reaction (PCR), and porcine aortic valve (Boatshed Butcher at Cottesloe, Perth, Western Australia, Australia) is a positive control for DNA content and immunogenic porcine α-gal by immunohistochemistry analysis.

Scanning electron microscopy

Samples for scanning electron microscopy (SEM) imaging were cut to 3 mm × 3 mm and mounted on a stub. A layer of platinum was then sputtered onto the samples. Then the samples were imaged under 1555 VP-FESEM (Zeiss, Baden-Württemberg, Germany) at an accelerating voltage of 5 kV in the Centre for Microscopy, Characterization and Analysis, University of Western Australia. The D-periodcity and diameter of the collagen bundles were measured using FIJI ImageJ (64-bit Java1.8.0_172).[19] At least 11 images were analysed for each membrane. For determining the porosity

1 Centre for Orthopaedic Research, Faculty of Health and Medical Sciences, The University of Western Australia, Nedlands, Western Australia, Australia; 2 Perron Institute for Neurological and Translational Science, Nedlands, Western Australia, Australia; 3 UWA Dental School, The University of Western Australia, Nedlands, Western Australia, Australia; 4 Oral and Maxillofacial Department, St John of God Subiaco Hospital, Subiaco, Western Australia, Australia

of all three collagen membranes, SEM images (three images per membrane) depicting three types of membranes were imported into ImageJ software (v 1.53m; National Institutes of Health, Bethesda, MD, USA), where the porous regions of the images were identified and selected through threshold segmentation techniques based on their distinct gray values. The orientation of fibres was analysed by a Java plugin for ImageJ, OrientationJ.[20] Images of SEM were used for quantification of the diameter and D-periodicity of the bundles. The diameter and D-periodicity of collagen bundles were measured by ImageJ. The D-periodicity of collagen fibrils measured by the repeating pattern of gap and overlap regions. The diameter of the bundles was determined by measuring the distance between the top and bottom of the bundles.

Micro-computed tomography

Samples were stained overnight with iodine Lugol solution (Sigma-Aldrich, St. Louis, MO, USA). All three samples (Striate+™, Bio-Gide®, Creos™ Xenoprotect membranes) were mounted together in a polypropylene tube and then scanned by using Nikon XT H 225 ST CT, Inspect-X version (Nikon, Tokyo, Japan) at 47 kV, 117 μA, power 5.5 W, with a resolution of 12 mm in three dimensions. Totally, three membranes of each brand were used for measurement. Samples were reconstructed with computed tomography Pro 3D Version. The thickness of the collagen membranes was measured using AVIZO software (v2022.1; Thermo Fisher, Waltham, MA, USA).

Determination of barrier property of collagen membranes

Measurement of the barrier properties of collagen membranes was performed by gravity-based filtration. Striate+™, Bio-Gide®, Creos™ Xenoprotect membranes, Whatman Filter paper Grade 1 and Whatman Filter paper Grade 5 (Whatman International Ltd., Maidstone, UK) were trimmed to 3 cm × 3 cm and placed into 3D printed funnels as filters. Standard beads (PPS-6K & NFPPS-52-4K, Spherotech Inc., Lake Forest, CA, USA) of different sizes and concentrations (0.22 and 0.45 μm at 1:20 concentration; 0.88, 1.25, 2.0, 3.3, 5.2, 7.88, 10.1 and 16.4 μm at 1:50 concentration) were mixed and slowly filtered (**Additional Figure 1**). Filtrates were collected and analyzed by flow cytometry (BD LSRFortessa, BD Life Sciences, San Jose, CA, USA). Samples were acquired for 30 seconds at high speed with 60 μL/min. FSC (voltage: 709) and SSC (voltage: 412) settings were used for small size beads (PPS-6K, 0.22–1.25 μm) and FSC (voltage: 418) and SSC (voltage: 247) setting for large size beads (NFPPS-52-4K, 2.0–16.4 μm). Additionally, control measurements were also performed with mixed standard beads before filtration. Data were analyzed by FlowJo™ v10 Software (BD Life Sciences) and GraphPad Prism (v8.0.1, GraphPad Software, San Diego, CA, USA, www.graphpad.com). At least three membranes of each brand were used for the filtration assay.

Determination of cell nuclei remnants by real-time polymerase chain reaction

DNA (total 100 μL) extracted from the collagen membranes (Striate+™, Bio-Gide®, and Creos™ Xenoprotect) of the same weight (0.082 g) were purified by DNeasy Mericon Food Kit (Qiagen, Hilden, Germany). Totally, four samples of each type of membrane were used for the real-time PCR. DNA was also extracted from the porcine mesentery. The same volume (2 μL) of the purified DNA samples from membranes was analysed by real-time PCR using iTaq™ Universal SYBR® Green Supermix (Bio-Rad, Hercules, CA, USA) and the published primers (PPA6-forward: 5′-CTA CCT ATT GTC ACC TTA GTT-3′& reverse: 5′-GAG ATT GTG CGG TTA TTA ATG-3′) (IDT Technology Ltd., Coralville, IA, USA) for detection of porcine DNA, by targeting porcine mitochondrial specific gene (mtATP6).[21] Technical triplicate was applied to each sample.

Determination of cell nuclei remnants by histological analysis

Paraffin sections of the three commercial membranes were stained with heamatoxylin and eosin (Sigma-Aldrich) according to a standard protocol and imaged under light microscope (Zeiss) at a range of objective magnifications.

Determination of DNA content and porcine α-gal immunohistochemistry analysis

Positive control sample (porcine aortic valve, Boatshed Butcher at Cottesloe, Perth, Western Australia, Australia) and the collagen membranes were embedded in OCT solution, frozen by immersion in iso-pentane cooled with liquid-N2 and stored at 80°C until required. Sections were prepared on a cryomicrotome at 10 μm thickness and placed on sialinated glass slides. Tissue sections were fixed by immersing them in pre-cooled acetone (–20°C) for 10 minutes, then washed twice with 1× phosphate buffered saline for 5 minutes each following by incubation with 0.1% Triton X for 5 minutes. Section were washed twice with 1× phosphate buffered saline for 5 minutes each and blocked with 3% bovine serum albumin. Sections were incubated with anti-DNA (1:1000, deposited by Voss, E.W., DSHB Hybridoma, Iowa City, IA, USA, RRID: AB_10805293) and anti-α-gal (1:1000, Isolectin GS-IB, Alexa Fluor 488 conjugate, Thermo Fisher, RRID: AB_2314662) at 4°C overnight. Sections stained with anti-DNA were then incubated with Alexa Fluor 680 donkey anti-mouse (1:500; RRID: AB_2762831, Thermo Fisher) at room temperature for 1 hour. After washing with 1× phosphate buffered saline three times, sections were stained with Hoechst 33342 (Thermo Fisher) and mounted with ProLong™ Diamond Antifade Mountant (Thermo Fisher). All sections were cover-slipped prior to imaging on a confocal laser scanning microscope (Nikon A1Si Confocal Microscope, Nikon, Tokyo, Japan).

Statistical analysis

Comparisons of multiple individual datasets were performed by one-way analysis of variance with Tukey's *post hoc* multiple comparison, after testing for the normal distribution of data. Statistical calculations were performed using GraphPad Prism software. The data are expressed as means ± standard error of mean (SEM), and we considered P values less than 0.05 as statistically significant.

Results

Surface topographic features of three collagen membranes

Resorbable collagen membranes (Creos™ Xenoprotect, Bio-Gide® and Striate+™) are derived from porcine tissue. In general, the membranes have a bilayer structure, with a rough and smooth side, which is a feature of the porcine source tissues. The smooth side refers to the side of the membrane with a relatively uniform surface and more parallel, aligned collagen bundles, while the rough side refers to the side with a porous, non-uniform surface with irregular collagen bundles. To understand the morphological differences between the collagen membranes, SEM was performed and images with different magnifications (364×, 19.75k×, 150k×) were selected and viewed in a side-by-side comparison. In all membranes, the smooth side had similar features, with no visible pores at 364× magnification (**Figure 1A**). At higher magnifications (19.75 k× and 150 k×), clear fibrillar collagen bundles were noted in all membranes (**Figure 1A**). Striate+™ and Creos™ Xenoprotect exhibited a more uniform smooth side than Bio-Gide® as their peaks of fibre orientation distribution were closer to zero degrees determined by OrientationJ (**Figure 1A**). On the rough side, Creos™ Xenoprotect, Striate+™ and Bio-Gide® demonstrated the irregular distribution of fibre bundles throughout the rough side of the membranes (**Figure 1B**). The peaks of fibre orientation distribution of all the membranes were found to be further away from zero degrees meaning that the fibres tend not to be parallel. On the other hand, Striate+™ showed significantly smaller porosity than Bio-Gide® and Creos™ Xenoprotect at the smooth side analyzed by Image J (**Figure 1C**). There is no significant difference of porosity in smooth side between Bio-Gide® and Creos™ Xenoprotect. Also, there is no significant difference of porosity in rough side of all membranes (**Figure 1D**).

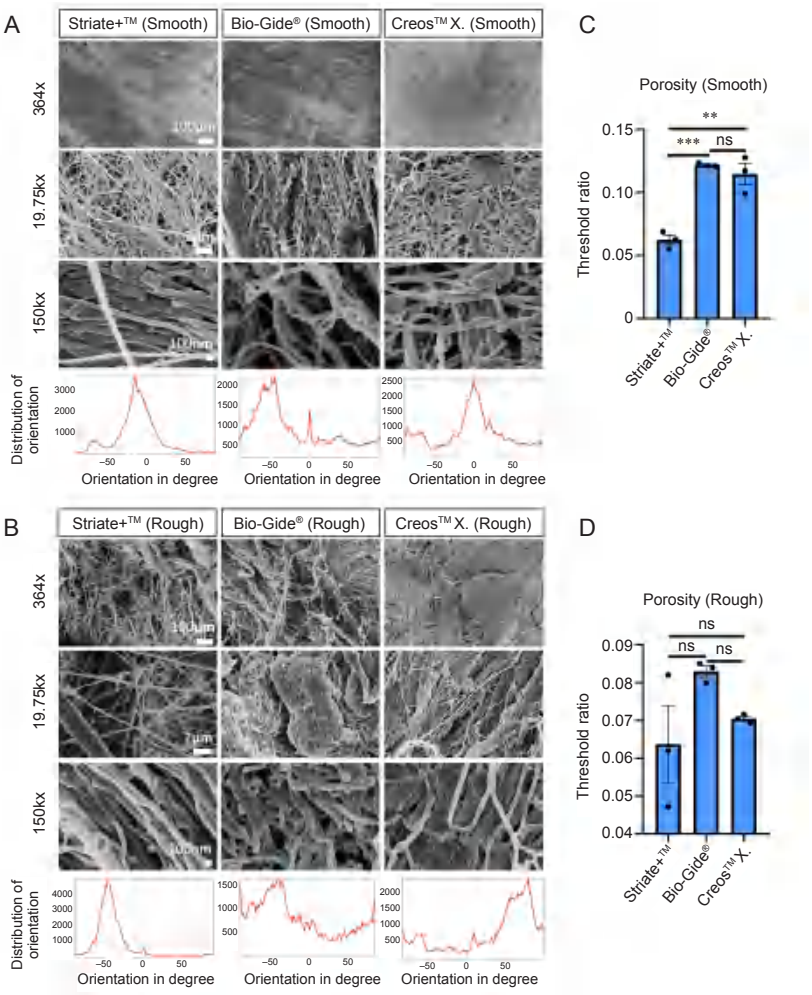

Figure 1. Scanning electron microscopy of porcine collagen membranes. (A, B) Smooth (A) and rough (B) sides of Striate+™, Bio-Gide® and Creos™ Xenoprotect. The smooth side of the collagen membranes showed a more uniform, smooth, and organized structure than the rough side. Scale bars: 100 μm (upper row), 2 μm (middle row), 100 nm (lower row). Representative scanning electron microscopy images of both smooth and rough sides of membranes at 150k× were analysed by OrientationJ for the orientation of fibres. Striate+™ and Creos™ Xenoprotect showed more uniform fibre orientation than Bio-Gide® on smooth side, whereas all three membranes showed random fibre orientation on rough side. (C, D) Porosity of smooth (C) and rough (D) sides of collagen membranes. Data are presented as means ± SEM. $^{**}P < 0.01$, $^{***}P < 0.001$ (one-way analysis of variance with Tukey's *post hoc* multiple comparison). ns: no significance.

Diameter and D-periodicity of collagen fibrils in three collagen membranes

In addition to the surface topological analysis, the intrinsic properties of collagen fibrils, such as diameter and D-periodicity in the three collagen membranes were examined, as these parameters are affected in the manufacturing process. SEM results showed there was no significant difference in fibril diameter among three membranes: Striate+™, Bio-Gide® and Creos™ Xenoprotect (**Figure 2A**). However, the D-periodicity of collagen fibrils in Striate+™ membrane was higher than those in Bio-Gide® and Creos™ Xenoprotect . The D-periodicity of collagen bundles of Striate+™, membrane is closest to the native one (67 nm).There was no significant difference in D-periodicity between Bio-Gide® and -Creos™ Xenoprotect (**Figure 2B**).

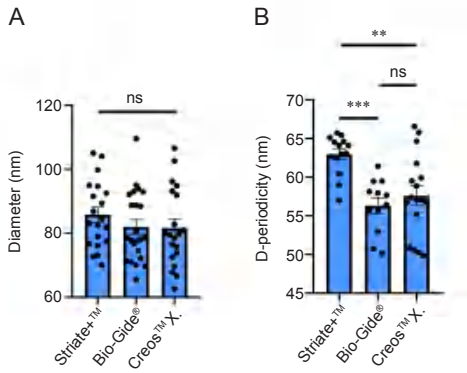

Figure 2. (A, B) Diameter (A) and D-periodicity (B) of collagen bundles in Striate+™, Bio-Gide® and Creos™ Xenoprotect (Creos™ X.). Data are presented as means ± SEM. $^{**}P < 0.01$, $^{***}P < 0.001$ (one-way analysis of variance with Tukey's *post hoc* multiple comparison). ns: no significance.

Thickness of the collagen membranes in three collagen membranes

To determine the thickness of the collagen membranes, micro-computed tomography was used to scan through the collagen membranes (**Figure 3A**). Membranes were oriented so that cross-sections were obtained (**Figure 3B**). Bio-Gide® membrane is the thickest membrane, while StriateTM is the thinnest one (**Figure 3C**).

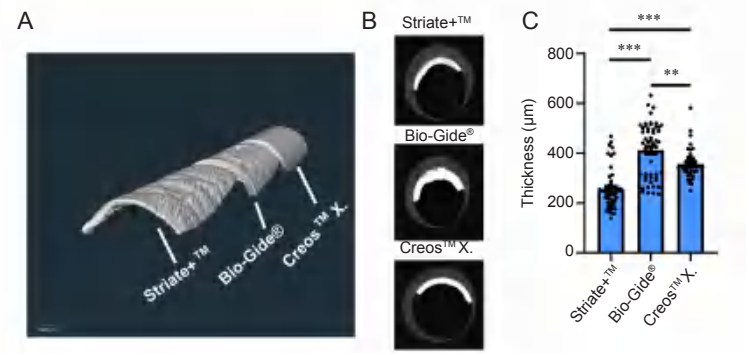

Figure 3. Thickness of porcine collagen membranes measured by micro-computed tomography. (A) Iodine-stained Striate+™, Bio-Gide® and Creos™ Xenoprotect (Creos™ X.) membranes were aligned in polypropylene tubes and scanned by micro-computed tomography. (B) Cross sections of Striate+™, Bio-Gide® and Creos™ Xenoprotect membranes were extracted by AVIZO software. (C) Thickness of three samples of each membrane. Data are presented as means ± SEM. At least 11 measurements were done on each membrane. $^{**}P < 0.01$, $^{***}P < 0.001$ (one-way analysis of variance with Tukey's *post hoc* multiple comparison). ns: no significance.

Barrier property of three collagen membranes

To evaluate the barrier properties of the collagen membranes, beads of different sizes were used to mimic fibroblasts and other soft connective tissue cells with a range of cell size in the socket cavity. Using a gravity-based filtration method, all collagen membranes showed superior barrier property by blocking the passage of all bead sizes (0.22–16.4 μm; **Figure 4A–C**), while grades 1 and 5 Whatman filter papers did not block 0.22, 0.45, 0.88 and 1.25 μm-sized beads (**Figure 4A** and **B**).

DNA contents and immunogens in three collagen membranes

Our previous study reported that several collagen scaffolds widely used for rotator cuff tendon repairs contain cellular/DNA components, which may be responsible for the severe

immune rejection reactions.[18] To determine if the three collagen membranes contain DNA and α-gal, we performed histology, immunohistochemical detection (for α-gal and double stranded DNA) and real-time PCR-based mitochondrial DNA assay. All collagen membranes showed eosin-stained collagen fibres in the histological evaluation. Basophilic nuclear staining with heamatoxylin was only present in the raw materials (porcine mesentery) but was not detectable in any of the commercial collagen membranes (**Figure 5**). By immunostaining using anti-DNA immunostaining and Hoechst nuclear staining, the positive control, aorta valve was shown positive staining in the nuclei (**Figure 6**). No immunostaining signal was detected in any commercial membranes. Next, we utilized a more sensitive method, real-time PCR, to determine the unknown DNA content in all membranes. The cycle threshold values of (0, 100 ng and 200 ng) porcine DNA and all membranes were plotted as a scatter plot shown in **Figure** 7. 0 ng porcine DNA, Striate+™ and Creos™ Xenoprotect showed high cycle threshold values at around 40 or beyond 40 detectable range, indicating that these two membranes have very few or no DNA contaminations. However, a relatively strong DNA signal (low cycle threshold) was detected in Bio-Gide® (1/50 portion of DNA extracted from 0.082 g membrane) similar to that of 100 ng porcine DNA (**Figure** 7).

Our anti-α-gal immunostaining analysis showed high α-gal expression in positive control porcine aorta, whereas all collagen membranes showed negative staining (**Figure 8**).

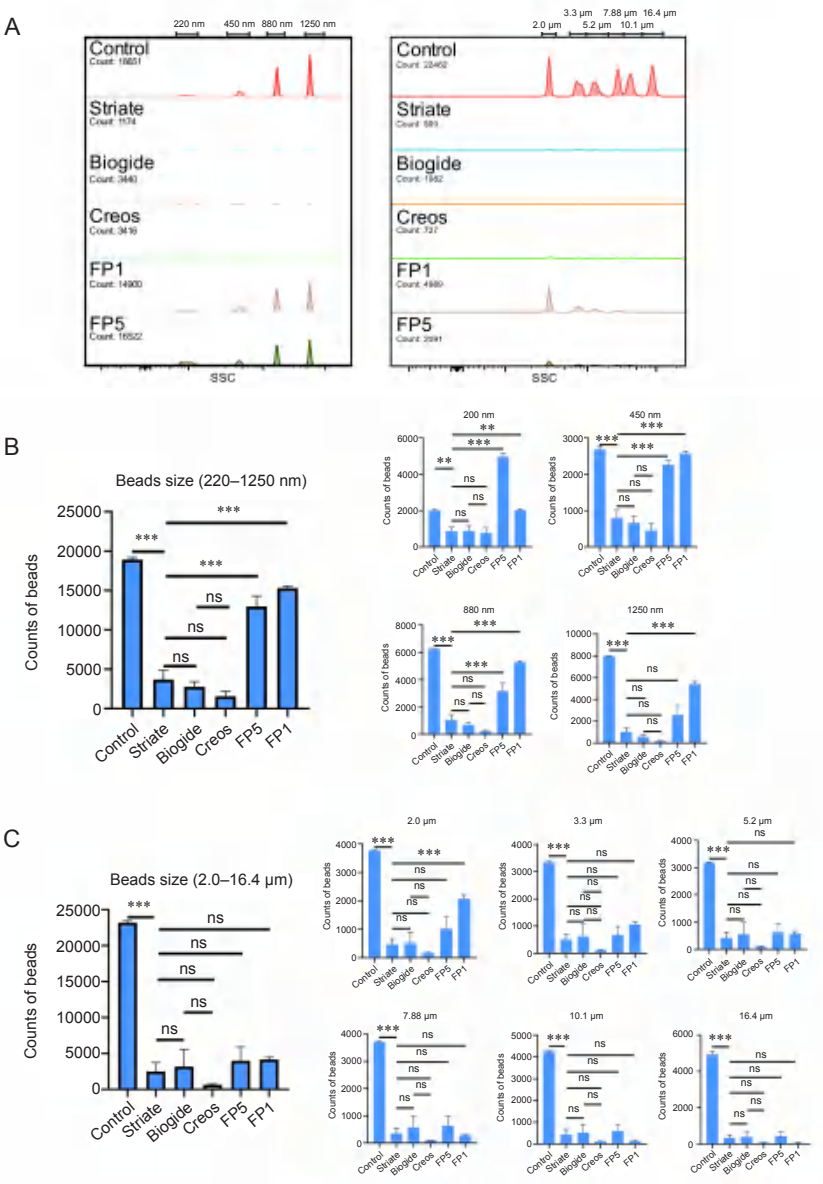

Figure 4. Barrier properties of three porcine collagen membranes measured by gravity-based filtration. (A) Representative results of collagen membranes' barrier property by filtration with mixed standard beads in different sizes. (B, C) Quantitative analysis of beads with all small (B, 220, 450, 880, and 1250 nm) and large (C, 2.0, 3.3, 5.2, 7.88, 10.1, and 16.4 µm) sizes passing through different collagen membranes. Data are presented as means ± SEM. $^{**}P < 0.01$, $^{***}P < 0.001$ (one-way analysis of variance with Tukey's *post hoc* multiple comparison). FP1: Whatman Filter paper Grade 1; FP5: Whatman Filter paper Grade 5; ns: no significance.

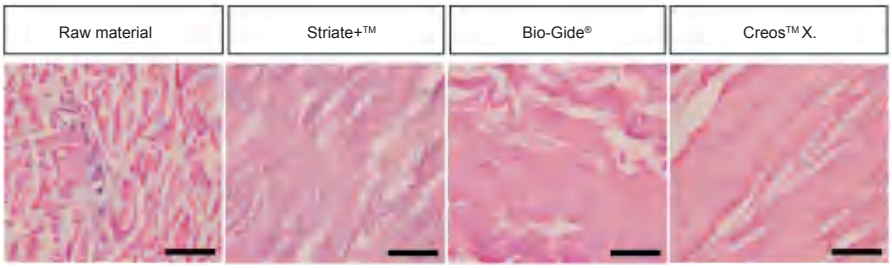

Figure 5. Heamatoxylin and eosin staining of different porcine collagen membranes. No heamatoxylin staining was found in all membranes. Scale bars: 50 μm. Creos™ X.: Creos™ Xenoprotect.

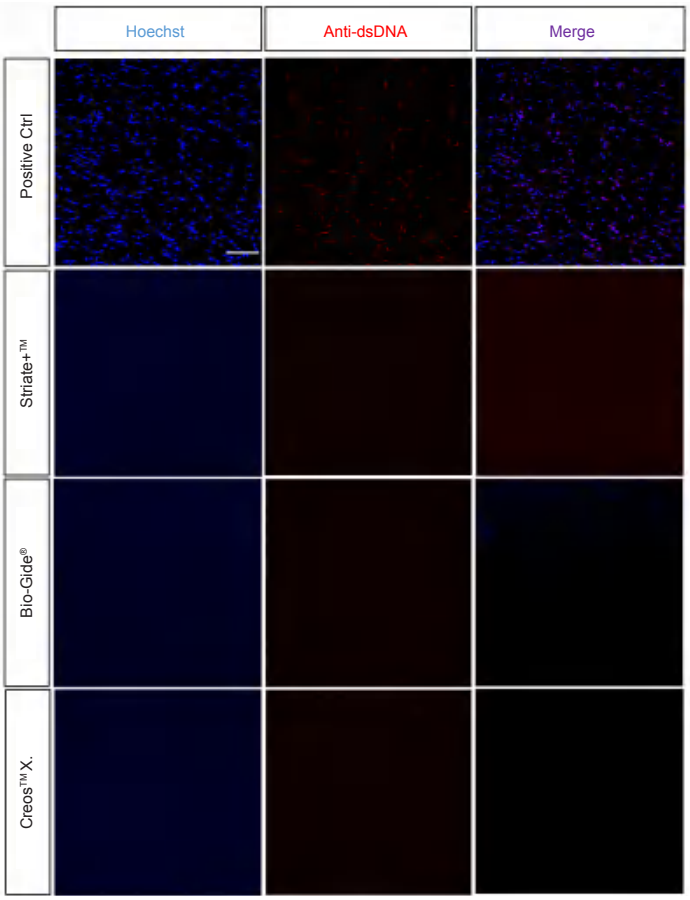

Figure 6. Anti-DNA immunostaining on different porcine collagen membranes. No DNA was found in all membranes by anti-DNA immunostaining. Positive control (Ctrl) indicates porcine aortic valve. Scale bar: 100 μm. Creos™ X.: Creos™ Xenoprotect; dsDNA: double stranded DNA.

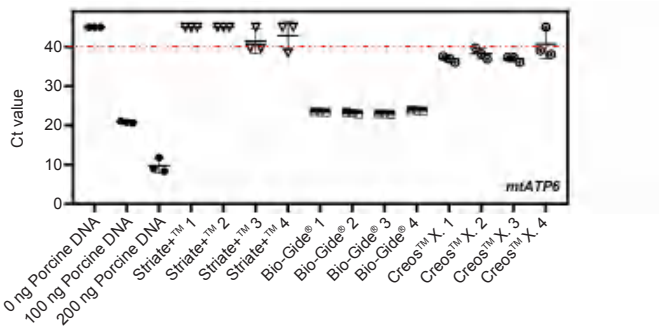

Figure 7. Determination of DNA content in different collagen membranes by real-time polymerase chain reaction. Among the three collagen membranes, only Bio-Gide® membrane showed significant DNA signal content. Data plotted above red dot line indicates undetectable within 40 cycles. Creos™ X.: Creos™ Xenoprotect; Ct: cycle threshold.

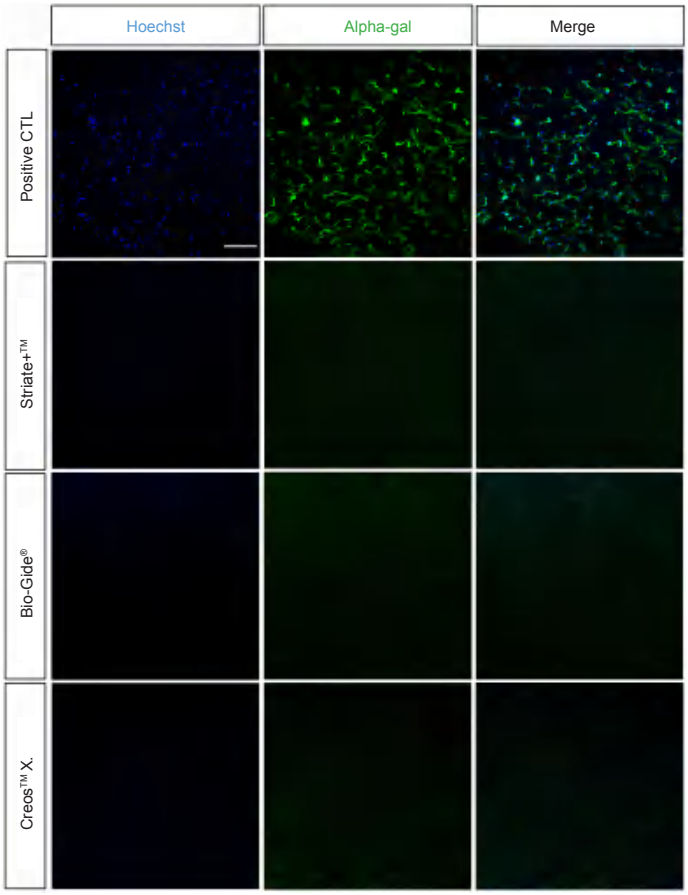

Figure 8. α-gal expression in different collagen membranes. No α-gal signal was detected in Creos™ Xenoprotect, Striate+™ and Bio-Gide® by anti-α-gal immunostaining. Positive control (Ctrl) indicates porcine aortic valve. Scale bar: 100 μm. α-gal: alpha-gal, galactose-α-1,3-galactose; Creos™ X.: Creos™ Xenoprotect.

Discussion

GBR is aided by the use of a barrier membrane to promote bone augmentation and osseointegration of dental implants. The barrier membrane prevents the growth of soft tissues into the wound to allow osteogenic cells to proliferate within the defect. Native collagen membranes (NCMs) have become popular as they are resorbed and degraded in-situ. NCMs can also promote soft tissue healing.[22] As NCMs are biodegradable, cross-linking of collagen membranes was developed to maintain the integrity and strength. However, a recent systematic review showed no difference in bone regeneration between cross-linked and resorbable collagen membranes.[23] Furthermore, cross-linked collagen membranes may impair soft tissue healing or cause wound infections.[24] Therefore, collagen barrier membranes without cross-linking have become widely used and studied.[3] The effective membrane for GBR must be able to act as a physical barrier against cell invasion but not inhibit bone regeneration on the other side of the membrane. NCMs must not contain immunogens which can cause severe immune reactions and result in poor bone regeneration, compromising the osseointegration of dental implants. This study is the first systematic examination of similar commercial native collagen membranes for GBR on their barrier properties, surface topological details, fibre diameter and D-periodicity, and immunogen contamination. We conclude that these membranes are not identical.

The surface topological examination focused on the distribution and density of collagen bundles in the three commercially available collagen membranes (Creos™ Xenoprotect, Bio-Gide® and Striate+™) by SEM. Our SEM analysis showed that all membranes have smooth and rough sides which can be easily distinguished from each other based on the density and distribution of collagen bundles. The smooth side of NCMs showed a high density of aligned collagen bundles, whereas the rough side showed relatively loose and irregular collagen bundles. At 364× magnification view, almost no pores were observed on the smooth surface of the collagen membranes. At 150k× magnification, most of the pores on both the smooth and rough side are smaller than 1 μm, which sufficiently prevent cells from passing through the membranes. In most cases, measurement of porosity was used to estimate their barrier property[25] probably due to the lack of an assay system. We designed an assay system using beads and gravity filtration as well as flow cytometry analysis. By using this assay system, all collagen membranes showed superior barrier property by gravity-based filtration, which is independent of the thickness of membranes, and thus explains why all the membranes can efficiently act as a physical barrier to prevent the in-growth of cells into the bone cavity.

The diameter of collagen fibrils is a result of the number and type of assembled collagen molecules, whereas the

D-periodicity of collagen fibrils is measured from overlap and gap regions between self-assembled collagen molecules. The diameter and D-peridocity of collagen fibrils in each of the three collagen membranes were measured by SEM at 150 k× magnification. No significant difference was found in the diameter of collagen fibrils between the three collagen membranes. Based on the 1.5 nm diameter of a mature collagen molecule,[9] approximately 54 tropocollagen molecules are self-assembled into collagen fibrils (81.62–85.82 nm in diameter) in these collagen membranes. The mean of D-periodocity of the collagen membranes Striate+™, Bio-Gide® and Creos™ Xenoprotect, were measured as 62.9, 56.3 m and 57.4 nm, respectively. Striate+™ showed the highest D-periodocity and is closest to the average D-periodicity of unprocessed natural collagen fibrils (67 nm)[5, 9-11] suggesting less deformation in the manufacturing process. The difference in the D-periodicity could be due to the origin of porcine tissues (age and/or tissue origin) and/or manufacture processing such as dehydration and compression.[13-15] Different D-periodicity of collagen fibrils does not affect the function as physical barriers which are mainly determined by the density and distribution of the collagen bundle, but it could affect their susceptibility to salivary collagenase.[15, 16] Furthermore, a recent study demonstrated that collagen membranes could be bio-inductive and facilitate the tissue repair.[26] GBR membranes have also been shown to have additional bone regenerative functions such as the triggering of expression of bone remodeling genes and differential concentration of bone morphogenetic protein-2 on the membrane surface.[27] Furthermore, a study suggested that collagen membranes may have an intrinsic transforming growth factor-β activity which may affect the tissue regeneration process.[28] It remains unclear whether maintenance of native superstructure of collagen fibrils such as D-periodicity could be important for bone and/or soft tissue regeneration during GBR or other tissue regenerations. As D-periodicity may also affect the susceptibility to collagenase degradation in saliva,[15, 16] the stability of all the membranes remains to be addressed.

Porcine small intestine submucosa, a collagen-rich tissue, has been used to manufacture collagen scaffolds for tissue regeneration. However, the immunogenic substances such as DNA present in small intestine submucosa can cause severe immunological reactions after implantation in the human body.[18] The removal of α-gal in collagen-based medical devices is important to prevent immunological rejection, especially in people with α-gal syndrome.[29, 30] These major immunogenic substances have to be removed during manufacturing of the collagen membranes. To test whether there was any immunogenic substance in the porcine-derived collagen membranes, we measured the DNA and α-gal content in the three porcine-derived collagen membranes by heamatoxylin and eosin staining, immunostaining and PCR. No α-gal and DNA, including nuclear remnants, were detected in any of the membranes by immunostaining and Hoechst staining. However, using real-time PCR, a relatively strong DNA signal was observed in the Bio-Gide® membrane but not in Creos™ Xenoprotect and Striate+™ membranes. The cycle threshold value of porcine specific gene (*mtATP6*) from Bio-Gide® membranes is similar to that of 100 ng porcine DNA. This could be possibly due to insufficient removal of immunogens during the manufacture of the Bio-Gide® membranes. Our data may explain why more inflammatory cells and cytokines were found in Bio-Gide® than another porcine collagen membrane in a recent study using a rat model.[25]

An ideal GBR membrane should include the following characteristics 1) good barrier property, 2) low immunogen content 3) good for soft tissue regeneration and 4) easy to handle. Our study has established robust assays for determining their barrier property and immunogenic content which are the key elements of GBR. The effects of the collagen membranes on soft and bone tissue regeneration have not been addressed which is also the limitation of this study. Further studies using animal GBR models can address both the extent of inflammation and tissue regeneration. On the other hand, the thickness of the membranes may potentially affect the quality of the surgical procedure. It appears to be more difficult to manipulate thicker membranes in GBR procedure. Rating by dentists could be a way to determine their handling experience. A more scientific assay system should be designed to address the handling property without bias.

In conclusion, our study showed that these three non-cross-linked membranes are similar but not identical, probably due to the different ages and sources of porcine tissues as well as different manufacturing processes. Striate+™ membrane is closest to the D-periodicity of natural, unprocessed collagen. Low residual DNA was detected in Bio-Gide® but not in Striate+™ and Creos™ Xenoprotect. All of these membranes have similar superior barrier properties. Further comparative studies are required to conclude their clinical outcomes.

Author contributions

MHZ, AT and EL designed the study; AT, EL and ZC conducted experiments and prepared figures; AT, EL, ZC, MT, BA, RR, DC, MG, HN and MHZ wrote and reviewed the manuscript. All authors have read and approved the final version of the manuscript.

Financial support

None.

Acknowledgement

The authors acknowledge the facilities, and the scientific and technical assistance offered by Ms. Alysia Hubbard, Ms. Diana Patalwala and Dr. Catherine Rinaldi of the National Imaging Facility, a National Collaborative Research Infrastructure Strategy (NCRIS) capability, at the Centre for Microscopy, Characterisation & Analysis, The University of Western Australia.

Conflicts of interest statement

MHZ holds shares of Orthocell Ltd., Australia. Other authors declare that no competing interests exist.

Additional file

Additional Figure 1: Determination of barrier property of collagen membranes by gravity-based filtration.

1. Dahlin, C.; Linde, A.; Gottlow, J.; Nyman, S. Healing of bone defects by guided tissue regeneration. *Plast Reconstr Surg.* **1988**, *81*, 672-676.
2. Sasaki, J. I.; Abe, G. L.; Li, A.; Thongthai, P.; Tsuboi, R.; Kohno, T.;

Imazato, S. Barrier membranes for tissue regeneration in dentistry. *Biomater Investig Dent.* **2021**, *8*, 54-63.

3. Sbricoli, L.; Guazzo, R.; Annunziata, M.; Gobbato, L.; Bressan, E.; Nastri, L. Selection of collagen membranes for bone regeneration: a literature review. *Materials (Basel).* **2020**, *13*, 786.
4. Lee, S. W.; Kim, S. G. Membranes for the guided bone regeneration. *Maxillofac Plast Reconstr Surg.* **2014**, *36*, 239-246.
5. Kadler, K. E.; Holmes, D. F.; Trotter, J. A.; Chapman, J. A. Collagen fibril formation. *Biochem J.* **1996**, *316 (Pt 1)*, 1-11.
6. Pace, J. M.; Corrado, M.; Missero, C.; Byers, P. H. Identification, characterization and expression analysis of a new fibrillar collagen gene, COL27A1. *Matrix Biol.* **2003**, *22*, 3-14.
7. Boot-Handford, R. P.; Tuckwell, D. S.; Plumb, D. A.; Rock, C. F.; Poulsom, R. A novel and highly conserved collagen (pro(alpha)1(XXVII)) with a unique expression pattern and unusual molecular characteristics establishes a new clade within the vertebrate fibrillar collagen family. *J Biol Chem.* **2003**, *278*, 31067-31077.
8. Exposito, J. Y.; Valcourt, U.; Cluzel, C.; Lethias, C. The fibrillar collagen family. *Int J Mol Sci.* **2010**, *11*, 407-426.
9. Hodge, A. J.; Petruska, J. A. Recent studies with the electron microscope on ordered aggregates of the tropocollagen macromolecule. In *Aspects of Protein Structure, Ramachandran*, G. N., Ed. Academic Press: New York, 1963; pp 289-300.
10. Chapman, J. A.; Tzaphlidou, M.; Meek, K. M.; Kadler, K. E. The collagen fibril--a model system for studying the staining and fixation of a protein. *Electron Microsc Rev.* **1990**, *3*, 143-182.
11. Orgel, J. P.; Irving, T. C.; Miller, A.; Wess, T. J. Microfibrillar structure of type I collagen in situ. *Proc Natl Acad Sci U S A.* **2006**, *103*, 9001-9005.
12. Wallace, J. M.; Chen, Q.; Fang, M.; Erickson, B.; Orr, B. G.; Banaszak Holl, M. M. Type I collagen exists as a distribution of nanoscale morphologies in teeth, bones, and tendons. *Langmuir.* **2010**, *26*, 7349-7354.
13. Kemp, A. D.; Harding, C. C.; Cabral, W. A.; Marini, J. C.; Wallace, J. M. Effects of tissue hydration on nanoscale structural morphology and mechanics of individual type I collagen fibrils in the Brtl mouse model of Osteogenesis Imperfecta. *J Struct Biol.* **2012**, *180*, 428-438.
14. Wells, H. C.; Sizeland, K. H.; Kelly, S. J. R.; Kirby, N.; Hawley, A.; Mudie, S.; Haverkamp, R. G. Collagen fibril intermolecular spacing changes with 2-propanol: a mechanism for tissue stiffness. *ACS Biomater Sci Eng.* **2017**, *3*, 2524-2532.
15. Watanabe-Nakayama, T.; Itami, M.; Kodera, N.; Ando, T.; Konno, H. High-speed atomic force microscopy reveals strongly polarized movement of clostridial collagenase along collagen fibrils. *Sci Rep.* **2016**, *6*, 28975.
16. Uitto, V. J.; Suomalainen, K.; Sorsa, T. Salivary collagenase. Origin, characteristics and relationship to periodontal health. *J Periodontal Res.* **1990**, *25*, 135-142.
17. Hilger, C.; Fischer, J.; Wölbing, F.; Biedermann, T. Role and mechanism of galactose-alpha-1,3-galactose in the elicitation of delayed anaphylactic reactions to red meat. *Curr Allergy Asthma Rep.* **2019**, *19*, 3.
18. Zheng, M. H.; Chen, J.; Kirilak, Y.; Willers, C.; Xu, J.; Wood, D. Porcine small intestine submucosa (SIS) is not an acellular collagenous matrix and contains porcine DNA: possible implications in human implantation. *J Biomed Mater Res B Appl Biomater.* **2005**, *73*, 61-67.
19. Schneider, C. A.; Rasband, W. S.; Eliceiri, K. W. NIH Image to ImageJ: 25 years of image analysis. *Nat Methods.* **2012**, *9*, 671-675.
20. Rezakhaniha, R.; Agianniotis, A.; Schrauwen, J. T.; Griffa, A.; Sage, D.; Bouten, C. V.; van de Vosse, F. N.; Unser, M.; Stergiopulos, N. Experimental investigation of collagen waviness and orientation in the arterial adventitia using confocal laser scanning microscopy. *Biomech Model Mechanobiol.* **2012**, *11*, 461-473.
21. Yoshida, T.; Nomura, T.; Shinoda, N.; Kusama, T.; Kadowaki, K.; Sugiura, K. Development of PCR primers for the detection of porcine DNA in feed using mtATP6 as the target sequence. *Shokuhin Eiseigaku Zasshi.* **2009**, *50*, 89-92.
22. Zitzmann, N. U.; Naef, R.; Schärer, P. Resorbable versus nonresorbable membranes in combination with Bio-Oss for guided bone regeneration. *Int J Oral Maxillofac Implants.* **1997**, *12*, 844-852.
23. Jiménez Garcia, J.; Berghezan, S.; Caramês, J. M. M.; Dard, M. M.; Marques, D. N. S. Effect of cross-linked vs non-cross-linked collagen membranes on bone: A systematic review. *J Periodontal Res.* **2017**, *52*, 955-964.
24. Becker, J.; Al-Nawas, B.; Klein, M. O.; Schliephake, H.; Terheyden, H.; Schwarz, F. Use of a new cross-linked collagen membrane for the treatment of dehiscence-type defects at titanium implants: a prospective, randomized-controlled double-blinded clinical multicenter study. *Clin Oral Implants Res.* **2009**, *20*, 742-749.
25. Zhu, M.; Duan, B.; Hou, K.; Mao, L.; Wang, X. A comparative in vitro and in vivo study of porcine- and bovine-derived non-cross-linked collagen membranes. *J Biomed Mater Res B Appl Biomater.* **2023**, *111*, 568-578.
26. Chen, P.; Wang, A.; Haynes, W.; Landao-Bassonga, E.; Lee, C.; Ruan, R.; Breidahl, W.; Shiroud Heidari, B.; Mitchell, C. A.; Zheng, M. A bio-inductive collagen scaffold that supports human primary tendon-derived cell growth for rotator cuff repair. *J Orthop Translat.* **2021**, *31*, 91-101.
27. Elgali, I.; Omar, O.; Dahlin, C.; Thomsen, P. Guided bone regeneration: materials and biological mechanisms revisited. *Eur J Oral Sci.* **2017**, *125*, 315-337.
28. Panahipour, L.; Kargarpour, Z.; Luza, B.; Lee, J. S.; Gruber, R. TGF-β activity related to the use of collagen membranes: in vitro bioassays. *Int J Mol Sci.* **2020**, *21*, 6636.
29. Kuravi, K. V.; Sorrells, L. T.; Nellis, J. R.; Rahman, F.; Walters, A. H.; Matheny, R. G.; Choudhary, S. K.; Ayares, D. L.; Commins, S. P.; Bianchi, J. R.; Turek, J. W. Allergic response to medical products in patients with alpha-gal syndrome. *J Thorac Cardiovasc Surg.* **2022**, *164*, e411-e424.
30. Steinke, J. W.; Platts-Mills, T. A.; Commins, S. P. The alpha-gal story: lessons learned from connecting the dots. *J Allergy Clin Immunol.* **2015**, *135*, 589-596; quiz 597.

Received: December 4, 2022
Revised: February 22, 2023
Accepted: March 2, 2023
Available online: March 28, 2023

Biomaterials Translational

Effect of radiation sterilisation on the structure and antibacterial properties of antimicrobial peptides

Xiaodan Wang[1,2,*], *Qinmei Li*[1], *Huawei Yang*[2,3,*]

Key Words:
antibacterial activity; antimicrobial peptides; radiation sterilisation

From the Contents

ABSTRACT

Antimicrobial peptides (AMPs) have recently been exploited to fabricate anti-infective medical devices due to their biocompatibility and ability to combat multidrug-resistant bacteria. Modern medical devices should be thoroughly sterilised before use to avoid cross-infection and disease transmission, consequently it is essential to evaluate whether AMPs withstand the sterilisation process or not. In this study, the effect of radiation sterilisation on the structure and properties of AMPs was explored. Fourteen AMPs formed from different monomers with different topologies were synthesised by ring-opening polymerisation of N-carboxyanhydrides. The results of solubility testing showed that the star-shaped AMPs changed from water-soluble to water-insoluble after irradiation, while the solubility of linear AMPs remained unchanged. Matrix-assisted laser desorption/ionisation time of flight mass spectrometry showed that the molecular weight of the linear AMPs underwent minimal changes after irradiation. The results of minimum inhibitory concentration assay also illustrated that radiation sterilisation had little effect on the antibacterial properties of the linear AMPs. Therefore, radiation sterilisation may be a feasible method for the sterilisation of AMPs, which have promising commercial applications in medical devices.

***Corresponding authors:**
Xiaodan Wang,
wxd@hygeamed.com;
Huawei Yang,
yanghw@ciac.ac.cn.

http://doi.org/10.12336/biomatertransl.2023.01.007

How to cite this article:
Wang, X.; Li, Q.; Yang, H. Effect of radiation sterilisation on the structure and antibacterial properties of antimicrobial peptides. *Biomater Transl.* **2023**, *4*(1), 51-61.

Introduction

Surfaces of indwelling medical devices, such as central venous catheters, prostheses and contact lenses, often suffer from microbial contamination, which ultimately leads to medical device-related infections and high risk to human health.[1-3] Therefore, extensive efforts have been made to develop effective, safe, and durable antimicrobial medical devices. In the clinical setting, antiseptic drug loading has been proven to be the most achievable method to create an antimicrobial surface on a medical device.[4-6] Silver ion-,[7,8] silver alloy-,[9,10] chlorhexidine-,[11-13] and antibiotic-impregnated central venous catheters[4,14] and urinary catheters have been widely used in hospitals and show lower risk of catheter-related infections. However, each approach possesses inherent limitations of overall poor biocompatibility and significant risks of drug resistance that will render it unsuitable for a specific product.[15,16]

Recently, antimicrobial peptides (AMPs) have attracted considerable attention for the development of antimicrobial medical devices by virtue of their broad-spectrum, rapid-acting antibacterial activity, excellent biocompatibility,[17-19] and less susceptibility to bacterial resistance evolution.[20-22] However, natural AMPs are not preferred for anti-infective medical devices due to their high-cost, unclear toxicology, and low immature stability.[17] Consequently synthetic AMPs which are less expensive and easier to prepare have been developed as good substitutes

for natural AMPs. Especially, AMPs prepared by ring-opening polymerisation (ROP) of *N*-carboxyanhydrides (NCAs) have tunable structures and properties that can be adjusted according to actual demands.[18, 23] In addition, surface-immobilised AMPs not only have high antimicrobial activity, but also exhibit much lower cytolytic potency towards mammalian cells.[24]

Sterilisation has been defined as any process that eliminates microorganisms from a surface, food, medication, or biological culture medium.[25] For medical devices, sterilisation has been recognised as an essential process.[26] Patients may suffer infection and mortality/morbidity issues when using improperly sterilised healthcare products.[26] Therefore, the AMPs loaded onto medical devices must be able to withstand the sterilisation process. Ethylene oxide gas and ionising radiation are the most widespread commercially-available non-thermal sterilisation methods for healthcare products.[27] For AMPs, amino groups are the main groups responsible for their bactericidal function.[28] Considering that an epoxy group will interact with active amino groups on the AMPs and affect their performance,[24, 29] ethylene oxide sterilisation is considered to be an unsuitable sterilisation method for AMPs, and radiation sterilisation is the preferred method. Nervetheless radiation may alter the chemical and physical properties of AMPs, to the best of our knowledge, there are no relevant studies on the validation of radiation sterilisation methods for AMPs and consequently detailed studies of potential degradation need to be performed.

In this study, fourteen AMPs consisting of different monomers and with varied topologies were synthesised through the ROP of NCAs. Validation of the AMPs against the radiation sterilisation was carried out by employing a commercial 10 MeV electron beam (e-beam). It has been reported that 25 kGy is the recommended dose for the sterilisation of medical devices with no further need to provide any biological validation.[30-34] Therefore, a radiation dose of 25 kGy was chosen for our tests. The influences of sterilisation on the structure and antibacterial properties of the AMPs were comprehensively analysed by matrix-assisted laser desorption/ionisation time of flight (MALDI-TOF) mass spectrometry (MS) and the minimum inhibitory concentration (MIC) assay.

Methods

Materials

Nε-tert-butyloxycarbonyl-L-lysine(Lys,97%),D-phenylalanine (Phe, 98%), triphosgene (99%), trifluoroacetic acid (99%), hexylamine (99%), and D, L-valine (Val, 98%) were obtained from Shanghai Aladdin Biochemical Technology Co., Ltd. (Shanghai, China). Star-shaped initiators were provided by Dendritech, Inc. (Midland, MI, USA). Sodium acetate (99.5%), dimethyl sulfoxide-d_6, chloroform-*d* were purchased from Anhui Senrise Technology Co., Ltd. (Anqing, Anhui, China). Anhydrous *N*, *N*-dimethylformamide (99.9%) and anhydrous tetrahydrofuran (99.9%) were provided by Beijing Innochem Technology Co., Ltd. (Beijing, China). Other reagents were analytically pure reagents and were used directly without treatment. *Escherichia coli* (*E. coli*, ATCC 25922) and *Staphylococcus aureus* (*S. aureus*, ATCC 6538) were purchased from Nanjing Clinic Biological Technology Co. Ltd. (Nanjing, Jiangsu, China). Bacterial culture medium and dialysis bags (molecular weight cut-offs of 3500 g/mol and 8000–12,000 g/mol) were provided by Dingguo Biological Technology Co., Ltd. (Beijing, China).

Instrumentations

^{1}H nuclear magnetic resonance spectroscopy (^{1}H-NMR) was carried out on a Bruker AV, 400 MHz spectrometer (Bruker Corporation, Billerica, MA, USA) to characterise the molecular structures of NCAs, AMPs and all intermediate products. Fourier transform infrared spectroscopy was performed on a Bruker Vertex 70 (Bruker Corporation) to ascertain the conversion rate of monomers. Gel permeation chromatography was performed on a system equipped with an isocratic pump (Model 1100, Agilent Technology, Santa Clara, CA, USA), a Dawn Heleos multi-angle laser light scattering detector (Wyatt Technology, Santa Barbara, CA, USA), and an Optilab rEX refractive index detector (Wyatt Technology). The detection wavelength of the laser light scattering detector was 658 nm. Separations were performed using serially-connected size-exclusion columns (100 Å, 500 Å, 1×10^3 Å and 1×10^4 Å Phenogel columns, 5 μm, 300 × 7.8 mm, Phenomenex Inc., Torrance, CA, USA) at 60°C using N, N-dimethylformamide containing 0.05 M LiBr as the eluent phase at a flow rate of 1.0 mL/min. MALDI-TOF MS was performed on a Bruker Daltonics FlexAnalysis system (Bruker Corporation) to measure the molecular weight of AMPs.

Preparation and characterisation of the antimicrobial peptides

In this study, fourteen AMPs consisting of different monomers and with different topological structures were synthesised by ROP of NCAs; the details are shown in **Figure 1**. ROP of NCAs is one of the most convenient methods to prepare AMPs. The specific synthetic processes of NCAs and AMPs have been reported elsewhere.[24, 35] The successful construction of all AMPs was confirmed by ^{1}H-NMR (**Additional file 1**).

Experimental process of radiation sterilisation

Each dry powdered AMP was placed in a 10 mL polypropylene tube and irradiated at room temperature at a dosage of 25 kGy by a 10 MeV e-beam accelerator at WEGO Holding Co., Ltd. (Weihai, Shandong, China) After irradiation, the samples were stored at room temperature for 5 months before characterisation. Un-irradiated samples were used as the controls to evaluate the changes caused by radiation.

1 Hygea Medical Technology Co., Ltd., Beijing, China; 2 State Key Laboratory of Polymer Physics and Chemistry, Changchun Institute of Applied Chemistry, Chinese Academy of Sciences, Changchun, Jilin Province, China; 3 Department of Applied Chemistry and Engineering, University of Science and Technology of China, Hefei, Anhui Province, China.

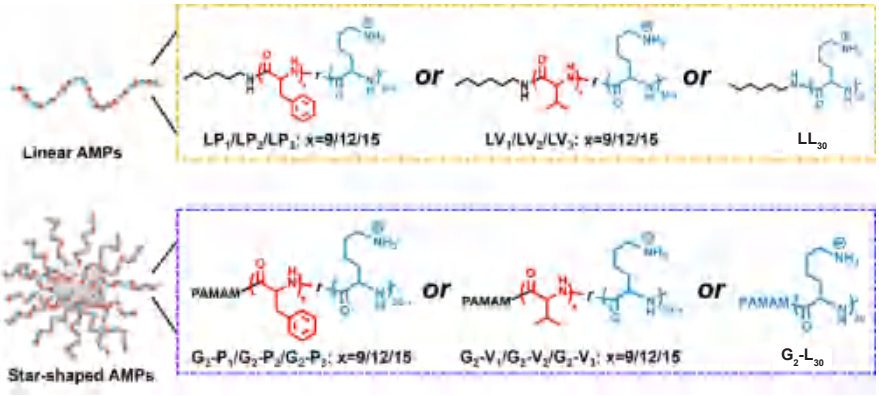

Figure 1. The molecular structure and abbreviation of each AMP in this study. AMP: antimicrobial peptide.

Evaluation of the structural changes of antimicrobial peptides

MALDI-TOF MS was used to analyse the influence of radiation sterilisation on the structure of the AMPs. Samples used for testing were prepared by dissolving in water at a concentration of 10 mg/mL.

Evaluation of the solubility of antimicrobial peptides

Approximately 10 mg of each AMP were weighed and dispersed in phosphate-buffered saline (PBS), PBS: acetic acid (v:v, 1:1) and hexafluoroisopropanol. The dissolution results were observed directly after sonication for 2 hours.

Evaluation of the antibacterial activity of antimicrobial peptides

The antibacterial activity of different AMPs before and after irradiation was determined by the MIC assay.[36, 37] The MIC of an antimicrobial agent refers to the critical concentration that inhibits bacterial growth absolutely. In this study, bacterial proliferation was analysed by measuring the optical density of the culture. *E. coli* and *S. aureus* were selected as representative Gram-negative and -positive bacteria for testing. The detailed process was as follows;[38] an overnight bacterial suspension was inoculated into Mueller-Hinton broth at 37°C with constant shaking. The bacteria were then harvested when in the logarithmic phase of growth. The bacterial density of the suspension was adjusted to 1×10^8 colony forming units (CFU)/mL, confirmed by an optical density value of 0.1 at 600 nm. Then the bacterial suspension was diluted 100 times to obtain a bacterial density of 1×10^6 CFU/mL. The AMPs were dissolved in PBS to obtain concentrations ranging from 1 μg/mL to 1000 μg/mL. Then, 100 μL of each AMP solution and 100 μL of bacterial suspension (1×10^6 CFU/mL) were added together to wells of a 96-well plate, which was then incubated at 37°C. The optical density values of the wells were measured using a microplate reader (Tecan Sunrise, Tecan Group Ltd., Männedorf, Switzerland) at 0, 6, 12, and 24 hours. A mixture of 100 μL PBS and 100 μL of bacterial solution (1×10^6 CFU/mL) was used as control.

Statistical analysis

All data are presented as mean ± standard deviation (SD). Each result is an average of at least three parallel experiments, calculated using Microsoft® Excel® 2019 (Microsoft, Redmond, WA, USA).

Results

Structural characterisation and solubility exploration of the antimicrobial peptides

First, fourteen AMPs were synthesised via ROP of three NCAs (**Figure 1**). All structures of the intermediate products and final AMPs were confirmed by ^{1}H-NMR. As shown in **Additional file 1**, the actual monomer components were consistent with the feed expectation. Combined with the results of gel permeation chromatography, the results proved that AMPs were successfully constructed. The detailed molecular parameters are shown in **Table 1**.

The solubility of AMPs before and after irradiation is shown in **Table 2**. All linear polypeptides could be dissolved in PBS regardless of irradiation, demonstrating that there was no effect of irradiation on solubility. In contrast, the star-shaped AMPs became insoluble in PBS after irradiation and only soluble in certain organic solvents, such as hexafluoroisopropanol. In order to prevent the interference of different solvents with the antibacterial properties of AMPs, linear AMPs with good solubility before and after irradiation in PBS were chosen for further investigation.

Structural changes to antimicrobial peptides caused by radiation sterilisation

Detailed information on the molecular structures and molecular weights of the monomers and AMPs is shown in **Figure 2**. The molecular weight of all AMPs ranged from 3500 to 4500, and MALDI-TOF MS was selected as a convenient instrumental method to determine the effect of radiation sterilisation on the molecular structure. (Fourier transform infrared spectroscopy and ^{1}H-NMR could not detect the tiny changes before and after sterilisation). **Figures 3–5** show the molecular weights of the linear AMPs before and after irradiation. Overall, the shapes of the MS spectrum of all samples maintained good consistency before and after irradiation. In the spectrum of the homopolymer of Lys (**Figure 3**), molecular weight intervals that corresponded to the molecular weight (128.2) of Lys monomer appeared, besides the peaks representative of $[M+H]^+$, $[M+Na]^+$, and $[M+K]^+$. Similarly, in the AMPs that copolymerised with Phe and Lys (**Figure 4**), a series of

Table 1. Detailed molecular parameters of the antimicrobial peptides

Sample	Arm No.	Designed Lys content (%)	Actual Lys content[a] (%)	Mn designed molecular weight (Da)	Mn determined molecular weight (Da)[b]	*Đ* determined molecular weight[b]
LP_1	1	70	70.8	6219.9	6200	1.07
LP_2	1	60	61.4	5976.6	6000	1.14
LP_3	1	50	51.2	5733.2	5700	1.24
G_2-P_1	16	70	71	101155.6	111200	1.05
G_2-P_2	16	60	60	97262.3	97300	1.08
G_2-P_3	16	50	48.2	93369	93400	1.12
LV_1	1	70	68.6	5787.5	5800	1.11
LV_2	1	60	59.3	5400	5500	1.09
LV_3	1	50	49	5012.5	5000	1.18
G_2-V_1	16	70	72.3	94236.4	94300	1.02
G_2-V_2	16	60	59.1	88036.7	88000	1.07
G_2-V_3	16	50	50	81837	81900	1.14
LL_{30}	1	100	100	6949.9	6900	1.05
G_2-L_{30}	16	100	100	112835.4	113000	1.13

Note: "a" represents Lys contents calculated by ^{1}H nuclear magnetic resonance spectroscopy. "b" represents the Mn and Đ determined by gel permeation chromatography. Đ: polydispersity; Lys: L-lysine.

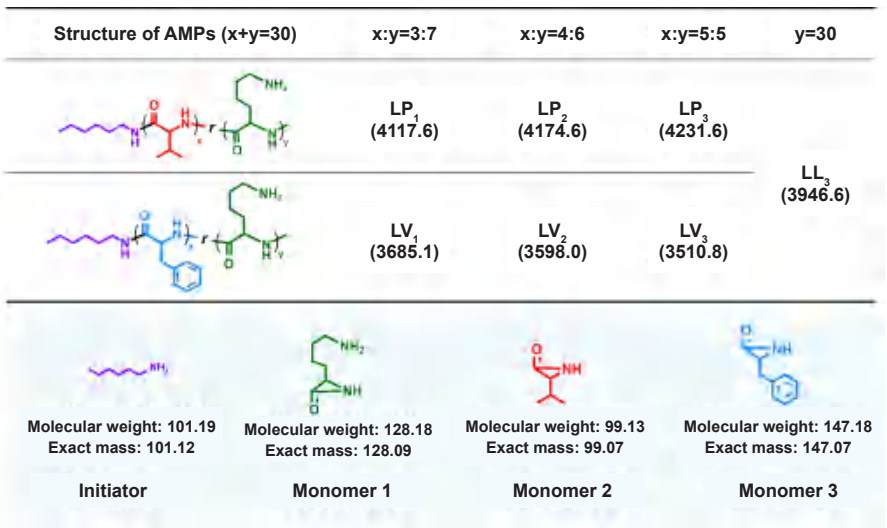

Figure 2. Molecular structure and molecular weight information of all linear AMPs. AMP: antimicrobial peptide.

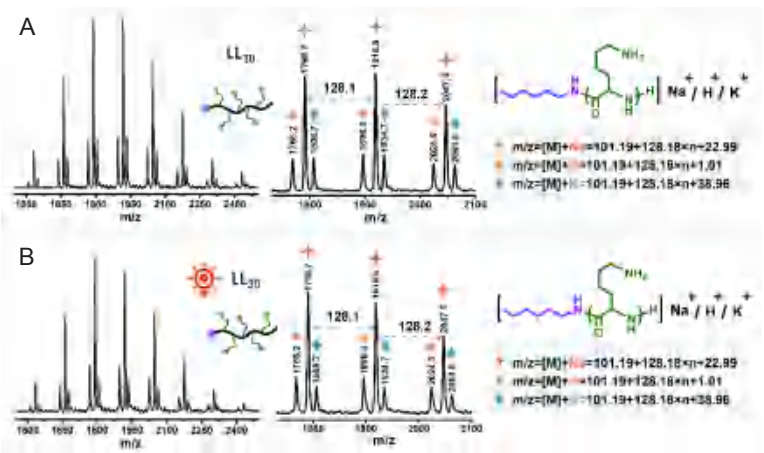

Figure 3. The spectra of LL_{30} before (A) and after (B) irradiation under matrix-assisted laser desorption/ionisation time of flight (MALDI-TOF) mass spectrometry.

Table 2. Solubility of the antimicrobial peptides before and after radiation sterilisation

	Before radiation sterilisation	After radiation sterilisation		
Sample	**PBS buffer**	**PBS buffer**	**PBS/AcOH**	**HFP**
LP_1	+	+	+	+
LP_2	+	+	+	+
LP_3	+	+	+	+
G_2-P_1	+	–	±	+
G_2-P_2	+	–	–	+
G_2-P_3	+	–	–	+
LV_1	+	+	+	+
LV_2	+	+	+	+
LV_3	+	+	+	+
G_2-V_1	+	–	–	±
G_2-V_2	+	–	–	±
G_2-V_3	+	–	–	±
LL_{30}	+	+	+	+
G_2-L_{30}	+	–	±	+

Note: "+" represents soluble, "–" represents insoluble, and "±" represents slightly soluble. AcOH: acetic acid; HFP: hexafluoroisopropanol; PBS: phosphate-buffered saline.

molecular weight intervals of 147.2, 128.2, 19.0, 109.1 and 90.2 could be seen in the spectra, which corresponded to the molecular weight of Phe monomer, Lys monomer and the molecular weight differences of Phe-Lys, 2Phe-Lys and 3Phe-2Lys (**Figures 2** and **4**). Also, for the copolymer products of Val and Lys (**Figure 5**), molecular weight intervals of 147.2, 128.2, 29.1, 70.1 and 41.0 appeared, indicating the molecular weights of Val monomer, Lys monomer, and the molecular weight differences of Lys-Val, 2Val-Lys and 3Val-2Lys (**Figures 2** and **5**).

Antibacterial performance of the antimicrobial peptides before and after irradiation

As shown in **Figures 6–8**, the antibacterial effects of all samples before and after irradiation against both Gram-positive *S. aureus* and Gram-negative *E. coli* were analysed. The MIC values are summarised in **Table 3**. The MIC of LV_2 against *S. aureus* and the MIC of LV_3 against *S. aureus* and *E. coli* increased by a factor of two after irradiation, showing a decrease in the antibacterial activity of LV_2 and LV_3. The MICs of all the other irradiated AMPs remained the same as before irradiation.

Table 3. The minimum inhibitory concentrations (μg/mL) of antimicrobial peptides against *S. aureus* and *E. coli* before and after irradiation

	S. aureus	***E. coli***
LL_{30}		
Before irradiation	16	16
After irradiation	16	16
LP_2		
Before irradiation	16	32
After irradiation	16	32
LP_2		
Before irradiation	16	32
After irradiation	16	32
LP_3		
Before irradiation	16	32
After irradiation	16	32
LV_1		
Before irradiation	16	8
After irradiation	16	8
LV_2		
Before irradiation	8	16
After irradiation	16	16
LV_3		
Before irradiation	16	32
After irradiation	32	64

Note: *E. coli*: *Escherichia coli*; *S. aureus*: *Staphylococcus aureus*.

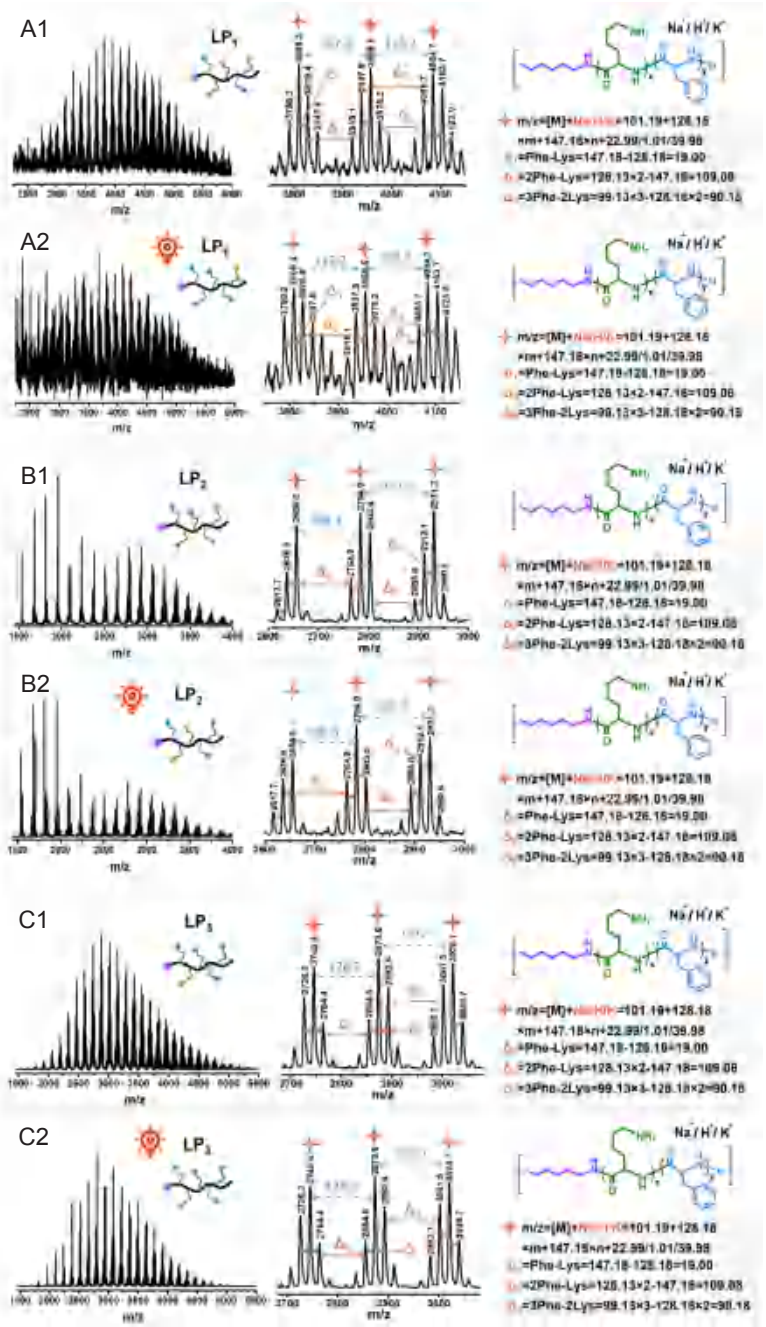

Figure 4. The spectra of LP_1–LP_3 before (A1–C1) and after (A2–C2) irradiation under matrix-assisted laser desorption/ionisation time of flight (MALDI-TOF) mass spectrometry.

Discussion

Structural changes of the antimicrobial peptides caused by radiation sterilisation

The purpose of the sterilisation process is to obtain material free from microorganisms. The ideal sterilisation process requires fully killing any pathogenic bacteria carried by a medical device. The instantaneity and high dose delivery of a high-energy e-beam allow sterilisation of products in hermetically-sealed packages. Meanwhile, the influence of radiation on the degradation of polymers is one of the most important concerns of scientific interest. Unpredictable degradation may affect their physicochemical properties, and thus affect the efficacy and safety of treatment.[32] It has been reported that ionising radiation may cause cross-linking or chain-scission.[26, 34, 39] When a cross-linking reaction occurs, the molecular weight of the polymer increases. In contrast, when the polymer undergoes a chain-scission process, the molecular weight of the polymer decreases. Therefore, the structural changes of the irradiated AMPs can be analysed by comparing the molecular weights of the corresponding AMPs before and after irradiation.

The process of radiation sterilisation had a negligible effect on the molecular weight of most AMPs. Nevertheless, careful comparison and analysis revealed a slight shift to lower

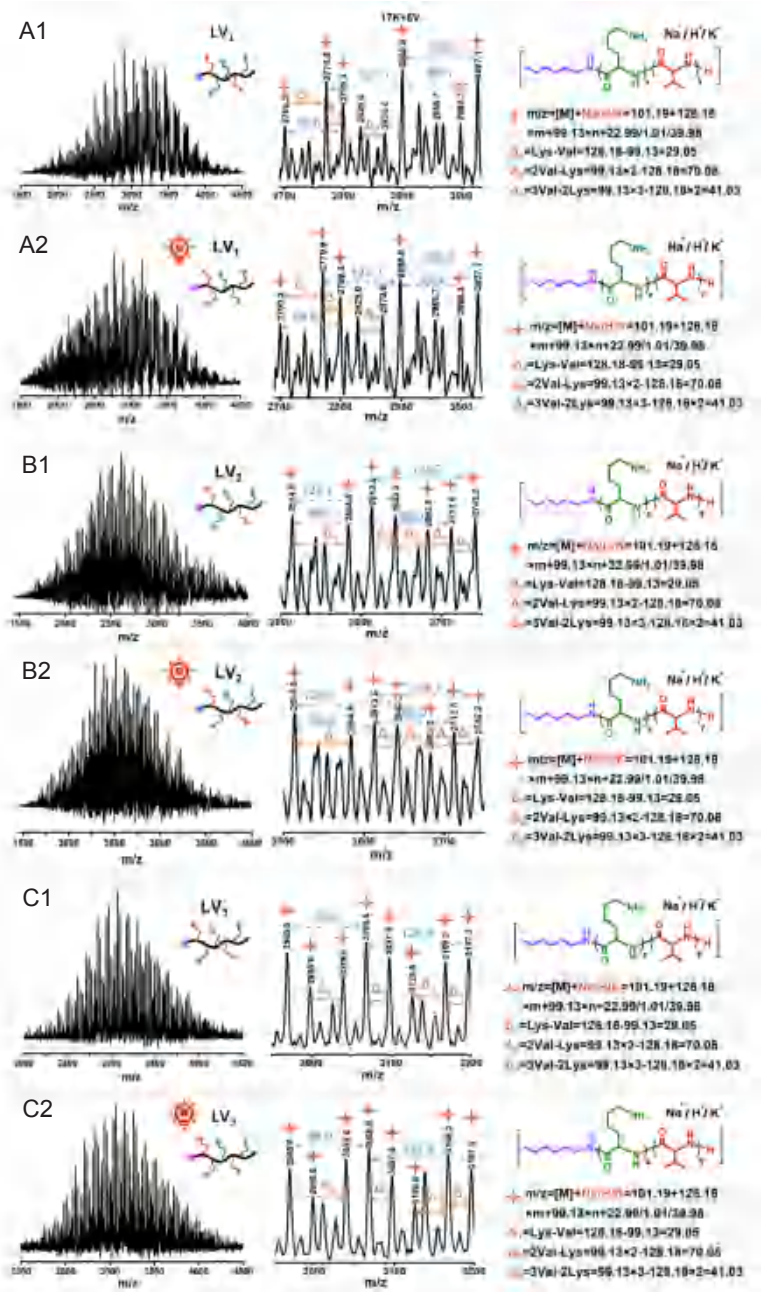

Figure 5. The spectra of LV_1–LV_3 before (A1–C1) and after (A2–C2) irradiation under matrix-assisted laser desorption/ionisation time of flight (MALDI-TOF) mass spectrometry.

molecular weight in some samples. The phenomenon was observed more obviously in the AMPs copolymerised from higher proportions of cationic Lys, regardless of whether they were copolymerised with either Phe or Val. For example, after irradiation, the molecular weight portions of LP_1 (**Figure 4A**) and LP_2 (**Figure 4B**) below 3000 g/mol were increased compared with the corresponding spectra before irradiation, indicating that molecular chains of the samples were partially broken. Similar phenomena were also observed in LV_1 (**Figure 5A**) and LV_2 (**Figure 5B**). However, the molecular weights of the samples with lower Lys, LP_3 and LV_3, showed no migration to low molecular weights. Some studies have reported that aromatic materials offer more resistance to radiation than aliphatic materials.[31] After being irradiated, the conjugated structure of aromatic rings can transfer and disperse the radiation energy by a delocalisation effect instead of concentrating on a certain bond, and as a consequence, the absorbed radiation energy will be converted into heat energy for release. Therefore, the materials generally show better radiation resistance when their main chain or side chain contains aromatic rings.[31] Accordingly, the AMPs composed of a higher proportion of Phe (LP_3) in this study showed better resistance to e-beam radiation than the AMPs with lower proportions of Phe (LP_1 and LP_2). However, these changes were tiny, and the results of MALDI-TOF MS demonstrated overall an insignificant influence of radiation sterilisation on the structure of AMPs. However, the mechanism behind the change of solubility of star-shaped AMPs was unclear.

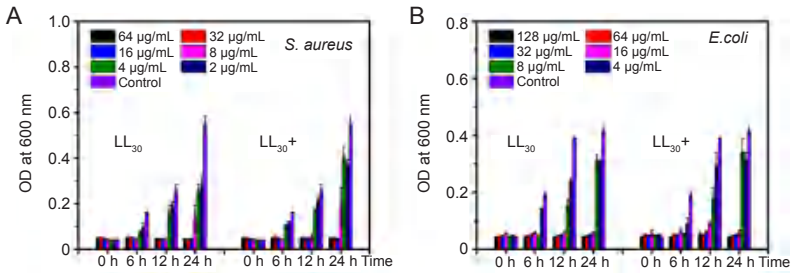

Figure 6. The minimum inhibitory concentrations of LL_{30} before and after irradiation. (A) *Staphylococcus aureus* (*S. aureus*). (B) *Escherichia coli* (*E. coli*). OD: optical density.

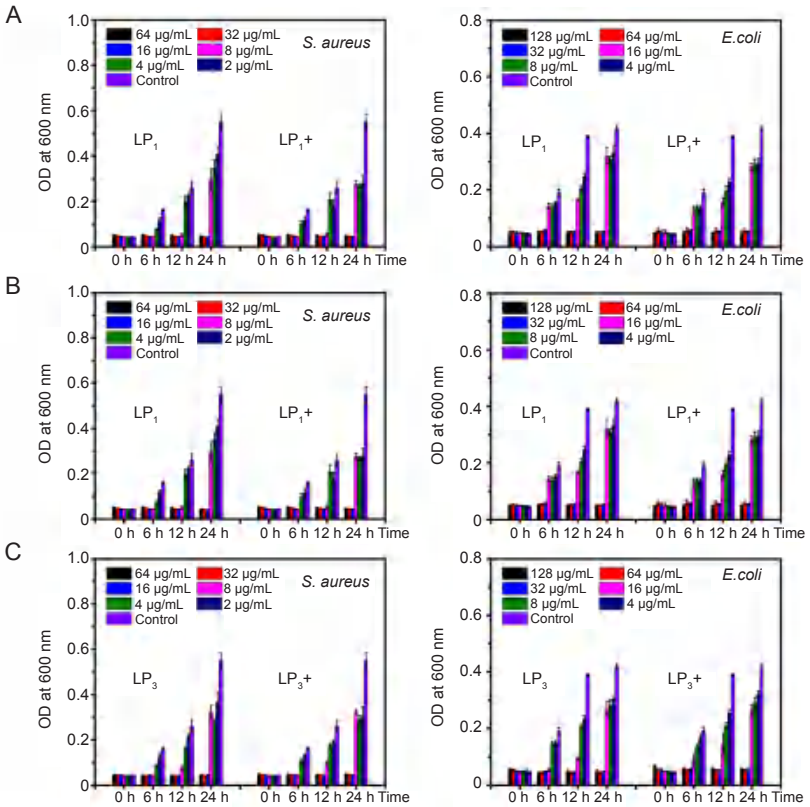

Figure 7. The minimum inhibitory concentrations of LP_1–LP_3 (A–C) before and after irradiation. *E. coli*: *Escherichia coli*; OD: optical density; *S. aureus*: *Staphylococcus aureus*.

Antibacterial property of antimicrobial peptides before and after irradiation

The antibacterial activity of AMPs is closely related to their architecture and monomer composition.[40-43] In order to explore universal laws governing the effect of radiation on the AMPs, fourteen AMPs with different architectures and varied monomer components were designed. As the star-shaped AMPs were found to be insoluble in water after radiation sterilisation, only the antibacterial properties of linear AMPs were analysed. The results of MALDI-TOF MS revealed that a high-energy e-beam caused the chain-scission of the samples. Free radicals can also be evoked in the process of chain-scission in an air atmosphere due to the presence of oxygen during the radiation process.[26, 31] Generally, decay reactions of free radicals will happen rapidly within hours to months, depending on the chemical structure of the samples, the radiation dose and the storage environment.[44-48] In order to eliminate the possible influence of free radicals, the samples were characterised at 5 months after irradiation to ensure the free radicals were fully consumed. From the results, MIC of most AMPs (except for LV_2 and LV_3) remained unchanged, indicating negligible effects of radiation on the antibacterial activity of those AMPs. Combined with the results of MALDI-TOF MS, radiation sterilisation could be considered as a feasible method to sterilise AMPs.

Conclusion

In conclusion, fourteen AMPs with different topologies (linear and star-shaped) and varied monomer components were designed and synthesised successfully. Commercial-scale 10 MeV e-beam radiation was selected as a promising sterilisation method for AMPs, and the AMPs were subjected

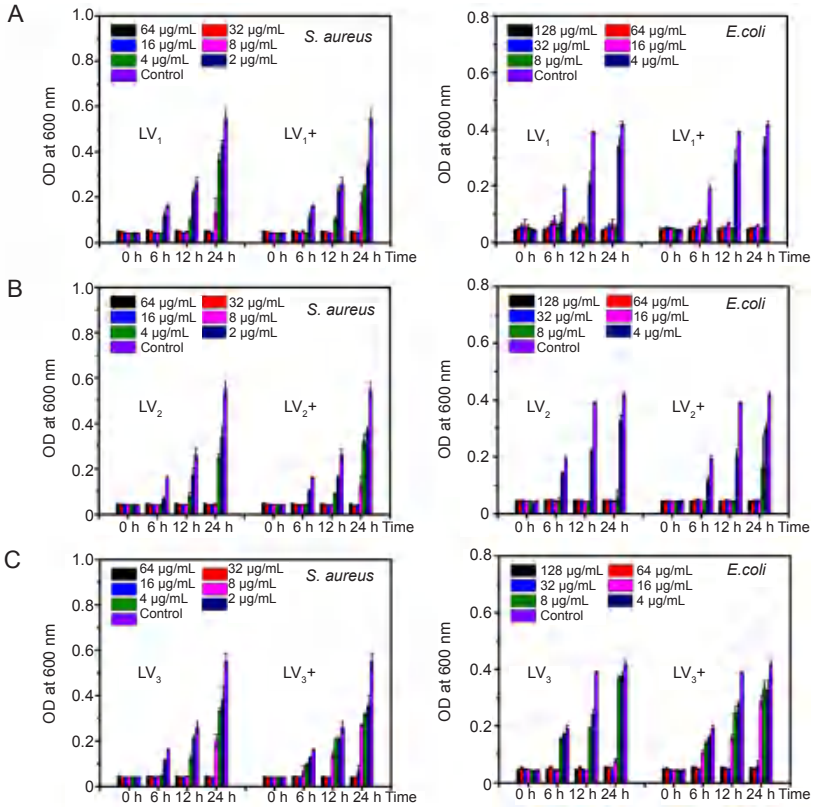

Figure 8. The minimum inhibitory concentrations of LV_1–LV_3 (A–C) before and after irradiation. *E. coli*: *Escherichia coli*; OD: optical density; *S. aureus*: *Staphylococcus aureus*.

to a dose of 25 kGy in order to explore the possible impact of radiation on their structure and antibacterial properties. It is worth mentioning that the water solubility of star-shaped AMPs changed from soluble to insoluble after irradiation. As for linear AMPs, the results of MALDI-TOF MS and MIC assay suggested negligible effects of radiation on the structure or antibacterial activity. Nevertheless, AMPs copolymerised with a higher proportion of Phe exhibited better resistance to radiation. In conclusion, radiation sterilisation is presented as an attractive and effective sterilisation strategy for AMP-based medical devices. However, there remain some problems that need further exploration. For example, characterisation of the structure and antibacterial properties of AMPs is relatively simple, but electronic paramagnetic resonance spectroscopy would be a more direct detection method for monitoring free radicals. In addition, a maximum dose that ensures the safety (biocompatibility) and performance (functionality) of the product over its lifetime also needs to be established.

Author contributions

Conceptualisation and methodology: XW, HY; investigation and resources: XW, HY, QL; formal analysis, visualisation, validation and manuscript draft: XW; manuscript revision, funding acquisition and project administration: HY; supervision: QL, HY. All authors approved the final version of the manuscript.

Financial support

None.

Acknowledgement

This study was supported by the National Natural Science Foundation of China (No. 51873213), High-Tech Research & Development Program of CAS-WEGO Group, and National Key Research and Development Program of China (No. 2021YFC2101700).

Conflicts of interest statement

There are no conflicts to declare.

Additional file

Additional file 1: Preparation and characterisation of the N-carboxyanhydrides and antimicrobial peptides.

1. Deusenbery, C.; Wang, Y.; Shukla, A. Recent innovations in bacterial infection detection and treatment. *ACS Infect Dis.* **2021**, *7*, 695-720.
2. Yu, Q.; Wu, Z.; Chen, H. Dual-function antibacterial surfaces for biomedical applications. *Acta Biomater.* **2015**, *16*, 1-13.
3. Bai, D.; Chen, J.; Li, P.; Huang, W. Perspectives on biomaterial-associated infection: pathogenesis and current clinical demands. In *Racing for the surface: pathogenesis of implant infection and advanced antimicrobial strategies*, Li, B.; Moriarty, T. F.; Webster, T.; Xing, M., eds.; Springer International Publishing: Cham, 2020; pp 75-93.
4. Lai, N. M.; Chaiyakunapruk, N.; Lai, N. A.; O'Riordan, E.; Pau, W. S.; Saint, S. Catheter impregnation, coating or bonding for reducing central venous catheter-related infections in adults. *Cochrane Database Syst Rev.* **2016**, *3*, CD007878.
5. Cloutier, M.; Mantovani, D.; Rosei, F. Antibacterial coatings: challenges, perspectives, and opportunities. *Trends Biotechnol.* **2015**, *33*, 637-652.
6. Campoccia, D.; Montanaro, L.; Arciola, C. R. A review of the biomaterials technologies for infection-resistant surfaces. *Biomaterials.*

2013, *34*, 8533-8554.

7. Chen, Y. M.; Dai, A. P.; Shi, Y.; Liu, Z. J.; Gong, M. F.; Yin, X. B. Effectiveness of silver-impregnated central venous catheters for preventing catheter-related blood stream infections: a meta-analysis. *Int J Infect Dis.* **2014**, *29*, 279-286.
8. Rupp, M. E.; Fitzgerald, T.; Marion, N.; Helget, V.; Puumala, S.; Anderson, J. R.; Fey, P. D. Effect of silver-coated urinary catheters: efficacy, cost-effectiveness, and antimicrobial resistance. *Am J Infect Control.* **2004**, *32*, 445-450.
9. Singh, R.; Hokenstad, E. D.; Wiest, S. R.; Kim-Fine, S.; Weaver, A. L.; McGree, M. E.; Klingele, C. J.; Trabuco, E. C.; Gebhart, J. B. Randomized controlled trial of silver-alloy-impregnated suprapubic catheters versus standard suprapubic catheters in assessing urinary tract infection rates in urogynecology patients. *Int Urogynecol J.* **2019**, *30*, 779-787.
10. Saint, S.; Elmore, J. G.; Sullivan, S. D.; Emerson, S. S.; Koepsell, T. D. The efficacy of silver alloy-coated urinary catheters in preventing urinary tract infection: a meta-analysis. *Am J Med.* **1998**, *105*, 236-241.
11. Safdar, N.; O'Horo, J. C.; Ghufran, A.; Bearden, A.; Didier, M. E.; Chateau, D.; Maki, D. G. Chlorhexidine-impregnated dressing for prevention of catheter-related bloodstream infection: a meta-analysis. *Crit Care Med.* **2014**, *42*, 1703-1713.
12. Lorente, L. Review: chlorhexidine-impregnated dressings reduce risk of colonisation of central venous catheters and risk of catheter-related bloodstream infection. *Evid Based Nurs.* **2015**, *18*, 91.
13. Srisang, S.; Nasongkla, N. Spray coating of foley urinary catheter by chlorhexidine-loadedpoly(ε-caprolactone) nanospheres: effect of lyoprotectants, characteristics, and antibacterial activity evaluation. *Pharm Dev Technol.* **2019**, *24*, 402-409.
14. Bayston, R.; Fisher, L. E.; Weber, K. An antimicrobial modified silicone peritoneal catheter with activity against both Gram-positive and Gram-negative bacteria. *Biomaterials.* **2009**, *30*, 3167-3173.
15. Luther, E. M.; Schmidt, M. M.; Diendorf, J.; Epple, M.; Dringen, R. Upregulation of metallothioneins after exposure of cultured primary astrocytes to silver nanoparticles. *Neurochem Res.* **2012**, *37*, 1639-1648.
16. Blair, J. M.; Webber, M. A.; Baylay, A. J.; Ogbolu, D. O.; Piddock, L. J. Molecular mechanisms of antibiotic resistance. *Nat Rev Microbiol.* **2015**, *13*, 42-51.
17. Tan, P.; Fu, H.; Ma, X. Design, optimization, and nanotechnology of antimicrobial peptides: From exploration to applications. *Nano Today.* **2021**, *39*, 101229.
18. Rasines Mazo, A.; Allison-Logan, S.; Karimi, F.; Chan, N. J.; Qiu, W.; Duan, W.; O'Brien-Simpson, N. M.; Qiao, G. G. Ring opening polymerization of α-amino acids: advances in synthesis, architecture and applications of polypeptides and their hybrids. *Chem Soc Rev.* **2020**, *49*, 4737-4834.
19. Luong, H. X.; Thanh, T. T.; Tran, T. H. Antimicrobial peptides - advances in development of therapeutic applications. *Life Sci.* **2020**, *260*, 118407.
20. Hancock, R. E.; Sahl, H. G. Antimicrobial and host-defense peptides as new anti-infective therapeutic strategies. *Nat Biotechnol.* **2006**, *24*, 1551-1557.
21. Ageitos, J. M.; Sánchez-Pérez, A.; Calo-Mata, P.; Villa, T. G. Antimicrobial peptides (AMPs): Ancient compounds that represent novel weapons in the fight against bacteria. *Biochem Pharmacol.* **2017**, *133*, 117-138.
22. Mowery, B. P.; Lee, S. E.; Kissounko, D. A.; Epand, R. F.; Epand, R. M.; Weisblum, B.; Stahl, S. S.; Gellman, S. H. Mimicry of antimicrobial host-defense peptides by random copolymers. *J Am Chem Soc.* **2007**, *129*, 15474-15476.
23. Deming, T. J. Synthesis of side-chain modified polypeptides. *Chem Rev.* **2016**, *116*, 786-808.
24. Wang, X.; Yang, F.; Yang, H.; Zhang, X.; Tang, H.; Luan, S. Preparation of antibacterial polypeptides with different topologies and their antibacterial properties. *Biomater Sci.* **2022**, *10*, 834-845.
25. Raza, S.; Iqbal, Y.; Ullah, I.; Mubarak, M. S.; Hameed, M. U.; Raza, M. Effects of gamma irradiation on the physico-chemical and biological properties of levofloxacin. *Pak J Pharm Sci.* **2018**, *31*, 181-186.
26. Gomes, A. D.; de Oliveira, A. A. R.; Houmard, M.; Nunes, E. H. M. Gamma sterilization of collagen/hydroxyapatite composites: Validation and radiation effects. *Appl Radiat Isot.* **2021**, *174*, 109758.
27. Domańska, I. M.; Oledzka, E.; Sobczak, M. Sterilization process of polyester based anticancer-drug delivery systems. *Int J Pharm.* **2020**, *587*, 119663.
28. Maturana, P.; Gonçalves, S.; Martinez, M.; Espeche, J. C.; Santos, N. C.; Semorile, L.; Maffia, P. C.; Hollmann, A. Interactions of "de novo" designed peptides with bacterial membranes: Implications in the antimicrobial activity. *Biochim Biophys Acta Biomembr.* **2020**, *1862*, 183443.
29. Yang, Z.; Xi, Y.; Bai, J.; Jiang, Z.; Wang, S.; Zhang, H.; Dai, W.; Chen, C.; Gou, Z.; Yang, G.; Gao, C. Covalent grafting of hyperbranched poly-L-lysine on Ti-based implants achieves dual functions of antibacteria and promoted osteointegration in vivo. *Biomaterials.* **2021**, *269*, 120534.
30. Bargh, S.; Silindir-Gunay, M.; Ozer, A. Y.; Colak, S.; Kutlu, B.; Nohutcu, R. The effects of gamma and microwave sterilization on periodontological grafts. *Chemical Physics Impact.* **2021**, *3*, 100046.
31. Sharma, A.; Anup, N.; Tekade, R. K. Chapter 21 - Achieving sterility in biomedical and pharmaceutical products (part-II): radiation sterilization. In *The future of pharmaceutical product development and research*, Tekade, R. K., ed. Academic Press: 2020; pp 789-848.
32. Nguyen, H.; Cassady, A. I.; Bennett, M. B.; Gineyts, E.; Wu, A.; Morgan, D. A.; Forwood, M. R. Reducing the radiation sterilization dose improves mechanical and biological quality while retaining sterility assurance levels of bone allografts. *Bone.* **2013**, *57*, 194-200.
33. De Guzman, Z. M.; Cervancia, C. R.; Dimasuay, K. G.; Tolentino, M. M.; Abrera, G. B.; Cobar, M. L.; Fajardo, A. C., Jr.; Sabino, N. G.; Manila-Fajardo, A. C.; Feliciano, C. P. Radiation inactivation of Paenibacillus larvae and sterilization of American Foul Brood (AFB) infected hives using Co-60 gamma rays. *Appl Radiat Isot.* **2011**, *69*, 1374-1379.
34. B.G. Porto, K. M.; Napolitano, C. M.; Borrely, S. I. Gamma radiation effects in packaging for sterilization of health products and their constituents paper and plastic film. *Radiat Phys Chem.* **2018**, *142*, 23-28.
35. Liu, H.; Zhang, X.; Zhao, Z.; Yang, F.; Xue, R.; Yin, L.; Song, Z.; Cheng, J.; Luan, S.; Tang, H. Efficient synthesis and excellent antimicrobial activity of star-shaped cationic polypeptides with improved biocompatibility. *Biomater Sci.* **2021**, *9*, 2721-2731.
36. Wiegand, I.; Hilpert, K.; Hancock, R. E. Agar and broth dilution methods to determine the minimal inhibitory concentration (MIC) of antimicrobial substances. *Nat Protoc.* **2008**, *3*, 163-175.
37. Li, P.; Poon, Y. F.; Li, W.; Zhu, H. Y.; Yeap, S. H.; Cao, Y.; Qi, X.; Zhou, C.; Lamrani, M.; Beuerman, R. W.; Kang, E. T.; Mu, Y.; Li, C. M.; Chang, M. W.; Leong, S. S.; Chan-Park, M. B. A polycationic antimicrobial and biocompatible hydrogel with microbe membrane suctioning ability. *Nat Mater.* **2011**, *10*, 149-156.
38. Wang, X.; Shi, H.; Tang, H.; Yu, H.; Yan, Q.; Yang, H.; Zhang, X.;

Luan, S. Electrostatic assembly functionalization of poly (γ-glutamic acid) for biomedical antibacterial applications. *J Mater Sci Technol.* **2020**, *59*, 14-25.

39. Haji-Saeid, M.; Sampa, M. H. O.; Chmielewski, A. G. Radiation treatment for sterilization of packaging materials. *Radiat Phys Chem.* **2007**, *76*, 1535-1541.
40. Liscano, Y.; Salamanca, C. H.; Vargas, L.; Cantor, S.; Laverde-Rojas, V.; Oñate-Garzón, J. Increases in hydrophilicity and charge on the polar face of alyteserin 1c helix change its selectivity towards Gram-positive bacteria. *Antibiotics (Basel).* **2019**, *8*, 238.
41. Palermo, E. F.; Lienkamp, K.; Gillies, E. R.; Ragogna, P. J. Antibacterial activity of polymers: discussions on the nature of amphiphilic balance. *Angew Chem Int Ed Engl.* **2019**, *58*, 3690-3693.
42. Judzewitsch, P. R.; Nguyen, T. K.; Shanmugam, S.; Wong, E. H. H.; Boyer, C. Towards sequence-controlled antimicrobial polymers: effect of polymer block order on antimicrobial activity. *Angew Chem Int Ed Engl.* **2018**, *57*, 4559-4564.
43. Lam, S. J.; O'Brien-Simpson, N. M.; Pantarat, N.; Sulistio, A.; Wong, E. H.; Chen, Y. Y.; Lenzo, J. C.; Holden, J. A.; Blencowe, A.; Reynolds, E. C.; Qiao, G. G. Combating multidrug-resistant Gram-negative bacteria with structurally nanoengineered antimicrobial peptide polymers. *Nat Microbiol.* **2016**, *1*, 16162.
44. Osmanoğlu, Y. E.; Sütçü, K. EPR studies of the free radicals generated in gamma irradiated amino acid derivatives. *J Mol Struct.* **2017**, *1145*, 240-243.
45. Duliu, O. G.; Bercu, V. Chapter 2 - ESr investigation of the free radicals in irradiated foods. In *Electron spin resonance in food science*, Shukla, A. K., ed. Academic Press: 2017; pp 17-32.
46. Atrous, H.; Benbettaieb, N.; Hosni, F.; Danthine, S.; Blecker, C.; Attia, H.; Ghorbel, D. Effect of γ-radiation on free radicals formation, structural changes and functional properties of wheat starch. *Int J Biol Macromol.* **2015**, *80*, 64-76.
47. Liu, W.; Wang, M.; Xing, Z.; Wu, G. The free radical species in polyacrylonitrile fibers induced by γ-radiation and their decay behaviors. *Radiat Phys Chem.* **2012**, *81*, 835-839.
48. Zhao, Y.; Wang, M.; Tang, Z.; Wu, G. ESR study of free radicals in UHMW-PE fiber irradiated by gamma rays. *Radiat Phys Chem.* **2010**, *79*, 429-433.

Received: January 5, 2023
Revised: Febraury 17, 2023
Accepted: March 9, 2023
Available online: March 28, 2023